Schweizerische Eidgenossenschaft
Confédération suisse
Confederazione Svizzera
Confederaziun svizra

Federal Department of the Environment, Transport, Energy and Communications DETEC

Swiss Federal Office of Energy SFOE
Energy Research and Cleantech

Final report

PeakMetal

Covering Winter Peaks of Heat and Electricity Demand by “Renewable Metal Fuels”

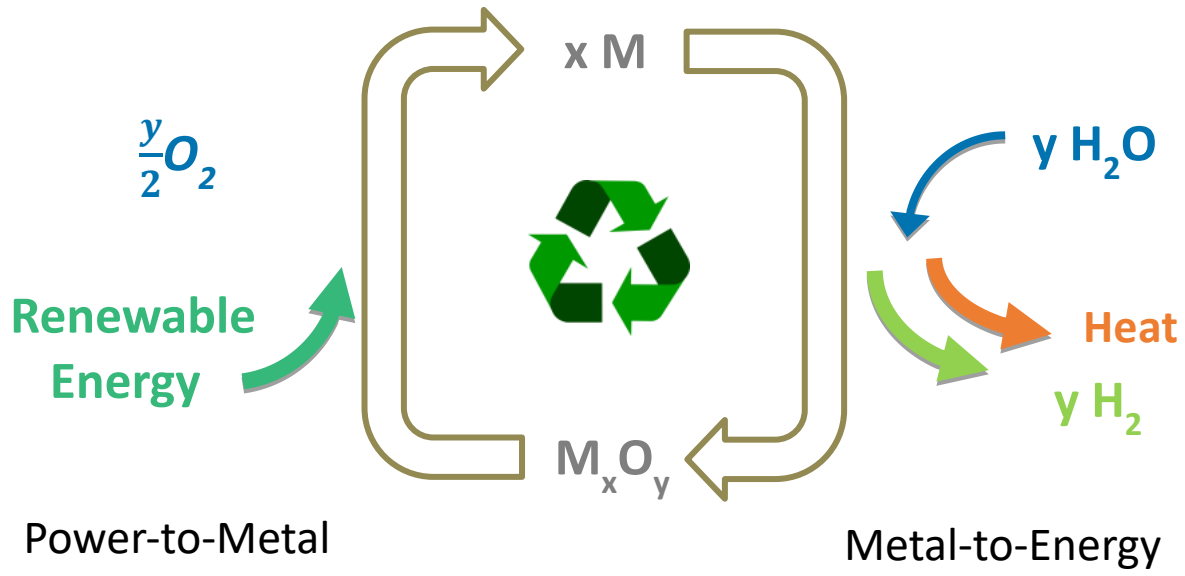

Source: © SPF 2024

Date: 05/07/2024

Location: Rapperswil

Subsidiser:
Swiss Federal Office of Energy SFOE
Energy Research and Cleantech Section
CH-3003 Bern
www.bfe.admin.ch

Co-financing
Energie 360° AG
Aargauerstr. 182
Postfach 805
8010 Zürich
www.energie360.ch

BWB-Altenrhein AG
Dorfstrasse 3

9423 Altenrhein
www.bwb-group.com/de/

Subsidy recipients:
SPF Institute for Solar Technology
Eastern Switzerland University of Applied Sciences (OST)
Oberseestr. 10, 8640 Rapperswil
www.spf.ch / www.ost.ch

Authors:
Yvonne I. Bäuerle, SPF, yvonne.baeuerle@ost.ch
Marcel Troxler, SPF, marcel.troxler@ost.ch
Michel Y. Haller, SPF, michel.haller@ost.ch

SFOE project coordinators:
Andreas Eckmanns, andreas.eckmanns@bfe.admin.ch
Nadège Vetterli, nadege.vetterli@anex.ch

SFOE contract number: SI/502545-01

Summary

Renewable Metal Fuels (ReMeF) are sustainable seasonal energy storage solutions that may deliver heat and power for buildings and reduce greenhouse gas emissions by replacing current fossil-fuel based systems in winter.

ReMeF are metals (M) that are produced from their oxides (M_XO_Y) by stripping oxygen (O_2) in a process that consumes renewable energy (Power-to-Metal). ReMeF are high density energy carriers that can be stored loss free for as long as needed and transported over long distances. When or where energy is needed, ReMeF can be oxidized again in either a single step using oxygen, or in two steps, of which the first is a metal-water reaction that produces hydrogen (H_2) and metal-hydroxide, and the second is oxidizing the hydrogen to produce electricity and heat. In order to close the material cycle, metal-hydroxide is then converted to metal-oxide that can be used in the production of new ReMeF. Thus, the material cycle of a ReMeF energy storage cycle is closed and meets the criteria of a circular economy.

Within the PeakMetal project, the focus was on

1. screening and rating metallic elements as candidates for ReMeF, selecting the most promising ones
2. evaluating the potential to reduce possible future winter energy gaps with the most promising ReMeF candidates for low temperature metal-water reactions

Screening and rating revealed that aluminium, iron, and silicon are the most promising candidates for ReMeF. Main advantages are their high abundance - they are the most abundant elements in the earth's crust besides oxygen - low cost and ease of handling as they are neither toxic nor highly reactive.

Power-to-Metal charging

The metallurgic industry of today uses carbon as a reducing agent for converting metal oxides to aluminium, iron or silicon. In this process, CO_2 is produced and emitted. It is therefore crucial for the use of metals as ReMeF, that the reduction of metal oxides is performed with new technologies such as inert anode electrolysis for aluminium or direct reduction by hydrogen for iron. The TRL of these new, CO_2-emission-free, Power-to-Metal processes is highest for hydrogen reduction of iron (TRL 6/7), followed by inert aluminium smelting (4-7) and similar technologies for silicon (4). The energetic efficiency of Power-to-Metal up to the point where the material is shaped into its desired form and stored until winter is estimated to reach 50 to 60%.

Metal-to-Energy discharging

When these metals are activated to react with water, hydrogen and heat are produced. The share of stored energy that converts to hydrogen compared to heat is highest (almost 100%) for the iron discharge process, and thus the share of electricity after hydrogen conversion in a fuel cell is much higher for iron (50%) than for aluminium and silicon. The metal-water reactions of aluminium and silicon are highly exothermic, and half of the stored energy is

released as heat, which leads to a metal-to-electric efficiency of roughly 25%. On the other hand, the energy density is considerably higher for aluminium and silicon compared to iron, both on a volumetric (>20 MWh/m^3 vs. 12 MWh/m^3) as well as on a gravimetric base (> 8.5 kWh/kg vs. 2 kWh/kg). Advantages of ReMeF compared to other long term Power-to-X storage options are:

- very high energy density, in particular per volume
- ease of transport
- non toxic and non explosive
- relatively low cost
- no need for cryogenic or pressurized storage vessels
- no carbon involved that needs to be (re)-captured at some point for climate neutrality

Potential to cover winter peak demand

Different scenarios of the Swiss energy system in the year 2050 were simulated, starting from the energy perspectives 2050+. Instead of producing hydrogen with electrolysers in summer and using fuel cells in winter to convert it to electricity again, the potential to produce ReMeF with excess summer electricity was evaluted. Subsequently, the potential to use ReMeF in multifamily buildings for the production of heat and electricity in winter was estimated, covering much of the heating and electricity demand of the buildings as well as feeding electricity into the grid in order to reduce a possible winter-gap of energy supply.

The results show for a Swiss energy system with high penetration of photovoltaics (45 TWh_{el}/a) a remaining winter gap of electricity of 8 – 9 TWh_{el} without ReMeF. Limiting the capacity of metal-to-energy conversion units to 10 kW_{th} installed in every multifamily building that is not connected to district heating, this winter gap could be reduced to 2-3 TWh_{el}, if aluminium- or silicon-water reactions are used for Metal-to-Energy. Using iron, which has a much higher share of electric output compared to thermal output, Switzerland would be able to export 2-4 kWh_{el} in winter with the otherwise same assumptions. Naturally, not all multifamily buildings will be equipped with ReMeF. However, additional potential exists for ReMeF in district heating and for industrial heat and electricity, which is not yet included in the above presented numbers.

Global warming

For Power-to-Metal based on carbon free metal production (TRL 4-7), the climatic effect of all considered ReMeF is determined by the greenhouse gas emissions of the electricity used for the Power-to-Metal process. This value must be lower than 35 – 50 gCO2-eq./MJ in order to reduce global warming when replacing a mini CHP (Combined Heat and Power) unit that is based on natural gas. Electricity generation with such low GWP can be achieved with hydro and wind energy (1-3 gCO2-eq./MJ) or with rooftop PV (10 gCO2-eq./MJ).

Installing ReMeF CHP in multifamily buildings in Switzerland with an average of 10 kW_{th} per building can reduce the winter gap of energy supply. Compared to achieving the same goal with natural gas turbine power plants, it would save greenhouse gas emissions of more than 3 Mio tCO_2eq per year.

Zusammenfassung

Renewable Metal Fuels (ReMeF) sind nachhaltige, saisonale Energiespeicherlösungen, die Wärme und Strom für Gebäude liefern und Treibhausgasemissionen reduzieren können, indem sie die derzeitigen Systeme auf Basis fossiler Brennstoffe im Winter ersetzen.

ReMeF sind Metalle (M), die aus ihren Oxiden (M_XO_Y) durch Abspaltung von Sauerstoff (O_2) unter Verwendung erneuerbarer Energie (Power-to-Metal) hergestellt werden. ReMeF sind Energieträger mit hoher Dichte, die verlustfrei und beliebig lange gespeichert und über weite Strecken transportiert werden können. Wenn oder wo Energie benötigt wird, können ReMeF entweder in einem einzigen Schritt unter Verwendung von Sauerstoff oder in zwei Schritten wieder oxidiert werden. Bei zwei Schritten ist der erste Schritt eine Metall-Wasser-Reaktion, bei der Wasserstoff (H_2) und Metallhydroxid entstehen. Im zweiten Schritt wird Wasserstoff in einer Brennstoffzelle zur Erzeugung von Strom und Wärme oxidiert zu Wasser. Um den Stoffkreislauf zu schließen, wird das im ersten Schritt entstandene Metallhydroxid in Metalloxid umgewandelt, das für die Herstellung von neuem ReMeF verwendet werden kann. Der Stoffkreislauf eines ReMeF-Energiespeicherkreislaufs ist also geschlossen und erfüllt die Kriterien der Kreislaufwirtschaft.

Im Rahmen des PeakMetal-Projekts lag der Schwerpunkt auf:

1. Screening und Bewertung metallischer Elemente als Kandidaten für ReMeF und Auswahl der vielversprechendsten Elemente
2. Bewertung des Potenzials zur Verringerung möglicher künftiger Energielücken im Winter mit den vielversprechendsten ReMeF-Kandidaten für Metall-Wasser-Reaktionen bei niedrigen Temperaturen

Screening und Bewertung ergaben, dass Aluminium, Eisen und Silizium die vielversprechendsten Kandidaten für ReMeF sind. Die Hauptvorteile sind ihre hohe Verfügbarkeit - sie sind neben Sauerstoff die häufigsten Elemente in der Erdkruste - ihre geringen Kosten und ihre einfache Handhabung, da sie weder giftig noch hochreaktiv sind.

Power-to-Metal - Einspeicherung

Die heutige metallurgische Industrie verwendet Kohlenstoff als Reduktionsmittel für die Umwandlung von Metalloxiden in Aluminium, Eisen oder Silizium. Bei diesem Prozess wird CO_2 erzeugt und emittiert. Daher ist es für die Verwendung von Metallen als ReMeF von entscheidender Bedeutung, dass die Reduktion von Metalloxiden mit neuen Technologien wie der inerten Anodenelektrolyse für Aluminium oder der direkten Reduktion mit Wasserstoff für Eisen durchgeführt wird. Die TRL dieser neuen, CO_2 -emissionsfreien Power-to-Metal-Verfahren ist für die Wasserstoffreduktion von Eisen am höchsten (TRL 6/7), gefolgt von der Aluminium-Elektrolyse mit Inert-Elektroden (4-7) und ähnlichen Technologien für Silizium (4). Der energetische Wirkungsgrad von Power-to-Metal bis zu dem Punkt, an dem das Material in seine gewünschte Form gebracht und bis zum Winter gelagert wird, wird auf 50 bis 60 % geschätzt.

Metall-zu-Energie-Entladung

Wenn Metalle aktiviert werden um mit Wasser zu reagieren, werden Wasserstoff und Wärme erzeugt. Der Anteil der gespeicherten Energie, der sich in Wasserstoff umwandelt, ist im Vergleich zur Wärme beim Eisenentladungsprozess am höchsten (fast 100 %). Daher ist der Anteil der Elektrizität nach der Wasserstoffumwandlung in einer Brennstoffzelle bei Eisen viel höher (50%) als bei Aluminium und Silizium. Die Metall-Wasser-Reaktionen von Aluminium und Silizium sind stark exotherm, und die Hälfte der gespeicherten Energie wird als Wärme freigesetzt, was zu einem Wirkungsgrad von etwa 25 % bei der Umwandlung von Metall in Strom führt. Andererseits ist die Energiedichte von Aluminium und Silizium im Vergleich zu Eisen wesentlich höher, sowohl auf volumetrischer (>20 MWh/m^3 vs. 12 MWh/m^3) als auch auf gravimetrischer Basis (> 8,5 kWh/kg vs. 2 kWh/kg). Die Vorteile von ReMeF im Vergleich zu anderen langfristigen Power-to-X-Speicheroptionen sind:

- sehr hohe Energiedichte, insbesondere pro Volumen
- Einachheit des Transports
- nicht giftig und nicht explosiv
- relativ geringe Kosten
- kein Bedarf an kryogenen oder unter Druck stehenden Lagerbehältern
- kein Kohlenstoff, der irgendwann (wieder)eingefangen werden muss (Klimaneutralität)

Potenzial zur Deckung des Spitzenbedarfs im Winter

Ausgehend von den Energieperspektiven 2050+ wurden verschiedene Szenarien des Schweizer Energiesystems im Jahr 2050 simuliert. Statt Wasserstoff im Sommer mit Elektrolyseuren zu produzieren und ihn im Winter mit Brennstoffzellen wieder in Strom umzuwandeln, wurde das Potenzial der Produktion von ReMeF mit überschüssigem Sommerstrom evaluiert. In der Folge wurde die Möglichkeit betrachtet, ReMeF in Mehrfamilienhäusern für die Produktion von Wärme und Strom im Winter einzusetzen, wobei dabei ein grosser Teil des Wärme- und Strombedarfs der Gebäude gedeckt wird und Strom zusätzlich ins Netz eingespeist werden kann, was zur Reduktion einer allfälligen Winterlücke beiträgt.

Die Ergebnisse zeigen für ein Schweizer Energiesystem mit hoher Photovoltaik-Durchdringung (45 TWh_{el}/a) eine verbleibende Winter-Stromlücke von 8-9 TWh_{el} ohne MeMeF. Mit einer thermischen Leistung von Metal-to-Energy auf 10 kW_{th} in allen Mehrfamilienhäudern die nicht an die Fernwärme angeschlossen sind, könnte diese Winterlücke mit Aluminium oder Silizium als ReMeF auf 2-3 TWh_{el} reduziert werden. Mit Eisen, das einen viel höheren Anteil an elektrischer im Vergleich zur thermischen Leistung hat, könnte die Schweiz unter sonst gleichen Annahmen im Winter sogar 2-4 kWh_{el} exportieren. Einerseits werden wohl nicht alle Mehrfamilienhäuser mit ReMeF ausgerüstet werden. Andererseits besteht jedoch ein zusätzliches Potenzial für ReMeF in der Fernwärme und für industrielle Wärme und Elektrizität, das in den oben dargestellten Zahlen noch nicht enthalten ist.

Globale Erwärmung

Unter Verwendung von Power-to-Metal welches auf einer kohlenstofffreien Metallproduktion basiert (TRL 4-7), wird die Klimawirkung aller betrachteten ReMeF durch die Treibhausgasemissionen des für den Power-to-Metal-Prozess verwendeten Stroms bestimmt. Dieser Wert muss unter 35 - 50 gCO2-eq./MJ liegen, um die globale Erwärmung zu reduzieren, wenn ein Mini-BHKW (Kraft-Wärme-Kopplung), das auf Erdgas basiert, durch ReMeF ersetzt wird. Eine Stromerzeugung mit einem solch niedrigen GWP-Wert kann mit Wasser- und Windenergie (1-3 gCO2-eq./MJ) oder mit Photovoltaik auf Dächern (10 gCO2-eq./MJ) erreicht werden.

Die Installation von ReMeF KWK in Mehrfamilienhäusern in der Schweiz mit einer durchschnittlichen Leistung von 10 kW_{th} pro Gebäude kann die Winter-Energielücke substantiell reduzieren. Verglichen mit dem Erreichen des gleichen Ziels mit Erdgas-Reservekraftwerken würden dadurch Treibhausgasemissionen von mehr als 3 Mio. tCO_2 eq pro Jahr eingespart.

Résumé

Les combustibles métalliques renouvelables (ReMeF) sont des solutions durables de stockage saisonnier de l'énergie qui peuvent fournir de la chaleur et de l'électricité aux bâtiments et réduire les émissions de gaz à effet de serre en remplaçant en hiver les systèmes actuels basés sur les combustibles fossiles.

Les ReMeF sont des métaux (M) qui sont produits à partir de leurs oxydes (M_XO_Y) par extraction de l'oxygène (O_2) dans un processus qui consomme de l'énergie renouvelable (Power-to-Metal). Les ReMeF sont des vecteurs d'énergie à haute densité qui peuvent être stockés sans perte aussi longtemps que nécessaire et transportés sur de longues distances. Lorsque l'énergie stockée est nécessaire, les ReMeF peuvent être oxydés à nouveau, soit en une seule étape en utilisant de l'oxygène, soit en deux étapes, dont la première est une réaction métal-eau qui produit de l'hydrogène (H_2) et de l'hydroxyde métallique, et la seconde est l'oxydation de l'hydrogène pour produire de l'électricité et de la chaleur. Pour clore le cycle des matériaux, l'hydroxyde métallique est ensuite converti en oxyde métallique qui peut être utilisé dans la production de nouveaux ReMeF. Ainsi, le cycle des matériaux d'un cycle de stockage d'énergie ReMeF est fermé et répond aux critères d'une économie circulaire.

Dans le cadre du projet PeakMetal, l'accent a été mis sur :

1. la sélection et l'évaluation des éléments métalliques candidats au ReMeF et la sélection des éléments les plus prometteurs
2. l'évaluation du potentiel de réduction des déficits énergétiques hivernaux éventuels grâce aux candidats ReMeF les plus prometteurs pour les réactions métal-eau à basse température

La sélection et l'évaluation ont révélé que l'aluminium, le fer et le silicium sont les candidats les plus prometteurs pour le ReMeF. Leurs principaux avantages sont leur abondance - ce

sont les éléments les plus abondants dans la croûte terrestre après l'oxygène -, leur faible coût et leur facilité de manipulation, car ils ne sont ni toxiques ni très réactifs.

Chargement "Power-to-Metal

L'industrie métallurgique actuelle utilise le carbone comme agent réducteur pour convertir les oxydes métalliques en aluminium, en fer ou en silicium. Ce processus produit et émet du CO_2. Il est donc crucial pour l'utilisation des métaux comme ReMeF que la réduction des oxydes métalliques soit effectuée à l'aide de nouvelles technologies telles que l'électrolyse à anode inerte pour l'aluminium ou la réduction directe par l'hydrogène pour le fer. Le TRL de ces nouveaux procédés "Power-to-Metal" sans émission de CO_2 est le plus élevé pour la réduction du fer par l'hydrogène (TRL 6/7), suivi de la fusion de l'aluminium inerte (4-7) et de technologies similaires pour le silicium (4). L'efficacité énergétique du procédé "Power-to-Metal" jusqu'au moment où le matériau est façonné dans la forme souhaitée et stocké jusqu'à l'hiver est estimée à 50 à 60 %.

Décharge métal-énergie

Lorsque ces métaux sont activés pour réagir avec l'eau, ils produisent de l'hydrogène et de la chaleur. La part de l'énergie stockée qui se convertit en hydrogène par rapport à la chaleur est la plus élevée (presque 100%) pour le processus de décharge du fer, et la part de l'électricité après conversion de l'hydrogène dans une pile à combustible est donc aussi beaucoup plus élevée pour le fer (50%) que pour l'aluminium et le silicium. Les réactions métal-eau de l'aluminium et du silicium sont fortement exothermiques et la moitié de l'énergie stockée est libérée sous forme de chaleur, ce qui conduit à un rendement métal-électricité d'environ 25 %. D'autre part, la densité énergétique est considérablement plus élevée pour l'aluminium et le silicium que pour le fer, tant sur une base volumétrique (>20 MWh/m^3 vs. 12 MWh/m^3) que sur une base gravimétrique (> 8,5 kWh/kg vs. 2 kWh/kg). Les avantages de ReMeF par rapport à d'autres options de stockage à long terme Power-to-X sont les suivants:

- une densité énergétique très élevée, en particulier par volume
- facilité de transport
- non toxique et non explosif
- coût relativement faible
- pas besoin de récipients de stockage cryogéniques ou pressurisés
- pas de carbone impliqué qui doit être (re)capturé à un moment ou à un autre pour être neutre sur le plan climatique

Possibilité de couvrir les pics de demande en hiver

Différents scénarios du système énergétique suisse en 2050 ont été simulés, à partir des perspectives énergétiques 2050+. Au lieu de produire de l'hydrogène avec des électro-lyseurs en été et d'utiliser des piles à combustible en hiver pour le convertir à nouveau en électricité, le potentiel de production de ReMeF avec l'électricité excédentaire de l'été a été évalué. Par la suite, nous avons considéré la possibilité d'utiliser ReMeF dans des immeubles collectifs pour produire de la chaleur et de l'électricité en hiver, tout en couvrant

une grande partie des besoins en chaleur et en électricité des bâtiments et en fournissant de l'électricité supplémentaire au réseau, ce qui contribue à réduire une éventuelle pénurie hivernale.

Les résultats montrent, pour un système énergétique suisse à forte pénétration de photovoltaïque (45 TWh_{el}/a), un déficit hivernal résiduel d'électricité de 8 à 9 TWh_{el} sans ReMeF. En limitant la capacité des unités de conversion du métal en énergie à 10 kW_{th} installées dans chaque bâtiment multifamilial non raccordé au chauffage urbain, ce déficit hivernal pourrait être réduit à 2-3 TWh_{el}, si les réactions aluminium ou silicium-eau sont utilisées pour la conversion du métal en énergie. En utilisant le fer, dont la part de la production électrique est beaucoup plus élevée que celle de la production thermique, la Suisse serait en mesure d'exporter 2 à 4 kWh_{el} en hiver avec les mêmes hypothèses. Naturellement, tous les bâtiments multifamiliaux ne seront pas équipés de ReMeF. Cependant, il existe un potentiel supplémentaire pour ReMeF dans le chauffage urbain et pour la chaleur et l'électricité industrielles, qui n'est pas encore inclus dans les chiffres présentés ci-dessus.

Réchauffement climatique

En utilisant le procédé Power-to-Metal soit basé sur une production de métal sans carbone (TRL 4-7), l'effet climatique de tous les ReMeF considérés est déterminé par les émissions de gaz à effet de serre de l'électricité utilisée pour le procédé Power-to-Metal. Cette valeur doit être inférieure à 35-50 gCO2-eq./MJ afin de réduire le réchauffement climatique lors du remplacement d'une mini unité de cogénération au gaz naturel. La production d'électricité avec un PRP aussi faible peut être obtenue avec l'énergie hydraulique et éolienne (1-3 gCO2-eq./MJ) ou avec l'énergie photovoltaïque en toiture (10 gCO2-eq./MJ).

L'installation de la cogénération ReMeF dans des immeubles collectifs en Suisse, avec une moyenne de 10 kW_{th} par immeuble, peut réduire le déficit hivernal de l'approvisionnement en énergie. Par rapport à la réalisation du même objectif avec des centrales électriques à turbine à gaz naturel, cela permettrait d'économiser des émissions de gaz à effet de serre de plus de 3 millions de tCO_2 eq par an.

Main findings

- Aluminium, iron, and silicon are considered the most promising candidates as Renewable Metal Fuel.

- In the case of iron, the metal-water reaction is not significantly exothermic and thus most of the stored energy can be transferred to hydrogen produced by this reaction.

- For aluminium and silicon, roughly half of the stored energy is released as heat in the metal-water reaction, which leads to a much lower potential to produce electricity with a hydrogen fuel cell per unit of energy originally stored in the metal, when compared to the iron-water reaction.

- The Power-to-Metal process must be CO_2-emission free, and electricity used for the process must have a carbon burden of less than 35 – 50 gCO2-eq./MJ to reduce global warming compared to fossil gas CHP units that produce heat and electricity.

- Various simulations of the Swiss energy system showcase the potential of Renewable Metal Fuels to substantially reduce the winter electricity deficit in 2050 and to save up to 3 Mio tCO2-eq per year compared to achieving the same reduction with power plants that use natural gas turbines.

Contents

Abbreviation

Al	Aluminium
BFE	Bundesamt für Energie
C	Combined-cycle gas turbine plants
CH	Switzerland
CHP	Combined Heat and Power
DHW	Domestic Hot Water
DRI	Direct Reduction of Iron
E	Renewable (Erneuerbar)
EF	Environmental Footprint
ETH	Eidgenössische Technische Hochschule
Fe	Iron
FED	Final Energy Demand
GH_2	Gaseous Hydrogen
GHG	Greenhouse Gas
GT	Gas Turbine
GWP	Global Warming Potential
HT	High-Temperature
LCA	Life Cycle Assessment
LCI	Life Cycle Inventory
LCIA	Life Cycle Inventory Assessment
LH_2	Liquid Hydrogen
LIB	Lithium-Ion Batteries
LME	London Metal Exchange
LT	Low-Temperature
MFH	Multi Family Homes
MG	Metallurical Grade
NEP	Neue Energiepolitik
PES	Pessimistic
PV	Photovoltaic
ReMeF	Renewable Metal Fuels
SFH	Singe Family Homes
Si	Silicon
SOG	Solar Grade
TRL	Technology Readiness Level
WPD	Winter Peak Demand

1 Introduction

1.1 Purpose of the project

The project PeakMetal focuses on the use of metal redox processes as a means for seasonally storing renewable energy. The project answers questions concerning the suitability of different metal sources and the implications that the source has on the environment as well as the potential for the Swiss energy system. Renewable energy can be stored during periods of excess electricity by producing Renewable Metal Fuel (ReMeF) in a centralized industrial plant. In this case, the ReMeF acts as an energy carrier which can be easily stored without losses over several months. Like wood chips or pellets, the ReMeF will be transported to homeowners or industrial sites to cover the heat demand during winter peaks. Furthermore, when releasing the energy of the ReMeF, not only heat but also electricity is produced (e.g., via hydrogen and fuel cell) which may be used for grid stabilization at peak demand times. Ideally, small, decentralized Combined Heat and Power (CHP) solutions based on ReMeF could eliminate the need for gas- or oil-fired power plants and backup systems in both the medium and long term. The use of renewable metal fuels in the building stock could provide the piece of the puzzle that is still missing in the Swiss energy system to make the electricity and heat supply completely renewable even in winter and make it independent of short-term supplies and dependencies of energy sources from abroad.

1.2 The concept of Renewable Metal Fuels

ReMeF redox storage cycles are based on the CO_2-free reduction of metal oxide (reaction (1) as indicated in Figure 1 on the left:

$$M_xO_y \rightarrow x\,M + \frac{y}{2}\,O_2 \qquad (1)$$

This, so called Power-to-Metal process (endothermic reaction) requires energy. Since most of the energy invested in this process is not lost but stored in the metal and can be released later by oxidation of the metal, this is a process of energy storage.

The concept utilizes renewable energy and stores it in the ReMeF during periods of abundant and low-cost availability of renewable electricity by producing ReMeF in a centralized industrial facility (Power-to-Metal, charging process). The only significant direct emission from the CO_2-free metal reduction process is oxygen. ReMeF serve as a durable energy carrier that is safe to store and easy to transport.

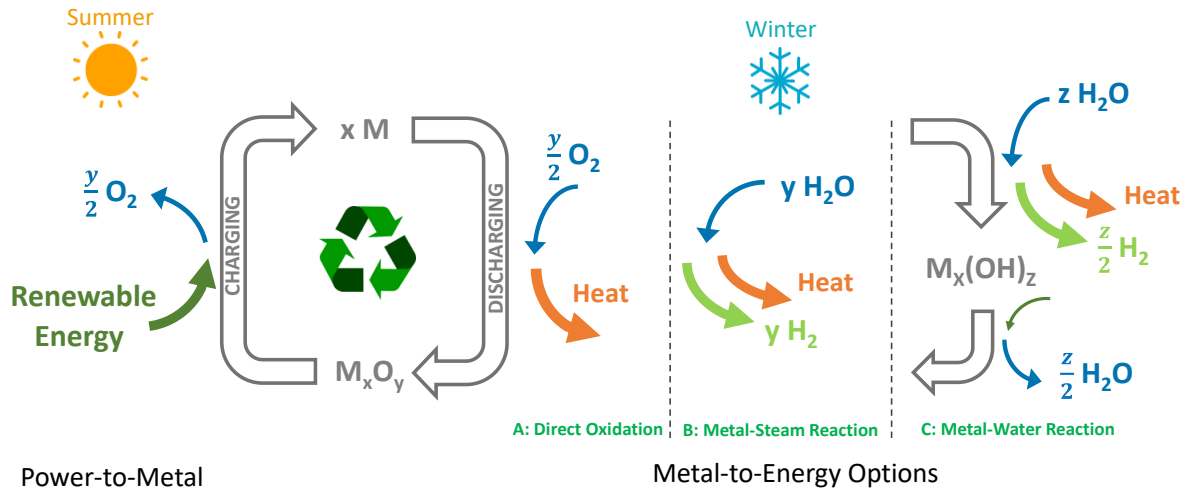

Figure 1: Illustration of the ReMeF redox storage cycle including the three options for the Metal-to-Energy process: A: Direct Oxidation or metal combustion, B: Metal-Steam reaction at high-temperature, C: Metal-Water reaction at low-temperature.

To cover winter peak demand locally, the renewable energy stored in the metal can be made available via the following Metal-to-Energy options: A: Direct oxidation as described in reaction (2) producing heat at very high combustion temperatures, B: Metal-steam process shown in reaction (3), and C: Metal-Water reactions (4 and (5) producing hydrogen and heat.

$$x\,M + \frac{y}{2}O_2 \rightarrow M_xO_y \quad (2)$$

$$x\,M + y\,H_2O \rightarrow M_xO_y \quad (3)$$

$$x\,M + z\,H_2O \rightarrow M_x(OH)_z + \frac{z}{2}\,H_2 \quad (4)$$

$$M_x(OH)_z \rightarrow M_xO_z + \frac{z}{2}\,H_2O \quad (5)$$

Hydrogen obtained from reactions (4 and (5 can be converted immediately to electricity and heat in a fuel cell system. In all cases, metal oxide or hydroxide is formed, which can be separated and fed back into the Power-to-Metal process, creating a closed-loop material cycle.

Decentralized ReMeF-based CHP solutions could replace gas- or oil-fired power plants or CHP units, contributing to long-term CO_2 reduction goals. For cold-season peaks of heat demand, ReMeF in buildings could complete the decarbonization puzzle, achieving 100% renewable electricity and heat supply, and reducing dependencies on foreign energy sources.

1.3 Objectives

The objective of the project is to investigate the contribution that ReMeF can make as CHP elements of the building stock a) to cover the local demand for electricity and heat and b) to feed electricity into the grid to support the energy system. In focus are metals as winter-energy suppliers with high availability, low cost, and favourable chemical properties to potentially reduce greenhouse gas emissions when compared to alternative import options like fossil-based systems.

Goals:

1. What role could ReMeF play in covering winter peaks (heat & electricity) in the Swiss building stock for the security of supply?
2. Can ReMeF eliminate the need for gas-fired power plants?

Detailed research questions to be answered:

3. Which metals can be considered as winter energy suppliers?
4. How efficient are ReMeF cycles (power-to-metal and metal-to-energy)?
5. What is the state of the art?
6. What is the potential for ReMeF in CH and can winter imports of energy be reduced?
7. How much CO_2 savings can potentially be achieved?

2 Procedures and methodology

The project objectives were comprehensively analysed by applying the following key evaluations (Figure 2):

- Analysis of ReMeF storage cycles using a key criteria evaluation to identify the most interesting ReMeF candidates, followed by a technology assessment of the ReMeF charging process (Power-to-Metal) and the discharging process (Metal-to-Energy).
- Environmental assessment applying a cradle-to-grave life cycle assessment of the identified ReMeF storage cycles, taking into account the production of renewable pathways currently under development.
- Simulations of the Swiss energy system in terms of heat demand and electricity balance for different electricity generation scenarios in 2050. These simulations assess the potential to cover winter heat demand and reduce winter electricity deficits by decentralized Metal-to-Energy plants in buildings, where the ReMeF is produced from surplus summer electricity at local central industrial plants in Switzerland.

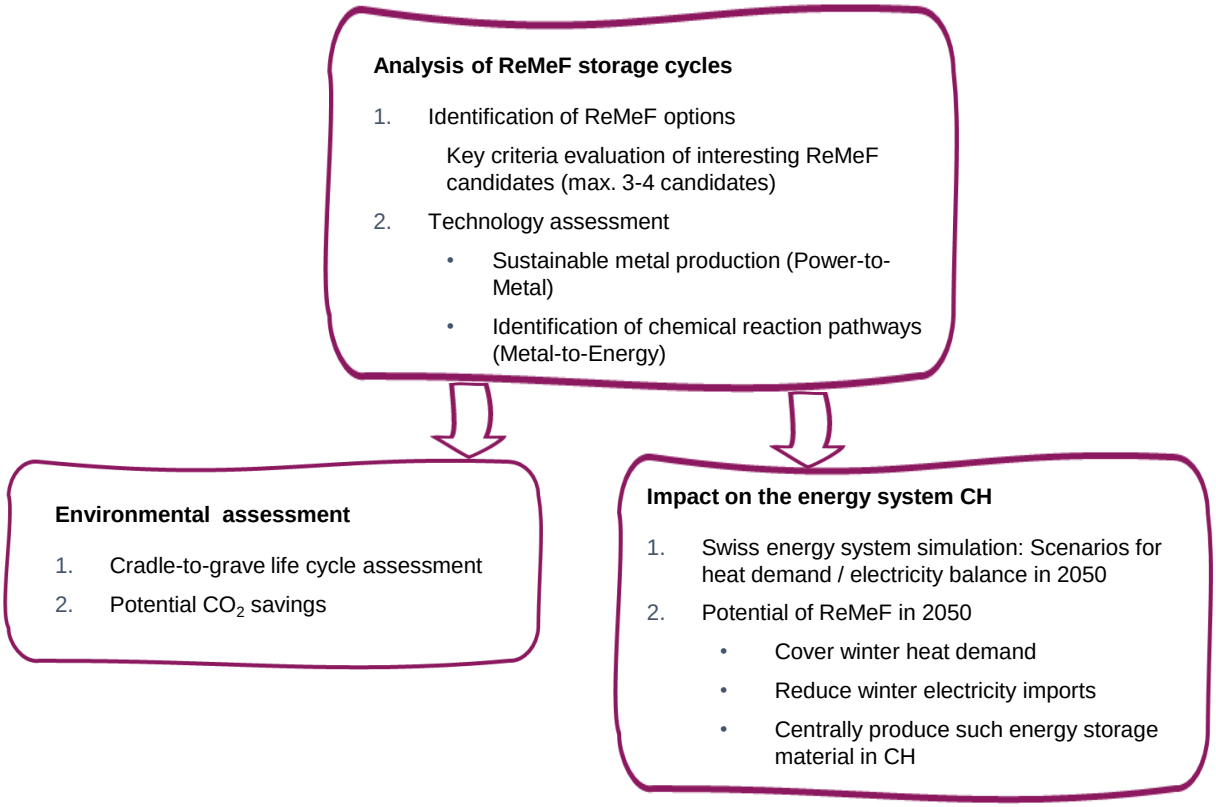

Figure 2: Overview of key evaluation procedure to analyse the project objectives.

The following chapters describe in more detail the methodology.

2.1 Analysis of ReMeF storage cycles

Based on the periodic table of the elements and prior work by Bergthorson et al. (2018) [1], various metals are analysed for their usability as ReMeF to generate heat and electricity in buildings.

2.1.1 Identification of ReMeF options

Based on the following criteria, the most favourable candidates are evaluated and selected:

- High availability of the metal
- Low cost of the raw material
- High achievable energy storage density
- Safety in handling (not explosive or too reactive)
- High potential for closing the material cycle
- Good reactivity during activation (power density)
- Simple and, if possible, loss-free storage

The environmental impact of metal production is a key selection criterion. However, the production technology and future decarbonization efforts of the industry should be taken into account to assess the individual environmental footprint which is part of the objectives of the project and is analysed in detail in Chapter 3.5.

In the first step, the following key criteria are used to identify and pre-select the most promising ReMeF candidates. Each criterion is weighted by a weighting factor that was discussed and verified by the advisory board (Table 1).

Table 1: Criteria for the identifying the most interesting ReMeF candidates, including weighting factor.

Identification criteria for ReMeF	Weighting factors
Energy density	0.2
Market price and its development	0.3
Abundancy	0.1
World reserves	0.2
Potential production increase for ReMeF compared to today's world market	0.2

It should be noted that the abundance and world reserves are both linked to the availability of the metal. In general, the concept of metal resources (abundancy) and reserves primarily

focus on the geological and economic aspects of metal deposits. The abundance refers to the amount of an element that exists in the Earth's crust, oceans, atmosphere, and other accessible natural sources (a natural occurrence). It is typically measured as a percentage or parts per million (ppm) by weight. In this analysis, only the abundance in the Earth's crust was evaluated. World reserves, on the other hand, refer to the estimated amount of an element that can be economically extracted from known sources, so reserves data are dynamic. This includes both identified reserves (deposits that have been found and can be exploited with current technology) and undiscovered reserves (deposits that are likely to exist but have not yet been discovered). The estimation of reserves depends on factors such as the cost of extraction, market demand, and technological advances. While a certain element may be abundant, it may not have large world reserves if it is difficult or expensive to extract, in contrast, an element may have a small abundance but large world reserves if it is highly valued and economically viable to extract.

Data on world reserves are retrieved from the Mineral Commodity Summary 2023 from the U.S. Geological Survey, which notes that obtaining national information on mineral reserves, focusing on the United States, Australia, Canada, and Russia, is challenging due to the lack of consistent criteria across different regions [2]. Therefore, these reserves data include historical data, reduction by historical production, and company, and government-reported reserves. It should be noted that material which will be recycled from current in-use stocks made available by recycling technology is not included. In addition, deep-sea reserves are not included in this data so far. In general, the assessment of world reserves is an ongoing process that varies by mineral commodity, country, and time period.

2.1.2 Deep sea mining of metal resources

Deep-sea mining is of controversial discussion and debate due to concerns about the potential environmental, ecological, and social impacts of extracting mineral resources from the deep seabed. Major resources found on the seabed are copper, silver, gold, zinc, manganese, cobalt, rare earth elements, tin and gas hydrates [3]. It is estimated that world reserve data from the U.S. Geological Survey of these specific metals represent only a very small proportion of on-land deposits, as the Clarion-Clipperton Zone (a vast plain in the Pacific Ocean between Hawaii and Mexico), which covers roughly 1.3% of the world's ocean floor, contains more nickel, cobalt and manganese by comparison [4]. As will be seen in chapter 3.1, out of the six elements considered for ReMeF, only two are possible candidates for deep sea mining: manganese and zinc.

The three most promising candidates for ReMeF – as will be seen in 3.1.5 – are extremely abundant in the earth's crust on land and therefore by no means candidates for deep sea mining.

2.1.3 Technology assessment

The technology assessment of the most interesting ReMeF candidates, as identified by the key criteria evaluation, involves a systematic and thorough review of current conventional production pathways and technology development to produce clean and sustainable metals in the future. In general, metal producers have strong incentives to move towards cleaner and more sustainable production pathways, driven by regulatory compliance, market demands, cost reduction, innovation, and changing stakeholder expectations.

Sustainability is therefore not only a regulatory requirement but also a strategic imperative for the long-term competitiveness and resilience of metal producers.

ReMeF energy storage cycles, a relatively new field of research, involve storing renewable energy during summer to produce a clean energy carrier. Evaluating sustainable methods of metal production will be the basis for further analysis (Chapter 3.2). In addition, a comprehensive analysis of possible chemical reaction pathways for the Metal-to-Energy process will be identified (Chapter 3.3).

The following key aspects of the ReMeF storage cycles are evaluated for both, the evaluated Power-to-Metal charging process and Metal-to-Energy discharging process:

- Energy and mass balance (Chapter 3.4)
- Process efficiency assessment (Chapter 3.4.4)

2.2 Environmental Assessment

2.2.1 Life Cycle Assessment

The environmental impact of the selected ReMeF is evaluated using the standardized procedure (ISO 104040 and ISO 104044 [5]) of a LCA which determines the environmental impact associated with the concept from resource extraction to end-of-life burdens. For this "cradle-to-grave" LCA, immediate physical flows are evaluated to depict the potential environmental impact by applying an avoided burden approach because the ReMeF concept is based on a closed-loop recycling procedure. It should be noticed that the choice of the LCA approach significantly shapes the environmental outcome of the ReMeF redox cycles. To support this decision, Dubreuil et al. emphasize that within the metal industry, there is a strong preference for the end-of-life recycling (avoided burden) approach compared to the recycled content approach (cut-off method) when it comes to environmental modelling, decision-making, and policy discussions related to metal recycling [6].

In general, this LCA includes a goal and scope definition (Chapter 3.5.1), a Life Cycle Inventory (LCI) collection (Chapter 3.5.2), a Life Cycle Impact Assessment (LCIA, Chapter 3.5.3), and an evaluation of the results (Chapter 4.2).

The functional unit has been defined to represent 1 MJ of energy produced. It is important to note that this functional unit includes a specific amount of heat and electricity (including the fuel cell system) depending on the choice of the ReMeF.

Additionally, the overall LCA results are compared with other options for covering winter peaks, such as gas-fired power plants or electricity imports. Conclusions are derived from this. The analysis uses SimaPro 9.5.0.1 and the Ecoinvent database version 3.9.

For this study, life cycle GHG emissions and their associated impacts on climate change are used as main indicators for the environmental performance of the ReMeF cycles. All Greenhouse Gas (GHG) emissions are assessed by the IPCC 2021 GWP 100a V1.03 method. Additionally, the Environmental Footprint (EF) V3.1 is used as a midpoint impact category assessment. The EF Initiative of the European Commission has developed and endorsed the EF method for evaluating the environmental impacts of products and organizations. Consequently, it is already designed for prospective utilization in consumer information [7].

2.2.2 Potential CO_2-savings from ReMeF storage cycles

The potential CO_2-savings from ReMeF storage cycles were assessed based on the ReMeF production scenarios for 2050 according to winter electricity deficit scenarios: PES and HighPV+,30°, as described in Chapter 2.3.2. The potential CO_2-savings from ReMeF winter peak demand scenarios were calculated in comparison with other options for covering winter peaks, such as electricity imports and gas turbine power plants:

Electricity from gas turbine power plants

Overall, the process of a gas turbine power plant converts the chemical energy of the fuel into mechanical energy, which is then converted into electrical energy. The electricity conversion efficiency of gas turbine power plants can achieve 20 to 35% [8]. In this case, utilization of produced heat is not implemented. In the case of Switzerland, reserve gas-turbines are planned for covering winter gaps or emergency situations in Birr (AG). The efficiency of the electricity production via these gas turbines is 29% (based on gross heating value) or 32% (based on net heating value) [9].

Winter electricity imports from neighbouring countries

Typical Swiss electricity scenarios assume winter electricity imports which are covered by countries that are members of the ENTSO-E network. The ENTSO-E transparency platform offers hourly data tailored to individual countries, detailing electricity consumption, generation by technology, and cross-border flows among nations [10]. Rüdisüli et al. provide GHG emission data based on Swiss winter electricity imports according to ENTSO-E, which were adapted for this analysis [11].

Comparisons with electricity from gas turbines or winter imports provide valuable insights into possible CO_2 reductions that Switzerland could achieve in the future by introducing ReMeF storage cycles into the energy system.

2.3 Swiss energy system

The year 2050 was chosen as the future energy system to look at. For the different input parameters, the "ZERO Basis" scenario of the Energy Perspectives 2050+ was used as a starting point [12].

The PowerCheck tool developed at the University of Applied Sciences of Eastern Switzerland was used to calculate the potential of ReMeFs by simulating future electricity consumption and production as well as heat consumption in Switzerland. An online version of this tool reflects the status before adaption for inclusion of detailed heat demand modelling: www.powercheck.ch.

2.3.1 Adaption of the PowerCheck tool

The PowerCheck tool that already existed (based on a model of Prof. Gunzinger from ETH and further developed by the Institute for Energy Technology IET at OST [13]) was transferred into a Python code and extended by a more detailed calculation of the heat demand of Switzerland. This included:

- a detailed modelling of space heat demand, depending on building stock, climate zones, refurbishment rates and types of heating systems.
- domestic hot water demand and type of heating system to cover it
- assumptions for the share and energy source of district heating
- industrial heat demand and technologies used to cover these demands

Space Heat Demand

The model for space heat demand was developed by the following procedure:

1. Six typical Swiss climate zones were defined.
2. For each climate zone, typical load profiles (15-minute profiles) were defined for single-family homes (SFH) and multi-family homes (MFH) with different construction periods or "thermal performance reference periods" (4 different periods). Thermal loads are expressed per m^2 of energy reference area.
3. For each climate zone, it is known how many m^2 of SFH and MFH buildings there are, and how many m^2 are heated with which type of heating system (status 2019, Table 2).

To reduce the complexity and number of categories, the following simplifications were made:

a. Double-family homes were included in the category SFH.
b. All “other” types of buildings (service sector, etc.) were included in the category MFH (increase of 25% heated area).

4. On this basis, the space heat demand of the different building categories and consequently for the whole of Switzerland is calculated.
5. To calculate the final energy demand, constant efficiencies were used for all heating systems other than heat-pumps. For heat-pumps, the efficiency was dynamically calculated based on the source and sink temperature.

Table 2: Distribution of the energy reference area among the different building types (left side) and the different heating systems for the year 2050. This table is calculated for SFH and MFH. It is the basis for further calculations of final energy demand.

Totals EBF for SFH in target year in Mio m2								
standard	**DH**	**electro**	**oil**	**gas**	**wood**	**HP**	**other**	**total**
before 1960	15.27	0.00	0.00	6.49	9.90	29.76	1.29	**62.71**
61 - 80	5.01	0.00	0.00	1.53	1.07	18.36	0.54	**26.51**
81-00	4.25	0.00	0.00	2.13	0.90	22.18	0.45	**29.90**
2000+	6.74	0.00	0.00	2.32	0.65	167.47	0.87	**178.06**
passivehouse	0.00	0.00	0.00	0.00	0.00	15.47	0.00	**15.47**
total	**31.27**	**0.00**	**0.00**	**12.47**	**12.52**	**253.24**	**3.15**	**312.65**

Domestic hot water and process heat

In addition to space heat demand, domestic hot water (DHW) and process heat are also calculated, although not in the same detail. Both annual trends are calculated starting from the annual final energy demand [14].

The annual trend for hot water can be represented by a sinusoidal curve over the year with a maximum in February (coldest temperature of water from the mains) and an amplitude of ±15% of the average (15% less than average in winter, 15% more in summer) [15].

For process heat, the annual demand is evenly distributed over the hours of the year.

2.3.2 Energy Scenarios 2050

Four different energy scenarios have been analysed. Starting from a pessimistic (PES) scenario for the development of renewable energies, a more realistic (HighPV) scenario was added. In addition, two more scenarios were created that are variations of HighPV (HighPV+ and HighPV+,30°). Both have a higher share of winter electricity production, either through alpine PV systems or additionally also due to higher mounting angles for the midland systems. For all generation scenarios, nuclear power and fossil fuel use has been set to zero. The availability of hydrogen has also been set to zero since it competes with the potential to use ReMeF.

The difference between the scenarios only affects electricity generation. Electricity demand, on the other hand, remains the same in all scenarios. A comparison of electricity production of the four scenarios with other scenarios carried out in Switzerland is shown in Figure 3. The same is shown for electricity demand in Figure 4. in the consumption scenarios, the use of electrolysers has been set to zero as these would compete with the potential to produce ReMeF in summer in this study. An overview of all scenarios that are compared can be found in Annex L [16].

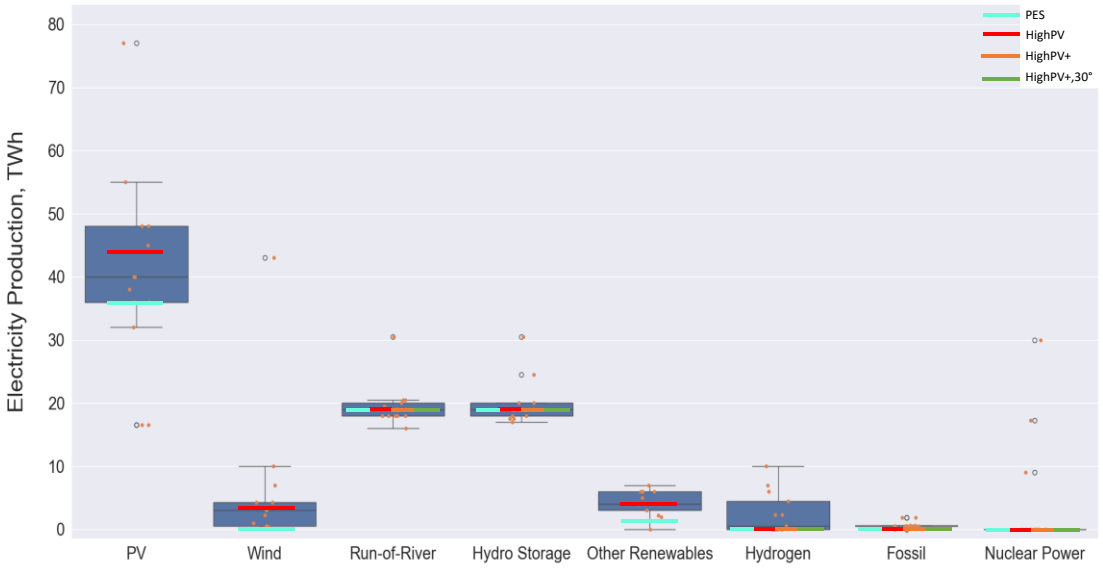

Figure 3: Comparison of different types of electricity production from different scenarios of the Swiss energy system 2050 [16] with the two scenarios of this study.

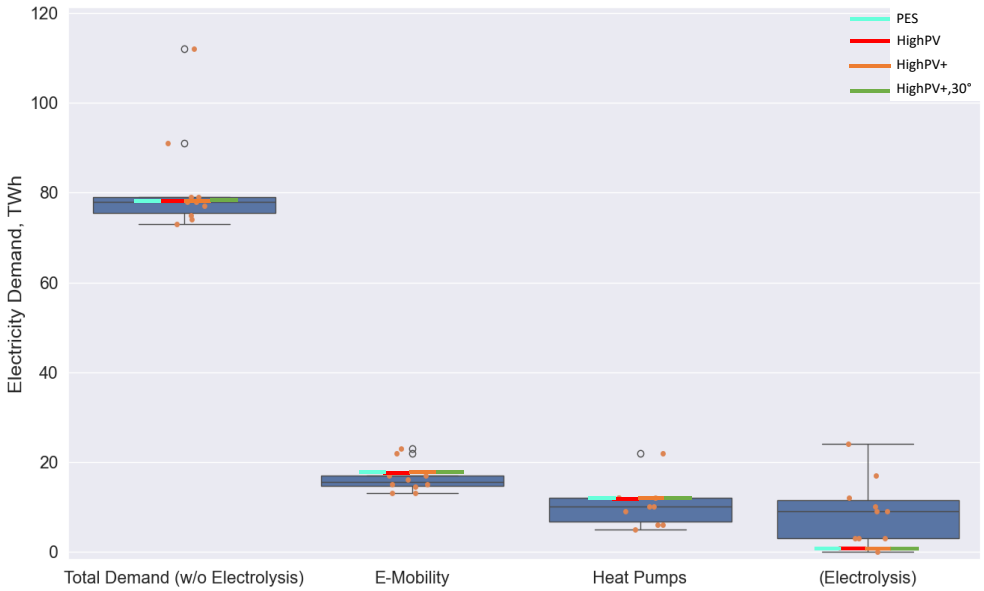

Figure 4: Comparison of different types of electricity demand from different scenarios of the Swiss energy system 2050 [16] with the two scenarios of this study.

Scenario PES

In this scenario, photovoltaic electricity production of 35 TWh (35.5 GW capacity) is assumed. This was adopted from the “ZERO basis” of the Energy Perspectives 2050+. For wind and other renewables (geothermal energy, biogas, MSWI), however, no increase compared to today is used. Figure 5 provides an overview of the share of electricity production by energy source assuming an annual electricity production of 79.9 TWh_e.

This is a more pessimistic assumption than in the Energy Perspectives 2050+, which assumes an expansion of wind and other renewables to around 4 TWh_e each. The assumptions for the ZERO base scenario are adopted for hydropower plants. A complete dismantling by 2050 is assumed for fossil-fuelled power plants and nuclear power plants. There is also no electricity production from hydrogen in this scenario, even if other scenarios assume some production here. The reason for this is that the seasonal storage of ReMeFs is assumed.

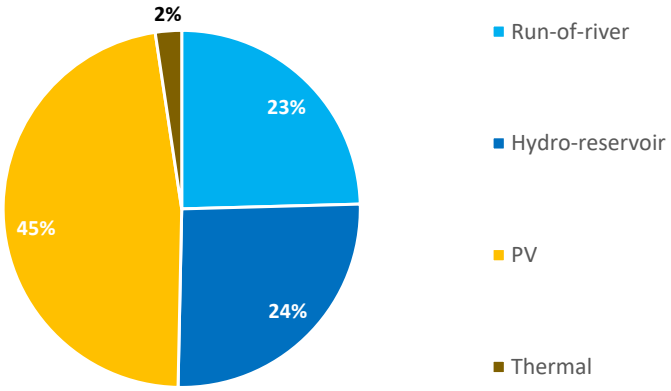

Figure 5: Share of electricity production by energy source for the PES scenario based on assumptions in Annex E.4.

Scenario HighPV

This scenario is more optimistic. In particular, the expansion of photovoltaics is higher here at 50 GW (45 TWh_e annual production). Wind production and the other renewables are also higher here than in the PES scenario and the same as in the ZERO basis scenario. Hydropower, hydrogen, fossil-fuelled power plants and nuclear power plants are the same as in the PES scenario. Figure 6 shows the share of electricity production by energy source assuming an annual electricity production of 95.8 TWh_e.

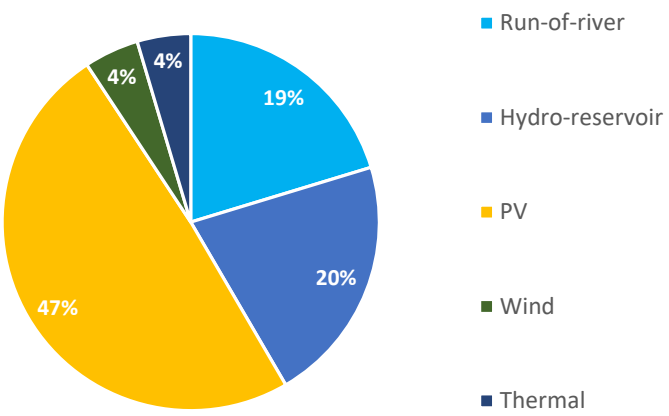

Figure 6: Share of electricity production by energy source for the HighPV scenario based on assumptions in Annex E.4.

Scenario HighPV+

The only difference between this scenario and HighPV is the inclusion of Alpine PV systems. The installed PV capacity is the same, but it was assumed that part of it was installed in the Alps instead of the flatlands. This was based on the Solarexpress, which is based on an annual production of 2 TWh by high alpine PV systems with a high winter share. These 2 TWh were not added to the total PV production of HighPV but used to replace the same amount of rooftop systems.

Scenario HighPV+,30°

In this scenario, it was assumed that an increase in the winter share would be more incentivised. The average elevation angle was increased from 15° to 30° for all rooftop systems, whereas the alpine systems of HighPV+ are maintained.

2.3.3 Balance comparison to other scenarios

Even though we based our simulation of the year 2050 on the ZERO Basis scenario, there are some differences which result in a higher summer surplus and winter deficit (both 9 TWh in ZERO Basis) (Figure 7). Possible reasons for this are listed below:

1. Photovoltaic Production:
    - ZERO Basis assumes a curtailment of renewable energies of 3 TWh which is not included in our simulation.

- ZERO Basis assumes a PV winter production share of 31% which is to be achieved through various measures. Scenarios PES and HighPV have a winter share of 27%, HighPV+ 28% and HighPV+,30° has a winter share of 30%.

2. Additional electricity consumption:
   - ZERO Basis assumes an electricity consumption of 1.7 TWh for carbon capture and storage. This is assumed to happen in waste incineration plants and cement production. This is not included in our simulation.
   - ZERO Basis assumes an additional electricity consumption of 3 TWh for electrolysis in summer which is also not included in our simulation.

3. Pumped hydro:
   - ZERO Basis assumes the construction of an additional 2.8 GW of turbine capacity through more pumped hydro power plants. This is also not included in our simulation as most of the plans for new pumped hydro have been cancelled and it is therefore assumed that no more pumped hydro plants will be built in the near future.

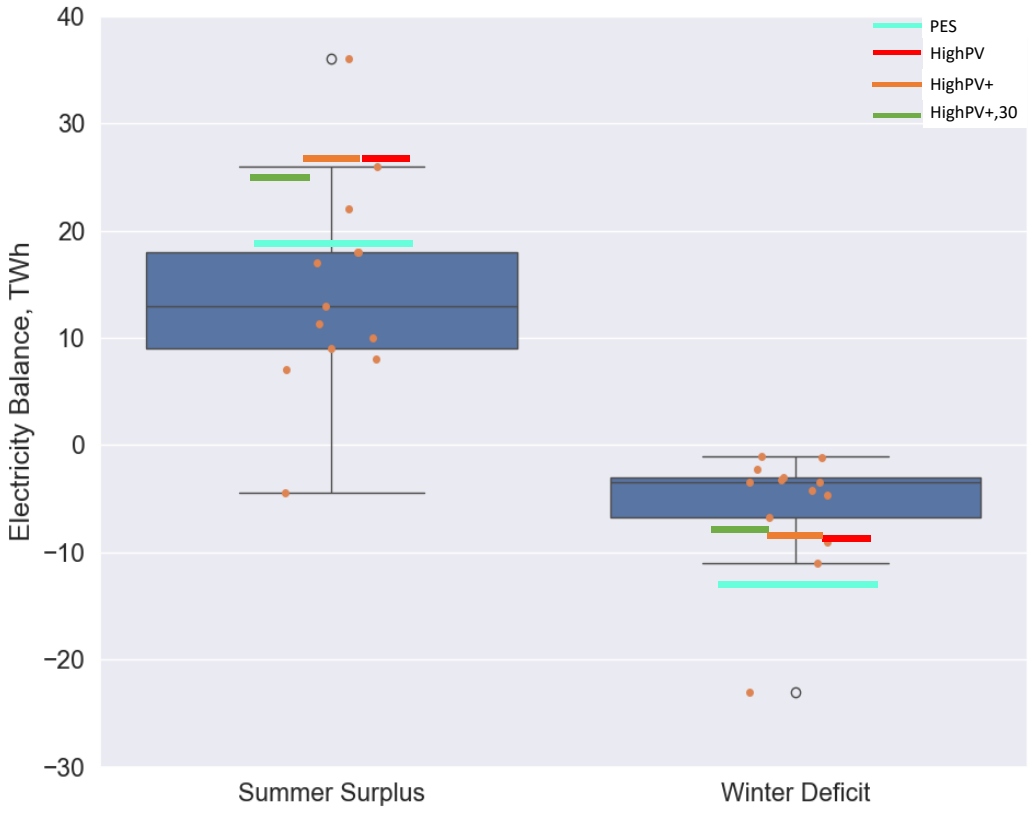

Figure 7: Comparison of summer surplus and winter deficit from different scenarios of the Swiss energy system 2050 [16] with the four scenarios of this study.

A detailed overview of the results of our simulation and the results of ZERO Basis is shown in Annex E.4.

2.4 Potential of ReMeF

The potential for ReMeF to cover heat and electricity at peak demand times in winter was based on the following assumptions for the year 2050:

Metal-to-Energy in winter

- Metal-to-Energy, i.e., the production of heat and electricity from metals, will be installed in multifamily buildings only. This is a simplification as these units could also be installed in single family homes or for district heating. However, it is expected that the total system comprising heat pump and Metal-to-Energy as well as thermal and electric (battery) storage, will be more economic for multifamily than for single family homes, as single family homes are smaller and have too little energy turnover to justify the installation of a more complex system. For district heating it is assumed that the operators of district heating plants pay much lower prices for energy carriers compared to building owners and have less economic advantage for producing their own electricity as they cannot realize self-consumption to the same extent.
- Only heat demand (space heat and DHW) covered by heat pumps was considered to be replaced by heat from ReMeF, as the heating structure of buildings in 2050 (in the scenario ZERO Basis of the “Energieperspektiven 2050+ [12]) is assumed to be 68% heat pumps, 23% district heating and 9% gas (biogas) and wood (Figure 8). Biogas and wood are already a “stored” form of energy and thus replacing them would not contribute to resilience or to reduction of the winter gap.
- It was assumed that either 50% or all (100%) of heat pump heated multifamily buildings are equipped with ReMeF. The total capacity (thermal and electric power) of these systems was determined based on the total load profile of these two cases, distinguishing a high capacity case and a low capacity case.

Power-to-Metal in summer

- There will be an excess of electricity in summer, mainly due to large penetration of photovoltaics and low heat demand in this season. This excess PV electricity can be used to produce ReMeF, since it would otherwise be exported at low price (as others will produce large amounts of PV energy in summer too) or curtailed.
- Part of this excess electricity is used to produce metals from their metal oxides or from their hydroxides in large central Power-to-Metal plants in industrial areas. The production capacity of these plants will be limited. For economic reasons, the more full-load hours these plants can be operated the better.

- Full-load hours multiplied with production capacity of the Power-to-Metal plant determines the amount that can be produced.

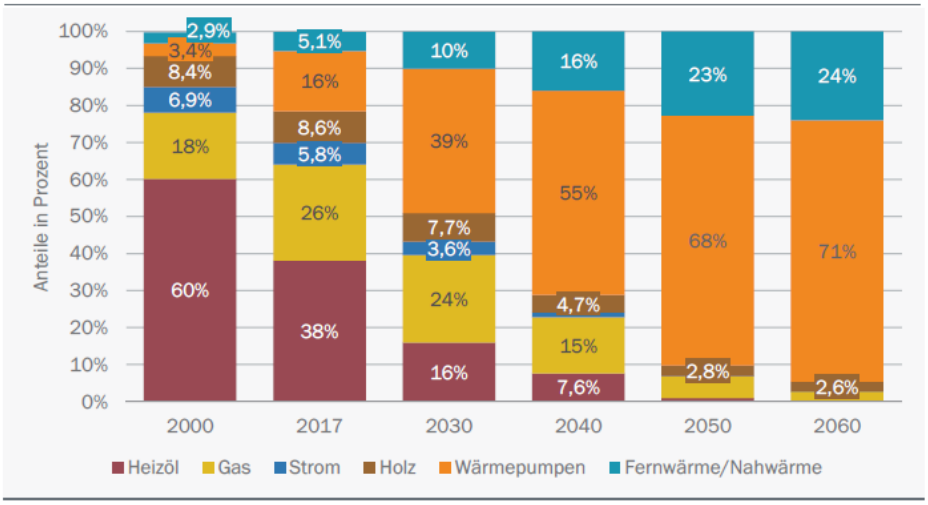

Figure 8: Heating structure of buildings in Switzerland in the scenario ZERO Basis [12].

3 Results and discussions

3.1 Potential ReMeF candidates

Recyclable metal fuels as energy carriers and the direct combustion of metal powders have been investigated by Bergthorson et al. (2015) [17]. The research group of Bergthorson screened the periodic table to identify interesting ReMeF candidates for their application (Figure 9). Metals and their oxides that are toxic or too expensive are excluded. Based on this evaluation, the remaining interesting candidates are lithium (Li), sodium (Na), potassium (K), magnesium (Ma), calcium (Ca), titanium (Ti), iron (Fe), zinc (Zn), aluminium (Al), silicon (Si), and boron (B).

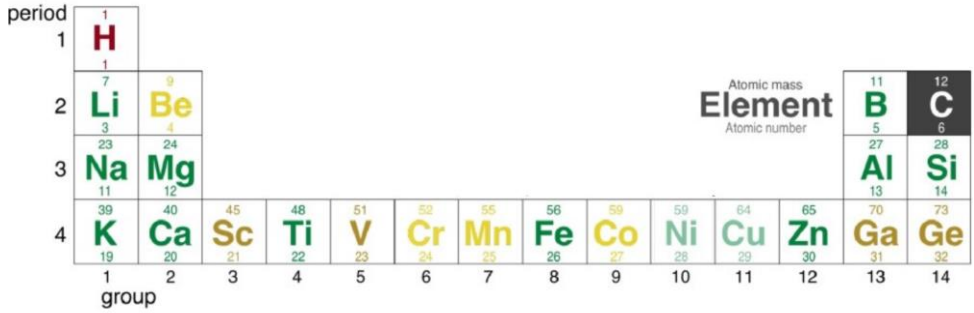

Figure 9: Subset of the periodic table illustrating potential metals for use as a ReMeF from Bergthorson et al. (2018) identifying metals that are too expensive for use as fuels (gold), and toxic metals or metal oxides (yellow). Interesting ReMeF candidates are shown in green [1].

In the last years, however, the price of lithium increased substantially from around 10'000 USD/tonne up to 80'000 USD/tonne due to the demand increase for electric vehicle batteries. Alongside this, the cost of nickel and cobalt increased substantially as well. Therefore, lithium (abundancy 0.002%, Figure 12) is excluded as a potential ReMeF candidate. Boron (abundancy 0.001%) is very attractive from an energy density point of view with the highest volumetric energy density of 38.2 MWh/m^3 compared to the other interesting candidates in Figure 9. It is mainly used in the glass and ceramics industry (approx. 50%), followed by agriculture (an essential nutrient for plants) and nuclear industries (neutron absorber). Boron is also an interesting candidate for the use in other renewable energy technologies (magnets for wind turbines and electric motors). Therefore, the demand keeps growing. Boron is produced only in Turkey and in the Mojave Desert in California and there are no known new large-scale mining projects. Projections show that boron demand will exceed its supply by 2024 and is in need of additional capacity already [18]. For this reason, boron is not suitable as a ReMeF candidate today. Sodium, potassium, and calcium are too reactive, and titanium and copper (abundancy 0.006%) are not reactive enough when in contact with water and are more expensive when compared to the other promising candidates [19].

For these reasons, **aluminium, iron, magnesium, manganese, silicon, and zinc** were shortlisted to be promising ReMeF candidates and are considered further in the criteria evaluation.

3.1.1 Energy density

By providing heat and electricity only in winter, ReMeFs act as seasonal energy storage solutions with the potential of several months of storage duration. In this case, high energy storage density and low capital cost for the storage medium and the installation of conversion facilities are of particular importance. The proposed ReMeF energy carrier must provide energy for several weeks or even up to several months. This means large amounts of energy are required which correlates with a large storage volume. Therefore, storage media achieving high volumetric energy storage density are most favourable, because this ultimately reduces the required storage volume and cost of containers, vessels or space needed.

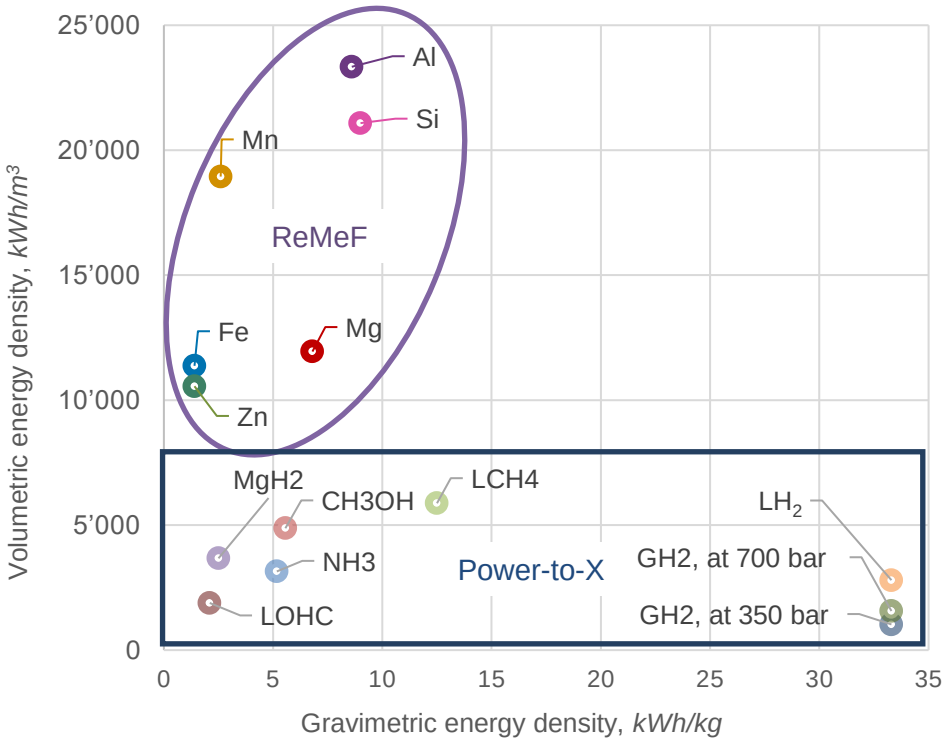

Figure 10: Gravimetric and volumetric storage density of long-term storage materials from [20], [21], [22], [23]. It has to be noted that this is without a container or equipment for charging or discharging. E.g., compressed hydrogen storage systems achieve typically less than 10% hydrogen weight per system weight and therefore, from a system perspective, not more than 3.5 kWh/kg.

Figure 10 illustrates the volumetric and gravimetric energy density of the selected ReMeF candidates and Power-to-X storage materials. Aluminium and silicon achieve the highest volumetric storage density; zinc and iron the lowest among the ReMeF candidates. Overall, gaseous hydrogen (GH_2) has the lowest volumetric storage density. It should be noted that the weight and size of the storage vessel are not included in the Power-to-X technologies. If the weight of the storage tank and "system" is considered, the gravimetric energy density of compressed hydrogen as a storage medium is reduced by a factor of ten or more. Based on the linear scoring function shown in Annex A.1, the individual metals achieved the following points and rank, respectively (Table 3):

Table 3: Overview of the points achieved for the energy density criterion:

	Points	Ranking
Aluminium	10	1
Silicon	9	2
Manganese	8	3
Magnesium	5	4
Iron	4	5
Zinc	4	5

3.1.2 Market price development

In general, market price trends are subject to various factors that can impact supply and demand, such as economic conditions, geopolitical events, and changes in technology and industry trends.

From 2018 until spring 2020, selected metal prices shown in Figure 11 declined steadily. But afterwards and until spring 2022, metal prices were on the rise. Magnesium and manganese reached very high price peaks of up to 7'000 USD a tonne. At the highest point, their value has increased four to even six times. China is the largest producer of magnesium with around 85% of the global production and this market behaviour has been attributed to a reduction of production in China due to high energy prices [24], [25]. From September to October 2021, Chinese producers have returned to a near 100% of their capacity for magnesium production and prices have fallen and stabilized under 3'000 USD per tonne.

Additional market surges were caused due to the Russia-Ukraine war and a temporary ban on exporting goods including metals. Additionally, energy prices in Europe skyrocketed. On the 2nd of March in 2022, the price of aluminium reached its peak of approx. 3'600 USD a tonne on the London Metal Exchange (LME) because smelters in Europe lowered their production lines due to high electricity prices and the aluminium supply has fallen to critical levels [26]. Since then, prices of most metals considered in this project have steadily fallen and stabilized. In general, market prices increased from approx. 1'500 to 2'500 USD per

tonne in 2018 to 2’000 and up to 3’500 USD per tonne in early 2023 where iron is the least expensive and silicon the most expensive of the selected metals.

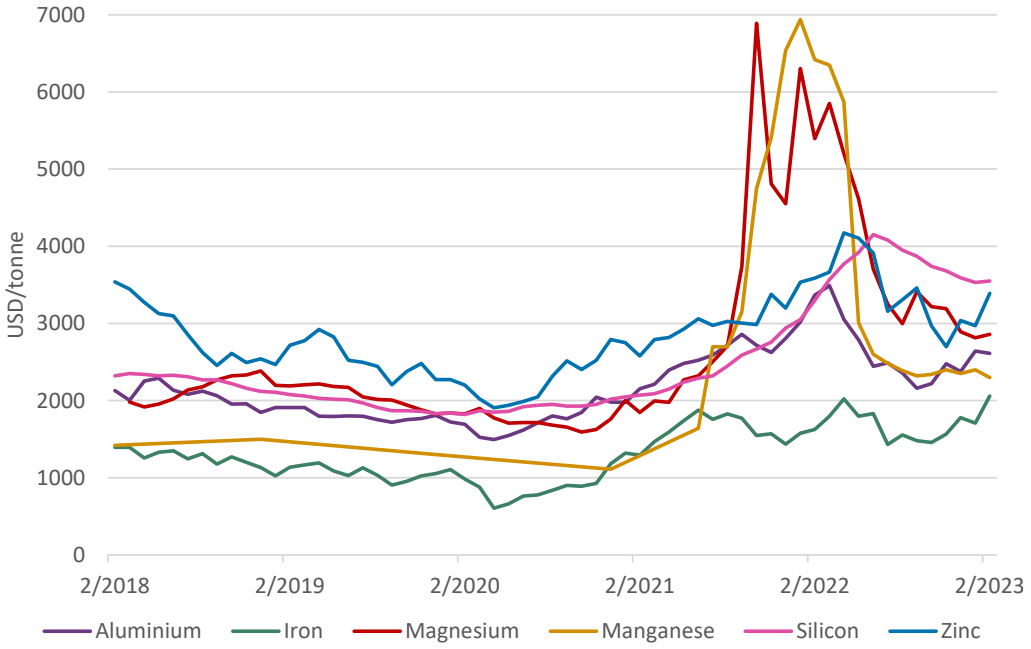

Figure 11: Historical metal prices (February 2018 to February 2023 [27], [28], [29], [30], [31], [32].

Based on the linear scoring function shown in Annex A.2, the individual metals achieved the following points (Table 4):

Table 4: Overview of the points achieved for the market price criterion:

	Points	Ranking
Iron	7	**1**
Aluminium	6	2
Magnesium	6	2
Manganese	6	2
Silicon	5	3
Zinc	4	4

On a side note, the market price of titanium in March 2023 is around 8’500 USD per tonne and the price of lithium skyrocketed from 5’600 USD per tonne in November 2020 to around 86’500 USD per tonne in November 2022. In March 2023, the market price of lithium has fallen again to around 50’000 USD per tonne.

3.1.3 Abundance and availability

Silicon is the second most abundant element in the earth's crust, followed by aluminium and iron, whereas manganese (0.095%) and zinc (0.007%) are the least abundant of the selected metals (Figure 12). The world's reserves, on the other hand, represent only a fraction of the level of abundance.

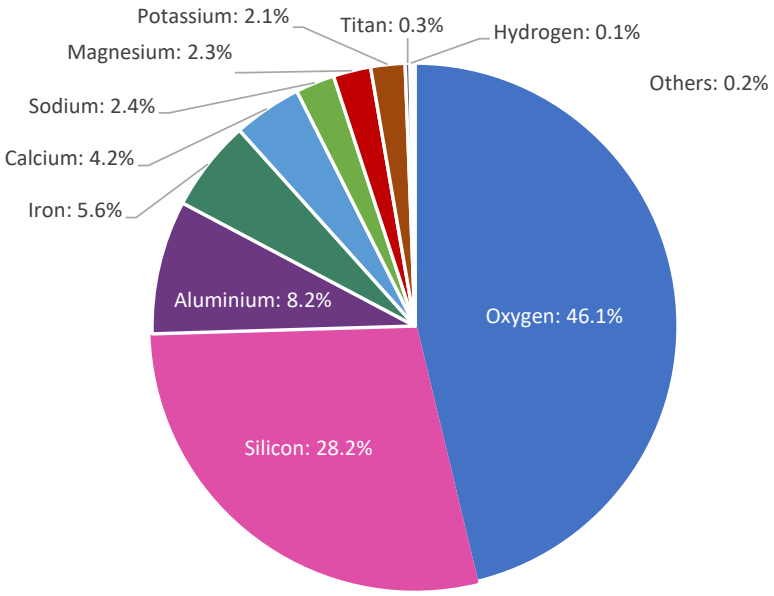

Figure 12: Distribution of the most common elements in the earth's crust. The abundance of manganese (0.095%) and zinc (0.007%) are included in others [33].

Based on the exponential scoring function shown in Annex A.3, the individual metals achieved the following points (Table 5):

Table 5: Overview of the points achieved for the abundance criterion:

	Points	Ranking
Silicon	10	1
Aluminium	9	2
Iron	8	3
Magnesium	7	4
Manganese	3	4
Zinc	2	6

Bauxite is the primary raw material used in the production of aluminium and approx. 4 kg of bauxite is needed to produce 1 kg of aluminium. Today, world reserves of bauxite are estimated at 29’700 Mio. tonne leading to around 7’400 Mio. tonne of aluminium. But bauxite resources are way higher (between 55 billion and 75 billion tonne). It should be noted that reported bauxite reserves can change over time, as more economically interesting deposits are discovered and mining technologies advance. Nevertheless, there are sufficient reserves to supply future demand. As of today, the aluminium industry would be able to more than double the amount of aluminium which was produced since industrialization (total global production in Figure 13.

Worldwide, the largest reserve of iron is in Australia (27’000 Mio. tonne), followed by Brazil (12’000 Mio. tonne), and Russia (14’000 Mio. tonne) [2]. The total iron content is estimated to be some 85 billion tonne. Meaning that the global quantity in circulation today (or rather the accumulated global production since 1943) could be doubled again.

Magnesium metal can be derived from seawater, natural brines, dolomite, serpentine, and other minerals. World reserves of magnesite are estimated at 2’400 Mio. tonne. But in general, reserves for this metal are sufficient to supply future requirements.

Manganese ore world reserves on land are estimated to reach 1’700 Mio. tonne (with an average of 40% manganese content). By far the largest reserves are found in South Africa. Demand for high-purity manganese is expected to increase 27-fold by 2035 due to the increase of electric batteries in vehicles. This number is based on a statement by GIYANI, the global supplier of high-purity manganese in China (90% of the global production) [34].

The source of silicon is silica in various natural forms, such as quartzite. Quantitative estimates of silicon reserves are not available. The reserves in most major producing countries are ample in relation to their demand.

The known world reserves of zinc have fluctuated slightly over the last decade and amount to 210 Mio. tonne in 2022 [35]. But about 1.9 billion tonne are identified as world zinc resources on land. According to the U.S. Geological Survey from January 2021, the accumulated global production of zinc amounts to 547 Mio tonne (data from 1990 to 2019) [36].

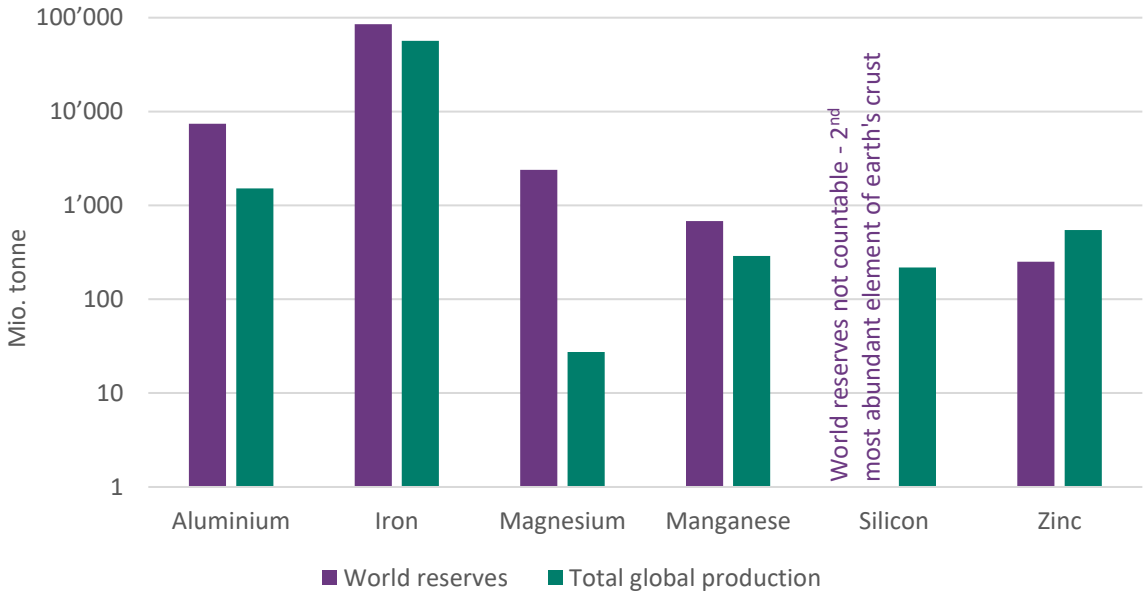

Figure 13: Comparison of world reserves and accumulated total global production since data collection [37]. Please note the logarithmic scale applied on the y-axis.

Based on the exponential scoring function shown in Annex A.4, the following points were achieved (Table 6):

Table 6: Overview of the points achieved for the world reserve criterion:

	Points	Ranking
Silicon	10	**1**
Iron	9	2
Aluminium	7	3
Magnesium	4	4
Manganese	2	5
Zinc	1	6

3.1.4 Production increase for ReMeF

Figure 14 provides an overview of the EU28 and its share of energy carriers and final energy demand (FED) for heating and cooling. Germany, France, UK, Italy, Spain, the Netherlands, and Belgium are the most relevant consumers of non-renewable energy for residential space heating, which can be decarbonized with the ReMeF concept. The population in these countries amounts to 369 million, which is more than 70% of the entire population of the EU plus the UK and Switzerland.

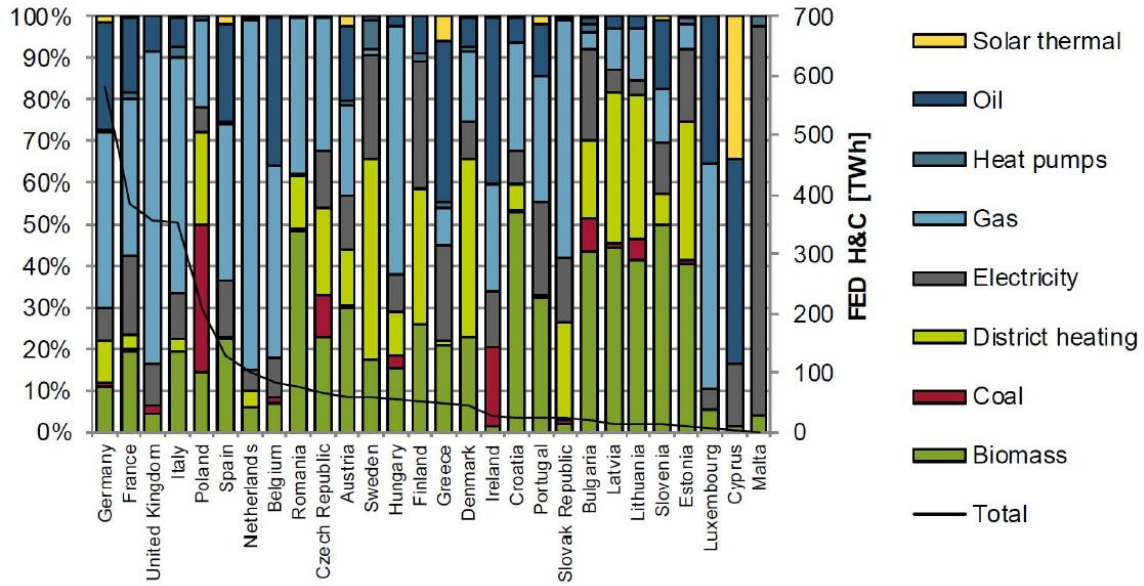

Figure 14: Share of energy carriers (bars, left axis) and final energy demand (FED, black line) for heating and cooling (H&C) in the residential sector of the EU28 in 2015, based on: www.heatroadmap.eu 1.

To estimate the winter energy demand for these counties, it was assumed that 20% of FED for heating and cooling could be assigned to the winter peak demand. Based on this "Heat Roadmap Europe", the target fraction of the non-renewable carriers for the heating and cooling demand (excluding biomass, solar thermal, and district heating) could be obtained. The following equation (6) was applied to receive the share of none renewable winter peak demand (TWh per year):

$$Winter\ peak\ demand_{none-renewable} = FED \cdot 20\% \cdot target\ fraction \qquad (6)$$

Furthermore, it was assumed that half of the target group cover their winter peak demand with the ReMeF application by 2050.

Table 7 gives an overview of the potential yearly winter peak supply from ReMeF systems for the selected EU countries and Switzerland by 2050.

[1] *Profile of heating and cooling demand in 2015, Deliverable 3.1 of the EU H2020 project "Heat Roadmap Europe" (No. 695989), 2017.*

Table 7: Potential winter peak energy (heat and electricity) in 2050 from ReMeF-CHP-systems considering that 20% of the heating and cooling demand for the residential sector is attributed to the winter peak demand and half of the target group is equipped with a ReMeF system by 2050.

Inhabitants, Mio		Final energy demand H&C (FED), TWh/a	Target fraction [a], %	Winter peak demand [a], TWh/a	Winter energy supply from ReMeF in 2050, TWh/a
Germany	83	580	80	93	47
France	67	380	75	57	29
UK	66	350	95	67	34
Italy	60	350	85	60	30
Spain	47	130	75	20	10
Netherland	17	100	90	18	9
Belgium	11	90	95	17	9
Switzerland	9	70	70	10	5
Austria	9	60	50	6	3
Total	**369**	**2110**		**348**	**176**

a) fraction of none-renewables, i.e., neither solar thermal, biomass nor district heating

Based on this winter energy supply from ReMeF in 2050 and the gravimetric energy density of the ReMeF candidate, a total yearly additional production increase over the next 25 years (2025 to 2050) can be estimated (Figure 15 – ReMeF demand per year). If compared to the global production capacity in 2019, this results in a capacity increase of 1.2% for aluminium, 0.3% for iron, 48% for magnesium, 13% for manganese, 9% for silicon, and 36% for zinc.

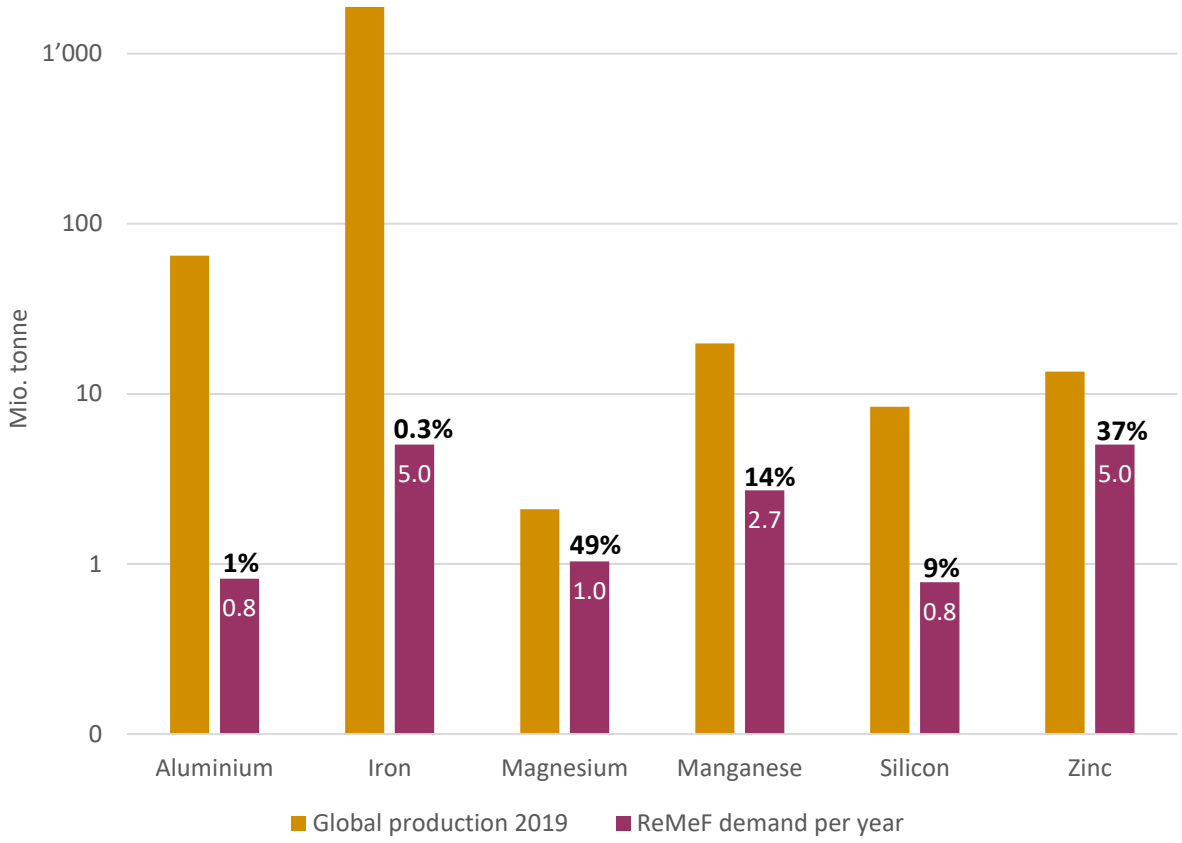

Figure 15: Global production of ReMeF candidates in 2019 in relation to the ReMeF demand per year forecasted until 2050 [37]. Please note the logarithmic scale that is applied to the y-axis.

Based on the exponential scoring function shown in Annex A.5, the following points were achieved (Table 8):

Table 8: Overview of the points achieved for the ReMeF production increase criterion:

	Points	Ranking
Iron	9	1
Aluminium	7	2
Manganese	3	3
Silicon	4	4
Zinc	2	5
Magnesium	1	6

The results of the complete criteria evaluation are shown in Table 9 with the defined weighting factors (see Chapter 2.1.1).

Table 9: Total weighted score and ranking list.

	Total weighted score	Ranking
Aluminium	8	1
Iron	7	2
Silicon	7	2
Magnesium	5	4
Manganese	5	4
Zinc	3	6

Aluminium reaches the highest overall score with 8 points, followed by iron and silicon with 7 points. Magnesium and manganese both achieve 5 points and zinc has the lowest score with 3 points.

3.1.5 Selection of most favourable ReMeF candidates

The criteria evaluation for ReMeF candidates assessed the abundance, world reserves (availability), cost, energy density, and ReMeF demand (an increase of capacity for ReMeF) to be able to identify the most promising ReMeF candidates. Figure 16 illustrates the complete assessment in a spider diagram.

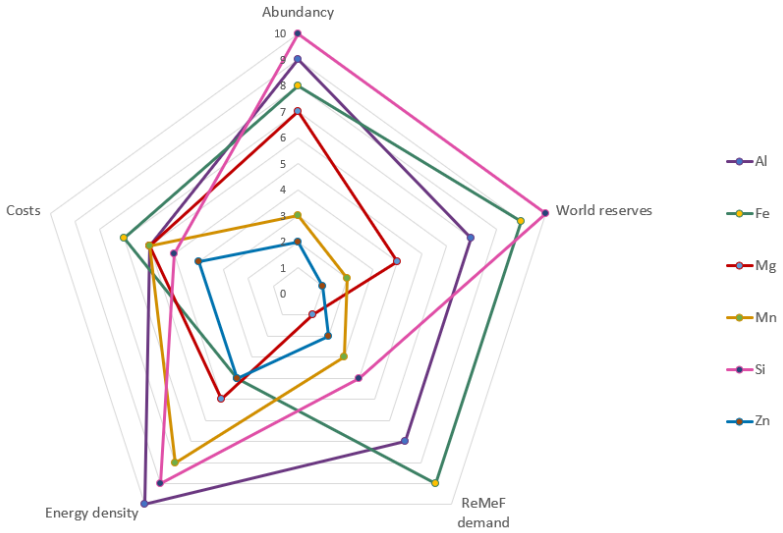

Figure 16: Overview of the individual criteria evaluation.

Overall**, aluminium, iron and silicon** achieved the highest scores and are therefore identified as the most favourable ReMeF candidates. The authors are keen to point out that there are large global reserves of these metals on land, and that their extraction from any seabed is not relevant or under discussion.

3.2 Charging process: Power-to-Metal

This section compares the options for a CO_2-free Power-to-Metal charging process on aluminium, iron and silicon with conventional technology. The entire process chain is analysed in terms of technological development and efficiency.

Conventional metal production, in the case of iron (in the form of iron ore), aluminium (in the form of bauxite) and silicon (in the form of quartzite), relies on carbon feedstocks due to the high reactivity and abundance of carbon. This is because carbon is an excellent low-cost reducing agent, i.e., it can remove oxygen from metal oxides. In this case, carbon reacts with the metal oxides to form carbon dioxide (CO_2) or carbon monoxide (CO). The use of carbon as a reducing agent in metal extraction has a long history and is supported by well-established technologies and infrastructure. It is estimated that steel production accounts for around 4 to 7% of global CO_2 emissions [38]. In the case of aluminium production, more than 80% of the greenhouse gas (GHG) emissions released originate from the use of electricity produced from fossil fuels (Scope 2) [39].

Therefore, Renewable Metal Fuels (ReMeF) must not only be produced exclusively using renewable energy but also by sustainable technologies, preferably without carbon as a reducing agent or with Carbon Capture and Storage (CCS).

3.2.1 Power-to-Aluminium

The traditional technology for producing primary aluminium is the Hall-Héroult process, which reduces alumina (Al_2O_3) in large electrolytic cells using carbon anodes which are consumed, releasing direct CO_2 emissions from the smelter process. However, the next generation of aluminium production lines will use carbon-free electrolysis with non-consumable inert anodes that release only oxygen.

Table 10: Technology comparison of the conventional Hall-Hérold and the inert anode smelter process.

	Hall-Hérold	**Inert anodes**
Cell design	Horizontal	Vertical
Anode material	Graphite (block of petroleum coke)	Non-consumable material
Cathode material	Carbon lining	Wettable cathode e.g., TiB_2
Reduction reaction	$2\ Al_2O_3 + 3\ C \rightarrow 4\ Al + 3\ CO_2$	$2\ Al_2O_3 \rightarrow 4\ Al + 3\ O_2$
Electrolyte	AlF_3, Na_3AlF_6	AlF_3, KF, Na_3AlF_6
Temperature	960 °C	700 to 800 °C
Efficiency	40.5% [40]; 50% [41]	Up to 65% [42]
Emissions	CO_2, CO, HF, $NaAlF_4$, CF_4, C_2F_6, PAH, SO_2	O_2, H_2O, HF, $NaAlF_4$, $KAlF_4$

Table 10 provides a technological overview of the conventional Hall-Héroult electrolysis process compared to a new inert anode cell design [39].

Both technologies are based on the electrolytic reduction of alumina (Al_2O_3) dissolved in a molten bath of sodium aluminium fluoride (cryolite). To neutralize sodium oxide (an impurity in the alumina), aluminium fluoride (AF_3) is used in significant excess compared to cryolite. The inert anode technology not only increases the overall efficiency of the process, it also eliminates significant emissions such as CO_2, CO, PAH, CF_x pollutants, tetrafluoromethane, hexafluoroethane, and sulfur oxide.

The molten aluminium obtained is tapped from the reduction cell into crucibles and transported to the casting plant to a holding furnace (approx. 750 °C) where the aluminium is refined (removal of impurities with fluxing salts and injected gas mixture), alloyed and cast (slabs, T-bars or billets, thin sheets, wire rod).

Because this study focuses on sustainable and renewable pathways to produce metal, only the inert-smelter technology applying reaction (7) is taken into account.

$$2\ Al_2O_3 \rightarrow 4\ Al + 3\ O_2 \qquad (7)$$

Process to obtain alumina (Al_2O_3) from aluminium hydroxide

In case the Metal-to-Energy process is operated at reaction temperatures below 280 °C, the oxidation reaction forms aluminium hydroxide ($Al(OH)_3$) (reaction (8). To recycle this reaction product within the ReMeF concept, the $Al(OH)_3$ needs to be dehydrated to form alumina according to the following reaction:

$$2\,Al(OH)_3 \rightarrow Al_2O_3 + 3\,H_2O \quad (8)$$

Bauxite ore is the natural resource of $Al(OH)_3$, and the mining industry obtains alumina from this ore via the so-called Bayer process to produce alumina which is the source material for the aluminium industry. The final step of the Bayer process is the calcination of $Al(OH)_3$ which induces dehydration and results in alumina formation [43]. In this case, $Al(OH)_3$ can be recycled within a centuries-established industrial process.

Technology development of carbon-free aluminium production

Gupta and Basu (2019) assess the technology development of primary aluminium production [44]. Several new technologies have been researched, such as cathode cells, inert anode, vertical electrode cells, etc. To fully reduce carbon emissions and minimize specific energy consumption, a combination of new developments is required. Arctus, IceTec and Sintef develop within the EU project REVEAL (from 2024 to 2026) such a revolutionary technology, which eliminates direct CO_2 emissions and improves energy consumption to demonstrate this process at a TRL of 4 [42].

In addition, in 2018 ELYSIS, a joint venture between ALCOA and Rio Tinto, announced a technology package and commercialization in 2024 for the world's first carbon-free aluminium smelting technology.

3.2.2 Power-to-Iron

Primary iron or steel is traditionally produced by reducing iron ore with a blast furnace process, and a basic oxygen furnace process. In the first step, iron ore and coal are smelted in the blast furnace to produce molten iron. This molten iron is then transferred to the basic oxygen furnace. Here, oxygen is used to decarbonize to the required carbon content and remove impurities such as silicon and manganese. Furthermore, fluxes like limestone are added to combine impurities and form a slag layer which floats on top of the molten iron.

After alloying and removal of the slag, the molten iron is poured into a ladle and further refined (vacuum degassing or ladle metallurgy) before being cast into ingots, slabs, or billets, depending on the intended use.

Figure 17 provides an overview of traditional and alternative steelmaking technology. The following processes can be identified:

- Traditional smelting reduction using carbon (coal and coke)
- Direct reduction using syngas, natural gas, or hydrogen
- Direct electrolytic decomposition in electric arc furnaces using electricity

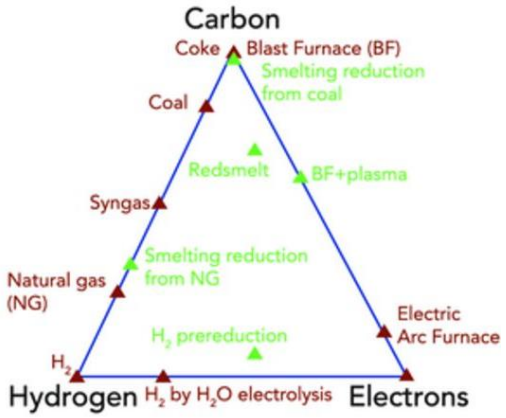

Figure 17: Pathways for iron extraction and some of their corresponding technologies for steelmaking provided by Allanore (2015) [45].

Debiagi et al. (2022) describe the global reduction reaction of iron ore via the traditional blast furnace process as follows [46]:

$$Fe_2O_3 + 3\,CO \rightarrow 2\,Fe + 3\,CO_2 \quad (9)$$

$$Fe_3O_4 + 4\,CO \rightarrow 3\,Fe + 4\,CO_2 \quad (10)$$

$$C + O_2 \rightarrow CO_2 \rightarrow CO_2 + C \rightarrow 2\,CO \quad (11)$$

From reactions (9) to (11), it becomes clear that the partial oxidation of coke is a very intensive CO_2-emitting process.

The direct reduction of iron (DRI) ore using hydrogen as a reduction agent has been developed in Sweden since 2009 and is suggested as one of the key pathways to reaching CO_2 neutrality in the sector. This solid-state process takes place at a temperature below 1'000 °C and is based on the following global reduction reactions [46], [47]:

$$2\,H_2O \rightarrow 2\,H_2 + O_2 \quad (12)$$

$$Fe_2O_3 + 3\,H_2 \rightarrow 2\,Fe + H_2O \quad (13)$$

$$Fe_3O_4 + 4\,H_2 \rightarrow 3\,Fe + 4\,H_2O \quad (14)$$

These reduction reactions (12) to (14) eliminate all CO_2 emissions, yielding H_2O vapour which has a negligible climate warming effect [48]. However, it should be noted that within this reduction process, sponge iron is produced with an iron content between 88 to 94% in the form of pellets, pebbles, or brisquets which is commonly used in steelmaking as a substitute for scrap metal. For steelmaking, sponge iron needs to be further processed in an electric arc furnace where it is melted and refined before it can be alloyed and cast. Nevertheless, sponge iron from DRI might even have advantages for the use as ReMeF not

only because of its pre-formed form (pellets or pebbles, and briquets) but also due to its porous structure with fine pores in the matrix, which can lead to favourable reaction efficiencies in the Metal-to-Energy process.

Early research on molten oxide reduction (direct electrolytic decomposition) using electrolysis cells with inert anodes was conducted at MIT (Massachusetts Institute of Technology, US) in the 2000s demonstrating lab-scale setups in 2010. Allanore et al. (2015) estimate an electricity consumption for a practical, optimized process at 3.7 MWh per t of Fe with the following global reaction (15) [45]:

$$2\,Fe_2O_3 \rightarrow 4\,Fe + 3\,O_2 \qquad (15)$$

This decomposition process takes place at a temperature level of 1'600°C using molten oxides such as CaO and MgO as the electrolyte, emitting only O_2 into the atmosphere but requiring a significant amount of electricity. Therefore, the GHG emissions from this process are highly dependent on the indirect emissions from the electricity production process, and only the use of renewable energy should be considered in this case.

Table 11 provides an overview of carbon-free production reduction technologies.

Table 11: Technology comparison of the direct reduction of iron ore and molten oxide electrolyte reduction of iron ore.

	Direct reduction using hydrogen	**Molten oxide reduction**
Iron ore	Pellets	Concentrates or pure oxides
Anode material	-	Non-consumable material
Cathode material	-	-
Reducing agent	Hydrogen	Electrons
Electrolyte	-	Molten oxides (CaO, MgO, etc.)
Temperature	< 1'000 °C	1'600 °C
Reduction efficiency	85% for DRI process; total P2Iron: 60% (H_2 electrolysis of 70%) [49], [50]	Up to 60% [45]
Product	Sponge iron	Pure metals or alloys
Emission	Water vapour	O_2

Technology development of carbon-free iron production

Suopajärvi et al. (2018) provide a technological overview of steelmaking processes and summarize alternative suitable reducing agents, such as biomass (charcoal) and hydrogen [38]. They conclude that the use of biomass in iron and steelmaking is limited due to its availability and competition issues but is a promising alternative to start the decarbonization efforts of this industry today.

HYBRIT (Hydrogen Breakthrough Ironmaking Technology), a Swedish joint venture between SSAB, LKAB, and Vattenfall, developed an innovative technology using the direct reduction of iron ore alongside hydrogen as a reducing agent [51]. They plan to demonstrate this technology in 2025 at a TRL of 7.

Boston Metal is on the way to commercialising an electrolytic cell using inert anodes, which was originally developed at MIT to eliminate direct (process) GHG emissions for iron extraction. The company plans to demonstrate this technology by 2025 at a TRL of 7 [52].

3.2.3 Power-to-Silicon

Silica (SiO_2) is the most abundant constituent of the earth's crust and thus correspondingly inexpensive. The following reduction pathways to produce silicon are being researched and developed:

- Traditional carbothermal reduction using coal as feedstock
- Carbothermal reduction using biomass as feedstock with CCS technology
- Electrochemical reduction using molten salts as electrolyte
- Metallothermic reduction using magnesium as a reducing agent

Today, high-purity quartz is the main raw material for the industrial preparation of silicon. The traditional carbothermal reduction of silica in industry, which uses an electric arc furnace at 2'000 °C, and carbon (coal, wood chips) as a feedstock is an endothermic process and can be described with the following reduction reaction:

$$SiO_2\ (s) + 2\ C\ (s) \rightarrow Si\ (l) + 2\ CO\ (g) \quad (16)$$

$$2\ CO + O_2 \rightarrow 2\ CO_2 \quad (17)$$

This reduction reaction (16) and (17) consumes a lot of energy and liquefies the silicon [53]. The obtained silicon has a purity of less than 99%, called metallurgical grade silicon (MG-Si) which is further purified by the modified Siemens method, resulting in the so-called solar grade silicon (SOG-Si) [54].

Inspired by the Hall-Héroult aluminium production process, R&D efforts started in the 1960s for the electrochemical reduction of silica, or "sand-to-silicon" electrolysis [55], [56] using inert electrodes containing hercynite [57]:

$$SiO_2 \rightarrow Si + O_2 \quad (18)$$

The reduction reaction (18), takes place in various electrolytes, such as molten salt, oxide, and fluorides, at temperatures between 400 - 900 °C releasing only O_2 into the atmosphere. De Mattei et al. (1981) report that the electrowinning of molten silicon was successfully demonstrated in a small experimental setup using a $BaO/SiO_2/BaF_2$ melt producing metallurgical grade (MG) silicon with 99.97% purity [58]. Lee et al. (2008) investigated the electrochemical reduction of silica with molten salt-based electrolytes, such as molten $CaCl_2$ or LiCl-KCl-$CaCl_2$ eutectic melt at 500 °C to solar-grade silicon and showed promising results

[59]. Recently, a scale-up pilot plant of a semi-continuous electro-reduction to nano-silicon wires for lithium-ion batteries (LIB) negative electrode application in molten salt was successful in Beijing [60], [61]. Tian et al. (2023) reviewed electrochemical pathways for the production of silicon, discussed the advantages and disadvantages of various electrolytes used, and concluded that for future development molten salts, are the most promising candidate for the electrochemical pathway, which is known as the so-called FFC Cambridge process [62]. However, reaching ultrapure Si quality is rather unlikely, but may also not be necessary for use as an energy carrier [55].

Overall, the advantages of molten salt electrolysis are the low energy consumption to produce very high qualities of silicon, low cost, and low pollution because it emits only O_2 into the atmosphere. However, the electrolysis deposition of this process is rather slow due to its poor conductivity, and therefore, an industrial production process will need a lot of time due to the large material amounts. Additionally, there are no obvious advantages in the overall energy efficiency, but the purity of the obtained silicon is higher when compared to the carbothermal reduction process. Therefore, more research is required at this development stage for the reduction process to become industrially attractive and available. Table 12 compares some parameters of the carbothermal and electrochemical reduction of silica.

Table 12: Technology comparison of the traditional carbothermal reduction and the electrochemical reduction of silica.

	Carbothermal reduction	**Electrochemical reduction**
Energy consumption	20 MWh_e per t MG-Si without energy content of carbon input [63] 75 - 130 MWh per t SOG-Si	10.5 MWh_e per t MG-Si [64] 13 MWh_e per t SOG-Si [62]
Anode material	-	Graphite / non-consumable anodes, e.g. hercynite
Reducing agent	Carbon:	Electrons
Electrolyte	-	Molten salt
Temperature	1’800 to 2’000 °C	650 – 900 °C
Product	Metallurgical silicon (MG-Si)	MG-Si or SOG-Si (depending on the electrolyte)
Emission	5 – 17 t CO_2 per t of MG-Si [64] 43 - 84 t CO2 per t of SOG-Si [63]	0.7 t CO_2 per t of SOG-Si from graphite anodes Only O_2 for inert anode technology

The exothermic metallothermic reduction, or rather the magnesiothermic reduction of silica can be described as follows in the temperature range of 550 – 650 °C:

$$SiO_2 + 2\,Mg \rightarrow Si + 2\,MgO \qquad (19)$$

Via this reduction process (19), nanostructured silicon can be produced. An undesired side reaction occurs which forms magnesium silicide but could be prohibited if mesoporous silica

channels are used [65]. This reduction process shows potential use for promising applications, but several research questions still need to be answered.

Process to obtain silica (silicon oxide) from silicon hydroxide (silicic acid)

In general, silicic acid is used in many industrial applications, such as catalyst or catalyst carriers in the petroleum, chemical industry, synthetic fibre, synthetic rubber, etc. To close the Power-to-Silicon and Silicon-to-Energy cycle, silicic acid ($Si(OH)_4$) needs to be dehydrated to form silica (SiO_2).

$$Si(OH)_4 \rightarrow SiO_2 + 2\,H_2O \qquad (20)$$

In general, this dehydration reaction (20) is controlled by the ratio of liquid to solid, reaction temperature, and time [66].

Technology development of carbon-free silicon production

Elkem is a company from Norway which produces silicon-based materials globally. Their sustainability report from 2022 provides insights into the roadmap to produce climate-neutral silicon [67]. To reach their net zero targets in 2050, several measures will be applied until then:

- Biomass smelter
- Increase in the usage of renewable electricity (China)
- Switch to a low-carbon supply chain
- Implementation of Carbon Capture and Storage (CCS)
- Other initiatives

Using charcoal from biomass and biomass waste in the carbothermal reduction of silica was investigated within the TOPBIO research project at WAI Environmental Solutions with other partners from SINTEF, etc. [68]. Additionally, the Norwegian University of Science and Technology (NTNU) and SINTEF successfully demonstrated on a pilot scale the recirculation of flue gas within the carbothermal reduction of silicon which is an important development step to efficiently implement CCS technology [69].

Although, raw material extraction for silicon production is significantly less expensive if compared to aluminium, research efforts on the electrochemical reduction of silica did not reach industrial application so far.

3.3 Discharging process: Metal-to-Energy

The chemical reaction pathways for the Metal-to-Energy process (discharge process) are identified. In general, there are three pathways to release energy from thermodynamic reactions with metals:

- Combustion (boiler with gas or steam turbine): oxygen as a reactant
- Electrochemical reaction (metal-air battery)
- Oxidation reaction with water or steam

In all reaction pathways, the geometric shape of the metallic fuel is decisive for the reaction time and thus for the energy released over time and metal oxide crystallisation.

A combustion process of ReMeF is applied in applications where high-temperature heat is required to drive a steam or gas turbine, for example, to generate electricity. In this case, only metal powders are suitable to achieve high efficiencies.

For the electrochemical pathway, on the other hand, the electrochemical potential of electrode materials determines the voltage level of the cell whereas the potential is a function of pH and temperature. Metal-air electrochemical cells use pure metal as anode material and an external cathode of ambient air typically with an aqueous electrolyte.

The metal-water or metal-steam oxidation reaction typically yields heat and hydrogen which can be further used in an electrochemical conversion such as a fuel cell system. The oxidation reaction kinetics and energy yield are dependent on the chemical property (oxygen bond, impurities) of the metal and on the reaction conditions (temperature, pH, etc.).

Figure 18 illustrates a metal A, such as iron (Fe) reacting with water and oxygen to form a corrosive layer (Fe_2O_3) which will grow over time. Aluminium and silicon, on the other hand, form a passivation layer as shown in metal B. This passivation occurs naturally with metals that bond readily with oxygen.

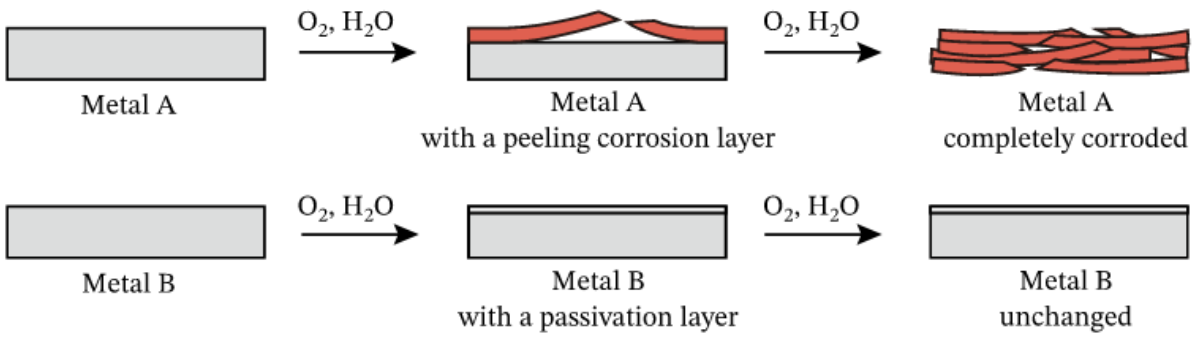

Figure 18: Pathways of metal-oxidation reaction to form corrosive or passivation layers [70].

Therefore, aluminium and silicon require a promoter, such as an alkaline or base solution to dissolve the oxide layer to start the oxidation reaction with water. At the same time, this passivation layer is a crucial advantage for long-term energy carriers because losses in standard conditions are very limited in this case.

The following sections focus on the oxidation reaction with water or steam because it is the most interesting pathway for the investigated applications in this project.

3.3.1 Aluminium-to-Energy

Depending on the oxidation reaction temperature, aluminium reacts with steam or water to form hydrogen and aluminium oxide (Al_2O_3) or aluminium hydroxide ($Al(OH)_3$). At temperatures above 280 °C, the oxidation reaction takes place with steam to form hydrogen and Al_2O_3 (reaction (21)), whereas at lower temperatures $Al(OH)_3$ (reaction (22)) is formed [71]:

$$2\,Al + 3\,H_2O \rightarrow Al_2O_3 + 3\,H_2 \qquad (21)$$

$$2\,Al + 6\,H_2O \rightarrow 2\,Al(OH)_3 + 3\,H_2 \qquad (22)$$

For both reactions, the same amount of hydrogen is produced. Additionally, these oxidation reactions are strongly exothermic.

As mentioned above, the aluminium surface rapidly forms a passivating layer when in contact with air or water, which can be removed if alkaline or base solutions are used. Dudita et al. (2019) suggest that sodium hydroxide (NaOH) is considered the best alkali solution to ensure ongoing oxidation and even enhance reaction kinetics [71]. The overall hydrogen generation quantity is independent of the NaOH concentration, but its kinetics highly depend on the concentration of the NaOH solution, the particle size, the porosity of the particles, and the reaction condition (temperature and pressure).

Technology development of the Aluminium-to-Energy process

Most research in hydrogen production from the aluminium water reaction is conducted using Al in the form of powder [72], [73], [74]. A research group at the University of Perugia in Italy, and the Helmholtz Institute and KIT in Germany investigate at a lab-scale the Al steam oxidation for large-scale industrial applications to produce hydrogen and heat at temperatures from 600 – 900 °C (melting point of aluminium is 660 °C) [75], [76].

In Switzerland at the Paul Scherrer Institute, the Al powder combustion was investigated and tested in 1990. However, the developed combustion unit was found not to be suitable for the use of Al powder due to high safety requirements because the Al powder is explosive [77].

Therefore, the research group at SPF only considers Al granulate as a source material for the Al oxidation reaction with water at temperatures below 100 °C. Figure 19 illustrates the research pathway which leads to the development and testing of a 4 kW CHP pilot plant for continuous operation at a TRL of 4/5 in 2026.

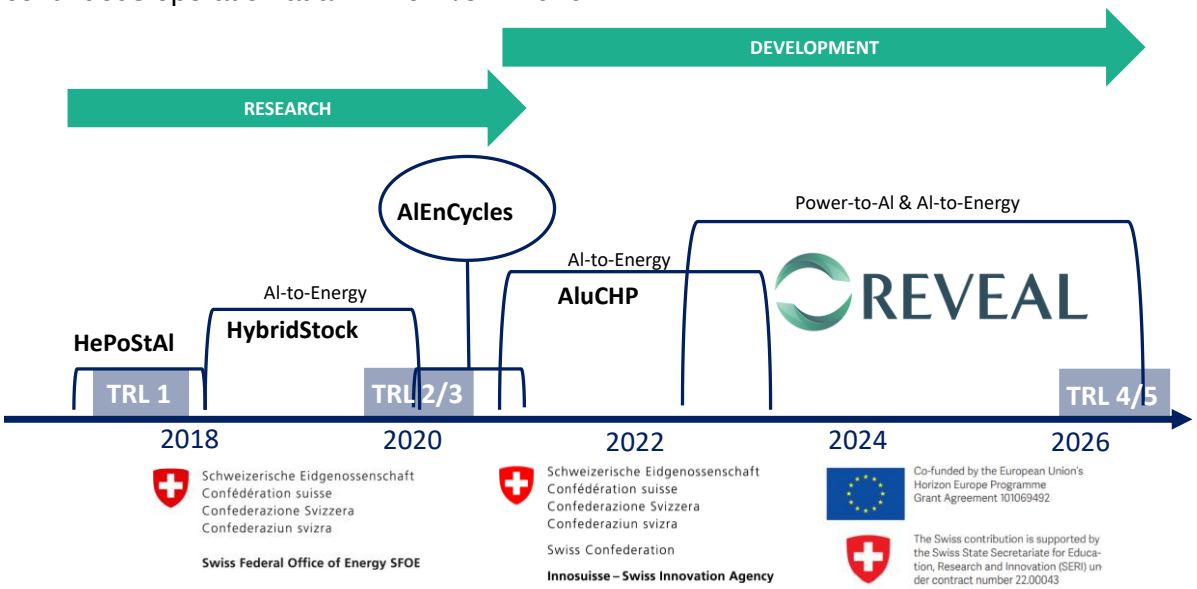

Figure 19: Overview of R&D projects of the Al redox storage cycle at SPF.

SPF and a research group at MIT (US) also focus on the use of aluminium scrap to produce hydrogen and heat [78], [39].

3.3.2 Iron-to-Energy

In general, metallic iron reacts with oxygen to form two main stable oxides 1) magnetite (Fe_3O_4) and 2) hematite (Fe_2O_3) following the global reactions [46]:

$$3\,Fe\ +\ 2\,O_2 \rightarrow Fe_3O_4 \qquad (23)$$

$$4\,Fe\ +\ 3\,O_2 \rightarrow 2\,Fe_2O_3 \qquad (24)$$

These thermochemical oxidation pathways occur rapidly at high temperatures releasing a significant amount of heat. Debiagi et al. (2022) propose the combustion of iron particularly for application in thermal energy systems to generate electricity [46].

As mentioned above, iron oxidizes in the presence of moisture (reactions (25), (26)). At first, loose porous rust or $Fe(OH)_3$ is formed which slowly transforms to crystallized Fe_2O_3:

$$4\,Fe\ +\ 3\,O_2\ +6\,H_2O \rightarrow 4\,Fe(OH)_3 \qquad (25)$$

$$4\,Fe(OH)_3 \rightarrow 2\,Fe_2O_3 + 6\,H_2O \qquad (26)$$

Literature suggests that the aqueous corrosion of iron is gradual. First, corrosion begins at anodic sites on the surface where ferrous ions are dissolved. Electrons are released from the anodic surface site and travel through the metallic structure to adjacent cathodic sites where they combine with oxygen and water to form hydroxyl ions. These react with the iron ions from the anodic site to form iron hydroxide, which is further oxidized in air to form hydrated iron oxide (rust, Figure 20).

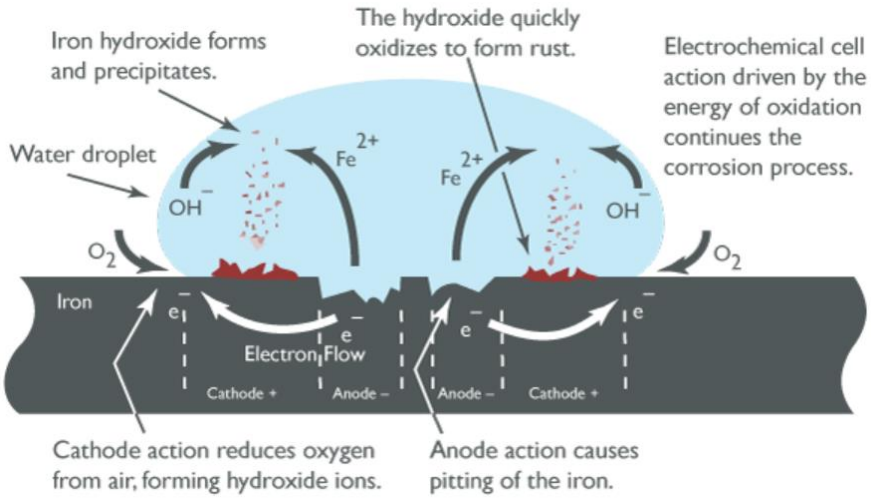

Figure 20: Description of iron corrosion [79].

The form in which iron is found in water after oxidation will primarily depend on the pH and the oxidation-reduction potential.

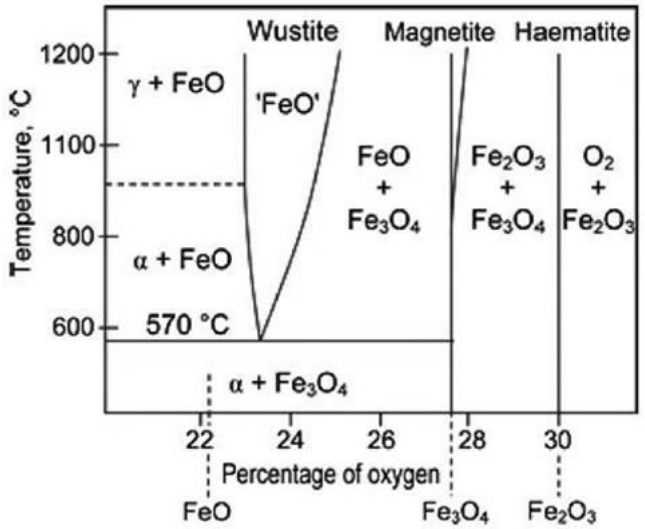

Figure 21: Iron oxygen phase diagram [80].

The reaction between iron and water proceeds at higher temperatures, i.e., with steam, according to the reaction (27) and (28) to a non-stoichiometric composition of Fe_xO_y – mixed iron (II, III) oxide and gaseous hydrogen (Figure 21) [80], [81]:

$$2\,Fe\ +\ 3\,H_2O\ (g) \rightarrow Fe_2O_3 + 3\,H_2 \qquad (27)$$

$$3\,Fe\ +\ 4\,H_2O\ (g) \rightarrow Fe_3O_4 + 4\,H_2 \qquad (28)$$

Long-term experiments of aqueous corrosion in the absence of oxygen at room temperature showed that magnetite (Fe_3O_4) is formed over several days following the oxidation reactions (29) to (32) leading to the global reaction (33) [82].

$$2\,Fe\ +\ 4\,H_2O\ (l) \rightarrow 2\,Fe(OH)_2 +\ 2\,H_2 \qquad (29)$$

$$Fe(OH)_2\ +\ H_2O\ (l) \rightarrow Fe(OH)_3 + 0.5\,H_2 \qquad (30)$$

$$Fe\ +\ 3\,H_2O\ (l) \rightarrow Fe(OH)_3 + 1.5\,H_2 \qquad (31)$$

$$2\,Fe(OH)_3 +\ Fe(OH)_2 \rightarrow Fe_3O_4 + 4\,H_2O\ (l) \qquad (32)$$

$$3\,Fe\ +\ 4\,H_2O\ (l) \rightarrow Fe_3O_4 + 4\,H_2 \qquad (33)$$

However, this oxidation process highly depends on the structure of the iron surface, as smooth surfaces can be kept almost infinitely in oxygen-free water. Additionally, it is assumed that the final oxidation product is a mixed form of hydrated ferric or ferrous hydroxide or oxide [82].

Technology development of the Iron-to-Energy process

Teamsolid, metalot and researchers at Eindhoven Technical University (TU/e) in the Netherlands are investigating the redox reaction between iron powder and oxygen (combustion process) to form iron oxide for power generation and transportation as well as for energy-intensive industrial applications. They claim to have proceeded from TRL 3 to 5 [83], [84]. A pilot plant at a Bavarian brewery was demonstrated in 2020 in the range of 100 kW and they plan to operate a 10 MW system in 2024 [85]. Additionally, Solid started in cooperation with several partners a project for the proof of concept of the iron-steam oxidation reaction which will form the basis for new innovative hydrogen storage solutions [86].

On a side note, research groups at Caltech and Northwestern University in the US conduct interesting experiments on thin film oxide (rust) layers generating electricity when in contact with flowing water [87].

3.3.3 Silicon-to-Energy

Bulk Si is extremely stable in aqueous solutions due to the nanometre-thin SiO_2 passivating layer [88]. But Ning et al. (2020) report on-demand hydrogen generation from porous silicon nanowires and nanoparticles fabricated via metal-assisted anodic etching method with water at ambient pressure without any energy input [89]. The steam oxidation of silicon forms silica (SiO_2) at high temperatures according to the reaction (34) [90]. Using a promoter such as an alkaline or base solution can activate the thermodynamic oxidation of silicon, for example in the form of powder, to produce hydrogen even at ambient temperatures according to the oxidation reaction (35) with a theoretical limit of 0.14 kg of H_2 per kg of Si [88].

$$Si + 2\,H_2O\,(g) \rightarrow SiO_2 + 2\,H_2 \quad (34)$$

$$Si + 2\,H_2O\,(l) \rightarrow SiO_2 + 2\,H_2 \quad (35)$$

$$SiO_2 + 2\,H_2O\,(l) \rightarrow Si(OH)_4 \quad (36)$$

$$Si + 4\,H_2O\,(l) \rightarrow Si(OH)_4 + 2\,H_2 \quad (37)$$

Furthermore, the surface SiO_2 layer dissolves in water through the reaction (36) to silicon hydroxide [89]. Combining the reaction (35) and (36) above, the overall reaction (37) is obtained. The overall hydrogen generation quantity is independent of the concentration of the alkali or base solution whereas its kinetics depends on the concentration of the solution, the particle size, the grinding degree or porosity of the silicon particles and the reaction condition [91]. Tin et al. (2020) report on hydrogen production from silicon slag by applying a wet grinding process for silicon slag recycling at room temperatures and pH levels of 8 – 9 [92]. However, the kinetics of the reaction using fine particle sizes of 74- 300 µm was rather slow, taking more than 6 hours to complete oxidation. Nevertheless, an increased pH level might accelerate the reaction kinetics further. But up to date, there is no literature confirming this assumption.

Technology development of the Silicon-to-Energy process

Research on hydrogen production from silicon and water focuses on using powder because reaction kinetics are favourable. Nakayama et al. (2022) investigated lab-scale experiments using silicon powder from waste stream sources and sodium hydroxide solution for hydrogen production, achieving the theoretical max. hydrogen yield [93]. A research group at the University of Buffalo suggests using this silicon redox cycle concept for small portable devices, such as satellite radio, GPS, laptops, lighting, watches, etc. [94]. EPRO Advance Technology (EAT) promotes its porous silicon nano powder (1 – 3 nm) product (vacuum packed or in an inert environment) as a renewable energy source, even suggesting backup generator applications and the replacement of marine fuel oil [95]. Additionally, EAT also developed scaled-up prototypes to generate up to 3 kg of hydrogen per day for 5 kW fuel cell systems [96]. It should be noted that the EAT's silicon redox concept is based on the open-

loop recycling of the produced silicates in zeolite e.g., as a drying agent and green cement production instead of closed-loop recycling within the concept.

Table 13: Overview of the CO_2-free Power-to-Metal process and the Metal-to-Energy process which are further considered in the following mass and energy balance and process efficiency assessment.

	Power-to-Metal process		Metal-to-Energy process
Aluminium	Inert anode		Oxidation reaction with water or steam producing heat and H_2 + fuel cell system
Iron	Direct Reduction of Iron via H_2 (DRI-H_2)	Molten oxide reduction	
Silicon	Electrochemical reduction (inert anode)		

Table 13 provides an overview of the ReMeF technologies which are further considered in the mass and energy (Chapter 3.4) and process efficiency analysis (Chapter 3.4.4). In addition, a summary of the results of this chapter is given in the conclusion (Chapter 4.1).

3.4 Mass and energy balance

The enthalpy of the reaction is a parameter that quantifies the amount of energy that must be added or released when chemical bonds change. It is thus a good measure for the conversion of chemical potential energy into heat or a combination of heat and electricity.

Therefore, the enthalpy of reaction was calculated for both, the Power-to-Metal and Metal-to-Energy processes, as discussed in detail in the following sections. For the oxidation reactions, high and low temperatures are considered according to the thermodynamic state of the water that enters the process in its gaseous (g) or liquid (l) state. Starting from liquid water, the net heat production of this process will be lower than starting with steam. However, if for a steam process, the enthalpy of conversion of water to steam is considered as an additional energy input that is required, the remaining difference is only due to different forms of the other reactants that participate in the reaction.

Additionally, from the reaction equation, the mass and energy balance were calculated by the formation enthalpy provided in Annex B. The hydrogen yield has been calculated based on the stoichiometric reactions, and its energy content is expressed based on the high heating value (HHV).

For the following mass and energy balance, a theoretical hydrogen conversion efficiency of the water-cooled fuel cell system with an electrical efficiency of 50% and a thermal efficiency of 50% was assumed. In this case, no losses are considered for the recovery of heat from the fuel cell.

3.4.1 Aluminium

Figure 22 provides an overview of the enthalpy of the reaction for the aluminium-redox-concept based on the reaction (7), (8), (21), and (22), including hydrogen to energy conversion via a fuel cell system according to the following reaction:

$$H_2 + O_2 \rightarrow H_2O \qquad (38)$$

Power-to-Aluminium

The Power-to-Aluminium-redox-concept starts either with Al_2O_3 or $Al(OH)_3$ initially.

According to Figure 22, at an oxidation reaction temperature below 280 °C, $Al(OH)_3$ is formed.

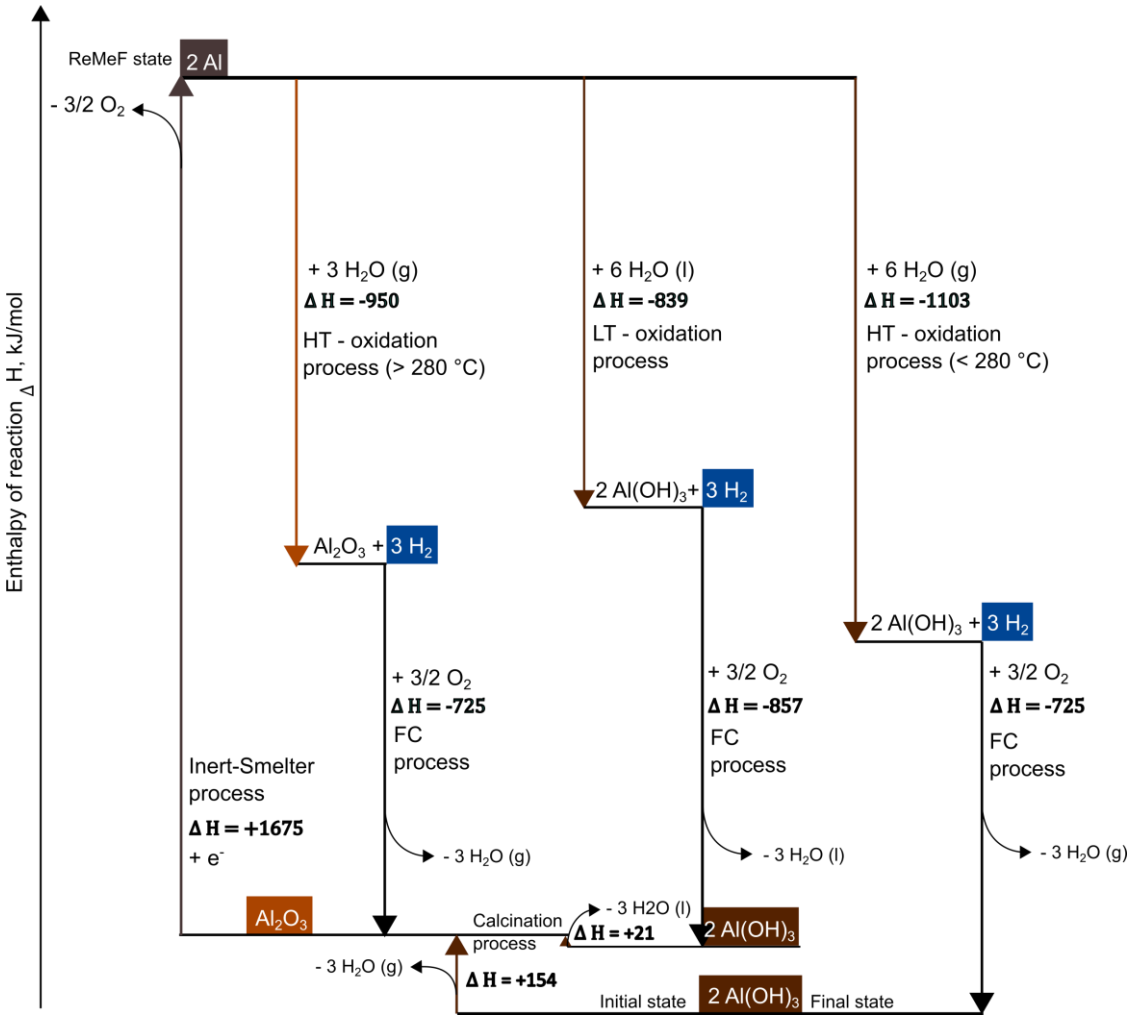

Figure 22: Enthalpy of reaction, ΔHr, 298 for the proposed aluminium redox cycle(s), considering a high-temperature HT-oxidation with steam and a low-temperature LT-oxidation with water. The enthalpy of the reaction from the fuel cell (FC) was also included.

It must be dehydrated by calcination, which requires 154 or 21 kJ of energy per 2 moles of $Al(OH)_3$, depending on the thermodynamic state of the reaction product, namely water in a gaseous (g) or liquid (l) state [71].

To form aluminium, the Al_2O_3 obtained requires 1675 kJ/mol of electricity using the inert-smelter process, which only releases oxygen.

Aluminium-to-Energy

Aluminium is oxidized releasing 839 kJ of heat per 2 moles of Al in the case of water (H_2O (l)) path and 950 or 1103 kJ per 2 moles of Al for steam (H_2O (g)) depending on the reaction product (Al_2O_3 or $Al(OH)_3$). However, independent of the reaction product, additionally 3 moles of hydrogen per 2 moles of Al is produced. The hydrogen conversion in the fuel cell process releases 857 or 725 kJ per 2 moles of $Al(OH)_3$ in the form of water or steam, respectively.

Figure 23 and Figure 24 illustrate the mass and energy flow for an ideal conversion of 100% of the original Al material, resulting in a total energy recovery of 8.6 and 8.7 kWh depending if Al_2O_3 or $Al(OH)_3$ is obtained.

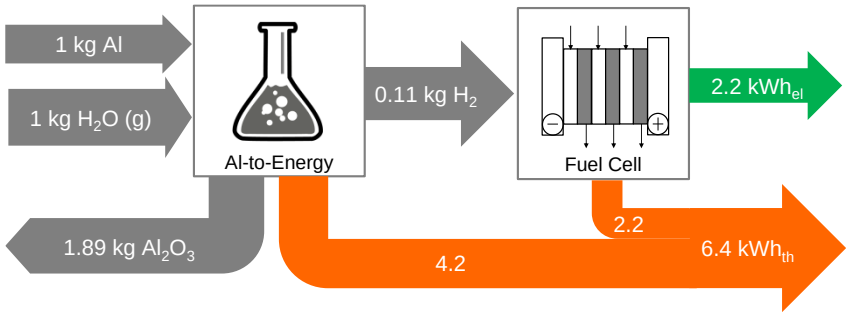

Figure 23: Mass and energy balance of the Alu-to-Energy process according to reaction (21) obtaining Al_2O_3. Water-cooled FC system efficiency: electrical 50%, thermal 50%.

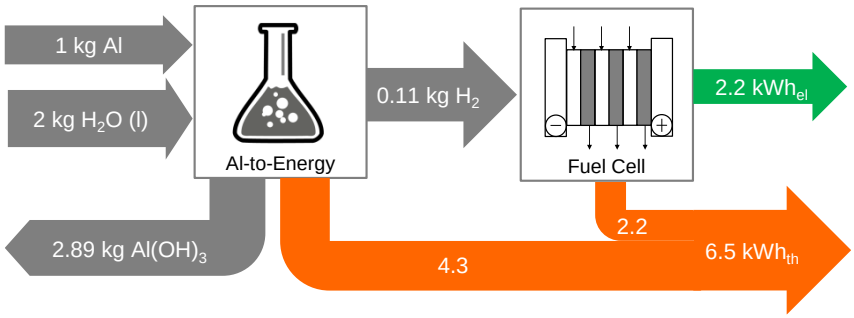

Figure 24: Mass and energy balance of the Alu-to-Energy process according to reaction (22) obtaining $Al(OH)_3$. Water-cooled FC system efficiency: electrical 50%, thermal 50%.

In general, the formation of $Al(OH)_3$ requires double the amount of water and leads to roughly 50% more solid reaction products after the precipitation of $Al(OH)_3$.

3.4.2 Iron

Figure 25 provides an overview of the enthalpy of the reaction for the iron-redox-concept with steam at high temperatures, based on the reaction (11), (12), (10), (23), and (24) including the fuel cell reaction, reaction (38).

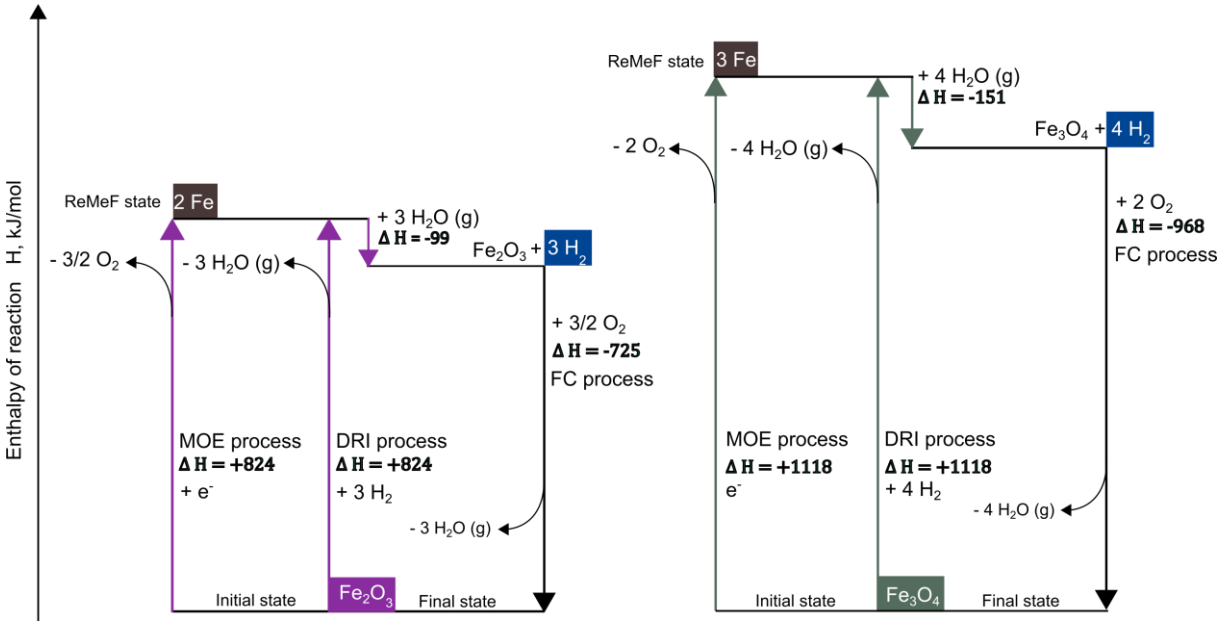

Figure 25: Enthalpy of reaction, ΔHr, 298 for the proposed iron redox cycle, considering oxidation with steam at high temperatures. The enthalpy of the fuel cell (FC) reaction was also included.

Figure 26 illustrates the iron oxidation with water (corrosion effect) described by reactions (14), (12), (29) to (32), and (38).

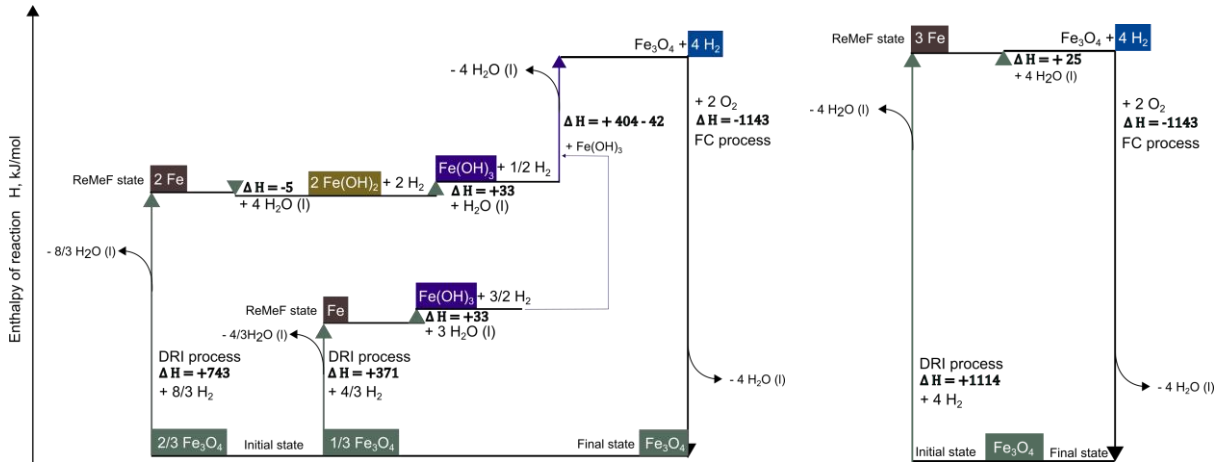

Figure 26: Enthalpy of reaction, ΔHr, 298 for the proposed iron redox cycle considering oxidation with water from reaction (29) to (32) on the left, and the global reaction (33) on the right. The enthalpy of the fuel cell (FC) reaction was also included. The final oxidation step requires 2 $Fe(OH)_3$ and $Fe(OH)_2$ to form Fe_3O_4 (34).

Power-to-Iron

The direct reduction of iron (DRI) process for reducing iron-oxides to iron uses hydrogen as a reduction agent, and the molten oxide electrolysis process requires 824 and 1118 kJ of hydrogen or electricity per mol of the initial starting product, namely Fe_2O_3 and Fe_3O_4, releasing oxygen or steam, H_2O (g).

If H_2O (l) is considered to be the reactant, 1114 kJ in the form of electricity or hydrogen is required to obtain 3 moles of iron from one mole of Fe_3O_4.

Iron-to-Energy

At high temperatures, iron is oxidized with steam, releasing 99 or 151 kJ/mol depending on the obtained reaction product (Fe_2O_3 and Fe_3O_4). In addition, this reaction produces 3 moles of hydrogen per mol of Fe_2O_3, and 4 moles of hydrogen per mol of Fe_2O_4, respectively. This results in the mass and energy balance illustrated in Figure 27 and Figure 28. Interestingly, the iron oxidation with steam releases only a small amount of heat, so most of the energy content of the iron is transferred to hydrogen.

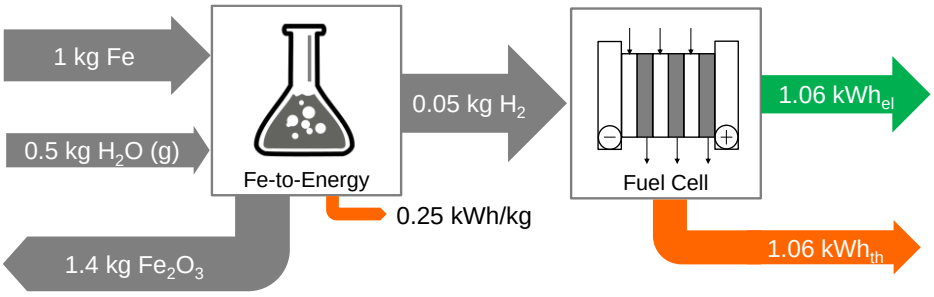

Figure 27: Mass and energy balance of the Fe-to-Energy process with steam according to reaction (27) obtaining Fe_2O_3. Water-cooled FC system efficiency: electrical 50%, thermal 50%.

Overall, 2.37 kWh of energy (heat and electricity) can be recovered per kg of iron from the hydrogen produced and, to a minor extent, from the heat of the reaction of the iron oxidation, when forming Fe_2O_3.

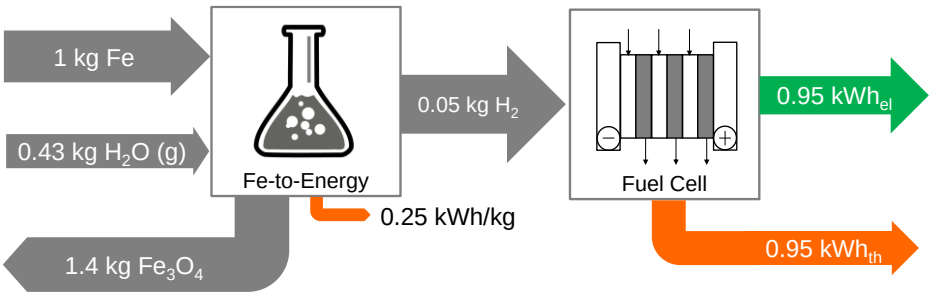

Figure 28: Mass and energy balance of the Fe-to-Energy process with steam according to reaction (28) obtaining F_3O_4. Water-cooled FC system efficiency: electrical 50%, thermal 50%.

However, the overall obtained reaction product of the iron-steam, H_2O (g) reaction is Fe_3O_4 with a hydrogen yield of 0.048 kg per kg of Fe leading to a total of 2.15 kWh of energy output (Figure 28).

Figure 29 shows the iron oxidation reaction with water, H_2O (l) producing 0.05 kg per kg of Fe. At the same time, about 1.4 kg of reaction product (Fe_3O_4) is formed.

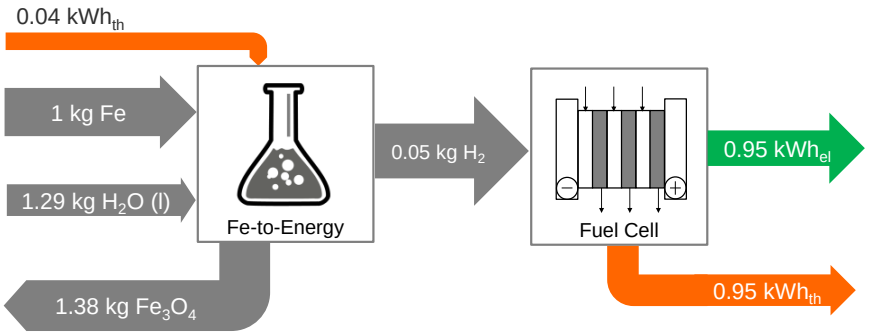

Figure 29: Mass and energy balance of the Fe-to-Energy process with liquid water according to the global reaction (33) obtaining F_3O_4. Water-cooled FC system efficiency: electrical 50%, thermal 50%.

It should be noted that the Fe-to-Energy process with liquid water is endothermic, i.e., it requires a continuous supply of heat to keep the reaction going. However, this energy demand corresponds only to one-tenth of the heat recovered from the fuel cell system (0.95 kWh$_{th}$).

3.4.3 Silicon

Figure 30 shows an overview of the enthalpy of the reaction for the silicon-redox-concept with steam at high temperatures based on the reaction (18), (20), (34), as well as the low-temperature pathway with water considering reaction (35), (36), and (37) including the fuel cell, reaction (38).

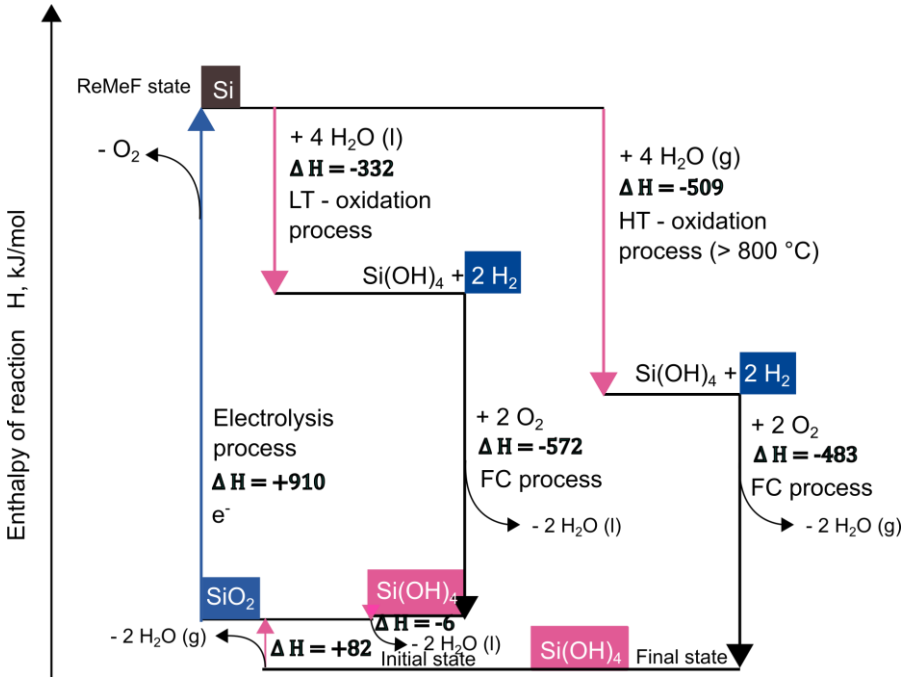

Figure 30: Enthalpy of reaction, ΔHr, 298 for the proposed silicon redox cycle considering oxidation with steam (H_2O (g)): reaction (34), and water (H_2O (l)): reaction (35) to (37). The enthalpy of the fuel cell (FC) reaction (38) was also included.

Power-to-Silicon

If the initial state of the source material is $Si(OH)_4$, the silica gel needs to be dehydrated to obtain SiO_2 which can be reduced in an electric arc furnace to MG-Si, i.e. silicon with a purity of up to 95 to 99.7% using molten salt electrolytes [57]. This molten salt electrolysis requires 910 kJ/mol of silicon as electric energy, releasing only oxygen to the atmosphere.

Silicon-to-Energy

Figure 31 and Figure 32 illustrate the silicon steam oxidation and silicon water oxidation reactions, respectively.

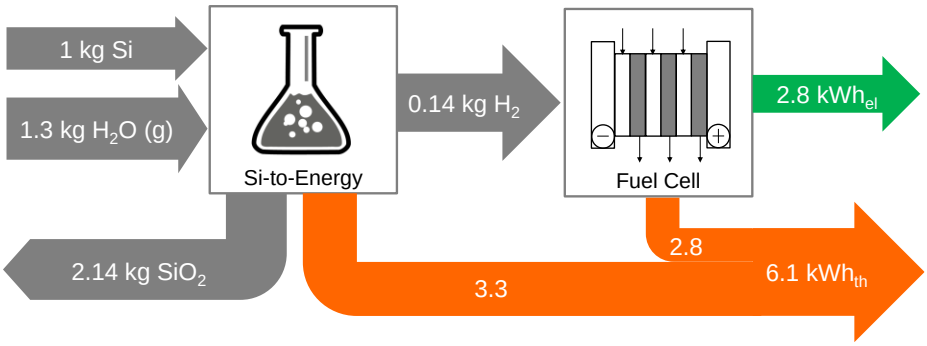

Figure 31: Mass and energy balance of the Si-to-Energy process according to the reaction (34) obtaining SiO_2. Water-cooled FC system efficiency: electrical 50%, thermal 50%.

For both pathways, the oxidation reaction is highly exothermic releasing energy in the form of heat (3.3 kWh_{th}) and 0.14 kg of hydrogen per kg of Si.

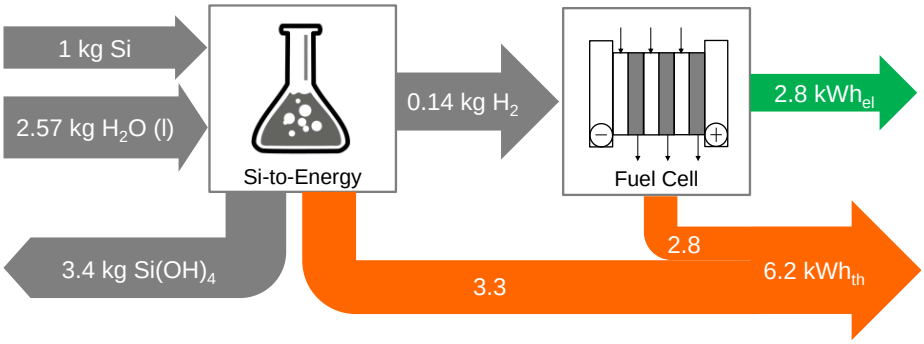

Figure 32: Mass and energy balance of the Si-to-Energy process according to the reaction (37) obtaining $Si(OH)_4$. Water-cooled FC system efficiency: electrical 50%, thermal 50%.

Overall, the energy yield of the Silicon-to-Energy process is similar to the Alu-to-Energy process. The results described are summarised in the conclusion (Chapter 4.1).

3.4.4 Energy efficiency

In general, the Power-to-Metal process is a centrally located industrial process. To provide a sustainable and renewable pathway, hydrogen, aluminium, or iron must be produced using only renewable electricity.

The Metal-to-Energy process, on the other hand, is operated in decentral CHP units for a small scale of approx. 4 to 10 kW in building applications or in large-scale MW industrial applications.

The overall Power-to-Metal-Storage efficiency ($\eta_{P2M,tot}$) is calculated as the product of the CO_2-free metal production efficiency (η_{P2M}), the efficiency of casting and shaping(η_{shape}), and an efficiency factor that accounts for eventual losses due to oxidation during storage (η_{Sto}):

$$\eta_{P2M,tot} = \eta_{P2M} \cdot \eta_{shape} \cdot \eta_{Sto} \qquad (39)$$

The efficiency of the metal reduction process is based on values from Chapter 3.2. The hydrogen electrolysis efficiency was considered 70%, based on the literature [97].A general process efficiency of 98% was assumed for the casting and shaping process of the liquid metal produced, irrespective of the type of metal (η_{shape}). For the long-term storage of the ReMeF, it was assumed that aluminium and silicon experience no losses over time due to the rapid formation of a protective oxide layer. However, iron is anticipated to rust by 2% over time, resulting in an iron storage efficiency of $\eta_{Sto} = 98\%$.

For the conversion of alumina to aluminium and the molten oxide electrolysis of iron without CO_2 emissions, a process efficiency of 65% for aluminium and 60% for iron can be expected, resulting in a total Power-to-Metal-to-Storage efficiency of 63% for Al and 57% for Fe (Figure 33). The energy consumption per tonne of sponge iron produced by direct reduction of iron (DRI) with hydrogen is approx. 2.8 MWh_e to produce hydrogen, resulting in the same overall charging and storage efficiency as molten oxide electrolysis (57%).

The total efficiency of the Power to Metal storage process as well as the contributions of the different subprocesses, is illustrated in Figure 33.

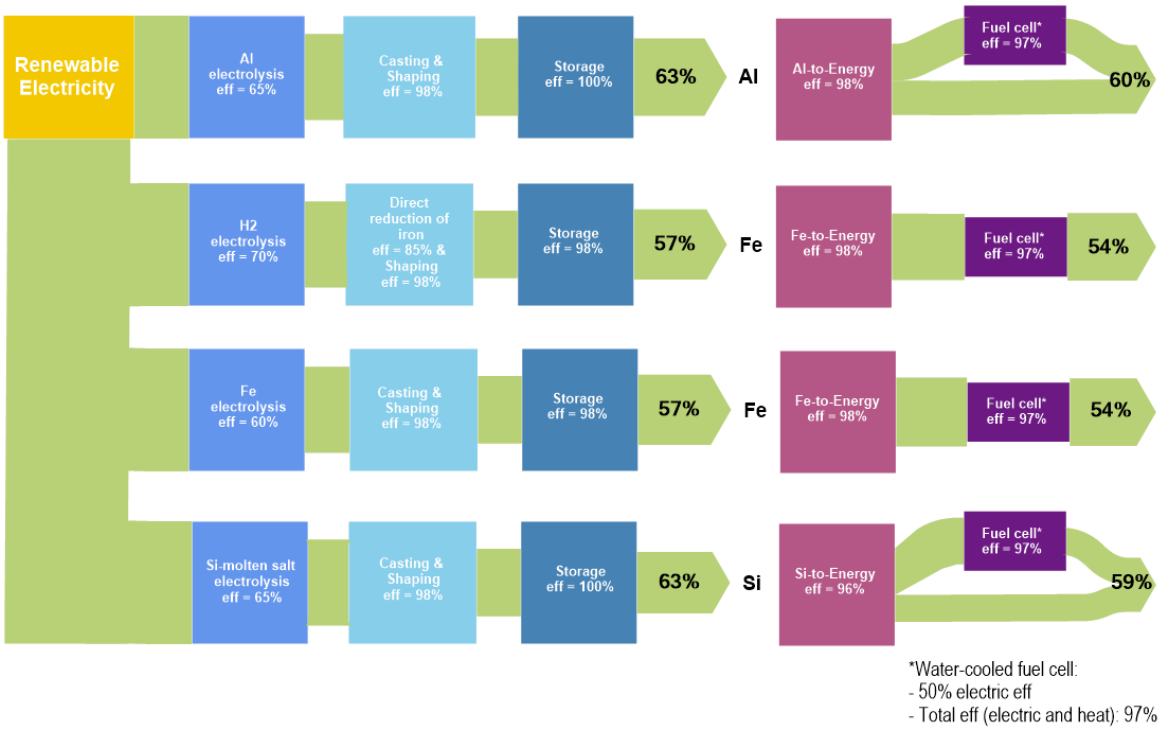

Figure 33: Efficiency of the different processes of the studies ReMeF cycles, composed of their subprocesses and their efficiency. Process and Power-to-Metal-to-Storage-to-Energy efficiency (eff) for ReMeF candidates.

The Power-to-Metal-to-Storage efficiency of silicon production by molten salt electrolysis reaches 63% which is equal to the production of aluminium by inert anodes. It should be noted, that the TRL of the Si molten salt electrolysis is rather low (4). As mentioned in Chapter 3.2.3, the silicon industry plans to implement a net-zero target scenario by 2050, still using the carbothermic reduction route. In this case, biomass pyrolysis is used to partially replace the carbon feedstock used as a reduction material. However, to fully achieve a net zero target, this route requires also CCS technology to compensate for carbon feedstock that is not of biomass origin, as shown in Figure 34.

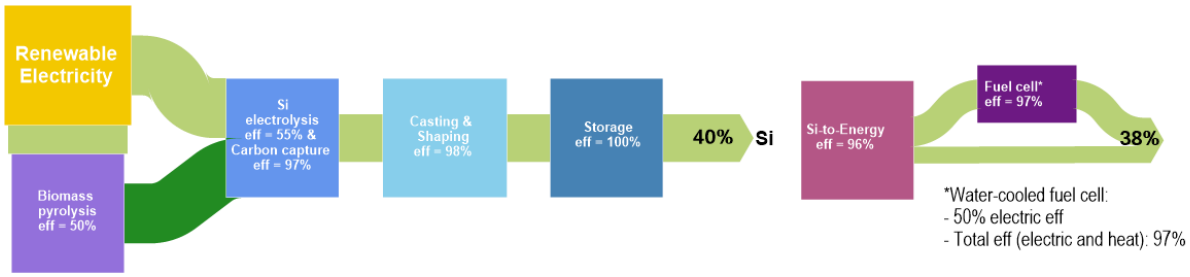

Figure 34: Process and Power-to-Metal-to-Storage-to-Energy efficiency (eff) for the silicon carbothermal reduction partially replacing carbon with biochar.

This pathway could also be implemented for a net-zero scenario of aluminium production using the traditional Hall Hèroult process. In this case, either the direct CO_2 emissions from the consumed carbon anode need to be captured and stored, or the carbon anodes would have to be produced from biochar.

For the Metal-to-Energy process, it can be concluded that the metal fully oxidizes if sufficient reactant is supplied and the passivating oxide layer on the metal surface (in the case of Al or Si) is dissolved. Therefore, if favourable oxidation reaction conditions are provided, a 100% reaction efficiency can be achieved. However, the kinetics of the reaction might not always be favourable. Most research on Metal-to-Energy processes provided is based on powder as source material since powder provides a higher surface-area ratio and therefore reacts faster [98], [99], [100], [91]. Also, porous metal, such as sponge iron, will lead to better reaction kinetics, i.e., faster energy release. Figure 33 and Figure 34 show the expected Metal-to-Energy efficiency based on the mass and energy balance evaluated in Chapter 3.4 (energy output to hydrogen (E_{H2}) and energy output to heat (E_{th})) for each ReMeF candidate (η_{M2H2}, η_{M2th}):

$$\eta_{M2H2} = \frac{E_{H2}}{E_{tot}} \quad (40)$$

$$\eta_{M2th} = \frac{E_{th}}{E_{tot}} \quad (41)$$

For the fuel cell system, an electric efficiency of 50% ($\eta_{fc,e}$) can be expected based on HHV [101]. In addition, a water-cooled fuel cell system is used, which assumed that the 50% heat loss ($\eta_{fc,th}$), can be recovered with a theoretical 95% heat recovery (η_{hx}) giving a fuel cell system efficiency of 97% ($\eta_{fc,tot}$):

$$\eta_{fc,tot} = \eta_{fc,e} + (\eta_{fc,th} \cdot \eta_{hx}) \quad (42)$$

$$\eta_{M2e} = \eta_{M2H2} \cdot \eta_{fc,e} \quad (43)$$

$$\eta_{M2th,tot} = (\eta_{M2th} \cdot \eta_{hx}) + (\eta_{M2H2} \cdot \eta_{fc,th} \cdot \eta_{hx}) \quad (44)$$

$$\eta_{M2E,tot} = \eta_{M2e} + \eta_{M2th,tot} \quad (45)$$

The Metal-to-Electricity efficiency (η_{M2e}) is based on Eq. (43), and the total Metal-to-Heat efficiency ($\eta_{M2th,tot}$) is calculated according to Eq. (44), resulting in the total Metal-to-Energy efficiency ($\eta_{M2E,tot}$, Eq. (45)). Therefore, the total Power-to-Metal-to-Storage-to-Energy efficiency ($\eta_{ReMeF-cycle}$) is given by Eq. (46):

$$\eta_{ReMeF-cycle} = \eta_{P2M} \cdot \eta_{M2E,tot} \quad (46)$$

This leads to a total ReMeF redox cycle efficiency of **60% for aluminium, 54% for iron, and 59% for the silicon** molten salt electrolysis pathway considering the oxidation reaction with water at low temperatures.

In general, the following ReMeF-to-electric and/or heat conversion units can be considered (LT = low temperature conversion, HT = high temperature conversion):

- LT-Al-water oxidation reaction & fuel cell (eff = 25% electric, and 70% heat [71])
- HT-Al-water oxidation reaction & steam cycle (eff = 59 to 70% [75])
- LT-Fe-water oxidation reaction & fuel cell (eff = 51% electric, and 44% heat)
- Si-water oxidation reaction & fuel cell (eff = 31% electric, and 64% heat)

3.4.5 Modulation of energy converters

Heat loads of buildings are usually slowly changing in the case of space heating and evened out or time-shiftable by the use of heat storage in the case of domestic hot water. Electric loads may be changing much faster, such that a Metal-to-Energy system may not be able to adapt fast enough. However, if short-term energy storage such as battery and heat storage units are integrated into the energy supply of a building, the Metal-to-Energy process can be run quite continuously with only slow changes in conversion output. Heat can be buffered in thermal storage, and a small hydrogen buffer within the converter can be used to adapt better to electric loads. A very fast response to quick changes in electric loads can additionally be achieved with battery storage.

3.5 Environmental assessment

The sustainable production of aluminium, iron, and silicon from renewable energy was assessed and the corresponding material flows of the ReMeF cycles were established and graphically presented. Based on this, the overall system boundary of the ReMeF cycles was determined. The identified individual process steps within the cycles allow for the allocation of the environmental impacts and thus for a more specific evaluation of these processes.

3.5.1 Goal and scope definition of LCA

The aim of this comparative LCA is to assess the environmental impact of the functional unit 1 MJ of energy (heat and electricity) produced from the complete metal redox cycle, including the industrial metal fuel production (Power-to-Metal), using the technologies identified in WP2, and the metal-to-energy conversion process (Metal-to-Energy) implemented decentral in buildings. The entire ReMeF circular economy concept will thus be implemented as interlinked processes. The transport of materials to and from the buildings is taken into account.

The results of this comparative "cradle-to-grave" LCA provide valuable insights into the proposed system concepts to examine and develop a sustainable system solution to cover the heating and electricity demand in buildings and act as seasonal energy storage at the same time.

Therefore, the authors emphasize that the LCA results of this study should not be used for comparative purposes outside of the defined system boundary and the intended application of the system. The proposed concept was specifically designed to produce domestic winter heat and electricity based on seasonally stored renewable energy, rather than to optimize the hydrogen production rate. Furthermore, it is the intention to directly convert the hydrogen to electricity via a fuel cell system and utilize the additional heat released from this conversion.

The geographical focus is on Switzerland and the EU-28 countries, with the ReMeF concept expected to enter the market in 2030. This means that neither the Power-to-Metal nor the Metal-to-Energy processes have reached the commercial phase at the time of writing, and therefore there is a lack of data on these technologies, which are filled with best approximations according to experts' opinions.

The intended audience of this LCA is the project partners and funding agency, the scientific community, as well as, the public. SPF will use the information from this study for public communications, to promote important insights for potential industry and to provide data for further projects regarding the research topic.

Figure 35 shows the system boundary of the complete metal redox concept. Within the material processing, the recovered reaction product (aluminium hydroxide, silicon hydroxide, or iron oxide) is treated (precipitation and separation), and calcinated in the case of aluminium and silicon storage cycle. Also, material losses of the reaction product are compensated. It is assumed that the process heat for the refining process is produced from renewable electricity with a 100% electricity-to-heat efficiency.

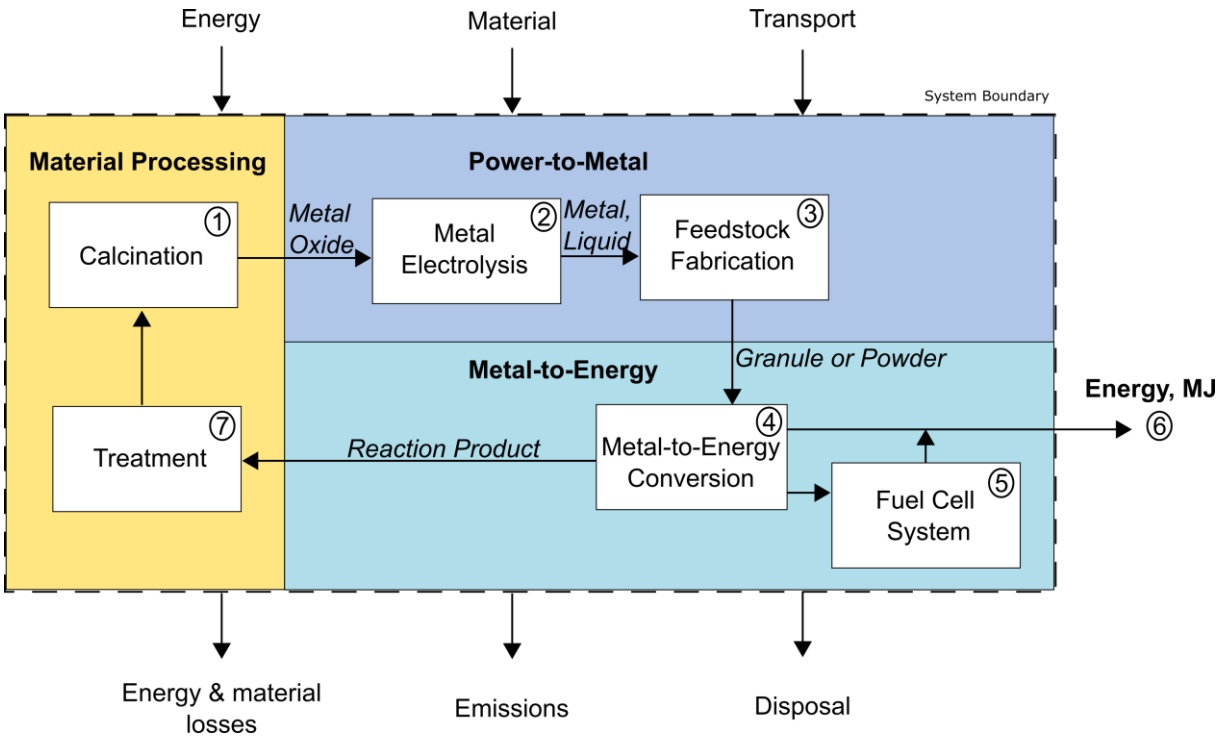

Figure 35: System boundary of the ReMeF circular economy concept using metal as source material. Reaction product which is lost in the process needs to be replaced. At the end of life, the metal is sent to the market for recycling.

The Power-to-Metal process is implemented according to the ReMeF technology identified and described in Chapter 3.3:

- Aluminium: Inert electrolysis
- Iron: Direct reduction with H_2
- Silicon: Inert electrolysis

The Metal-to-Energy process is implemented by applying the low-temperature pathway with winter energy production.

3.5.2 Life Cycle Inventory (LCI)

Minor or negligible inputs and outputs that will not significantly change the overall conclusions of the study are determined and subsequently omitted (Annex D). Specific process data on energy and material inputs are based on the technology assessment, the energy and mass balance and the energy efficiency evaluation according to Chapters 3.2 to 3.4.4. Based on current assumptions for the transport of heating oil, the transport of ReMeF to and from buildings was considered. The detailed LCI for the aluminium redox cycle is

given in D.3, for the silicon redox cycle in D.4 and for the iron redox cycle in D.5. Ecoinvent 3.9 datasets applied for resource extractions of aluminium hydroxide, iron oxide and sand assume standard mining practice (on land) and state-of-the-art technology used today (D.2).

The following section (Table 14 to Table 20) describes the LCI of the different redox cycles. Based on the system boundary, the LCIs are categorised according to their interlinked processes.

Table 14: Description of the calcination process to produce metal oxides for the different redox cycles.

Calcination (Figure 35 – 1, section material processing)	
Aluminium	In- and outputs of aluminium oxide/hydroxide are calculated according to the stoichiometry (1.53 kg$Al(OH)_3$ => 1 kg Al_2O_3 + 0.53 kg H_2O). The Bayer process to replace lost aluminium hydroxide: The $Al(OH)_3$ extraction process involves adding milled bauxite to a hot caustic soda (NaOH) solution, dissolving the aluminium-bearing minerals (gibbsite, boehmite and diaspore) present to form a sodium aluminate supersaturated solution or “pregnant liquor”. Flocculants are added to aid settling and the solution is progressively cooled causing aluminium hydroxide crystals to precipitate. Calcination process to produce aluminium oxide: Hydrate alumina crystals are heated in the calcination process. The heat in the calciners drives off combined water leaving alumina deposited.
Silicon	In- and outputs of silicon oxide are calculated according to the stoichiometry (1.6 kg $Si(OH)_4$ => 1 kg SiO_2 + 0.6 kg H_2O). Because silicon dioxide (SiO_2) is equivalent to sand, its production does not require an energy-intensive process to replace lost material. Hydrated silica crystals are heated during the calcination process. The heat in the calciners drives off the combined water, leaving silica as a deposit.
Iron	As the Fe-to-Energy conversion process directly produces iron oxides, no calcination process is required for the iron redox cycle.

Table 15: Description of the electrolysis and casting process to produce renewable metals for the various redox cycles.

Metal Electrolysis (Figure 35 – 2, section Power-to-Metal)	
Aluminium	In- and outputs of aluminium oxide/hydroxide are calculated according to the stoichiometry (2 $Al_2O_3 \rightarrow$ 4 Al + 3 O_2). Electrolysis: Cells equipped with inert anodes will not emit any CO_2 and CO from the electrolysis process. There will also be no emissions of CF_x as carbon anodes are eliminated. In addition, all emissions of PAH (from coal tar pitch used in the anodes, especially Söderberg anodes) and sulfur compounds, mainly SO2 (from sulfur compounds in the carbon anode raw materials) will be eliminated. Due to a new vertical inert cell design, the energy requirement is expected to be 13.2 kWh_e per 1 kg of aluminium produced. In

	this case, aluminium is generally produced by the electrolytic reduction of alumina (Al_2O_3), dissolved in a molten bath of potassium fluoride, sodium fluoride, and aluminium fluoride at a temperature of approximately approx. 800 °C. Casting: After the electrolysis, aluminium is refined to remove impurities such as sodium, calcium oxide particles and hydrogen. This refining stage is performed by the injection of a gas into the molten metal usually in an in-line reactor. Liquid aluminium is directly used to fabricate granules (see fabrication process). Additional small quantities of skimming are also produced at this stage and are removed from the surface of the molten metal (dross).
Silicon	Electrolysis: This dataset represents the production of 1 kg of metallurgical-grade silicon (MG-silicon) with a purity of 99% in molten salt electrolysis cells. Based on the literature, the minimum theoretical electricity input is 7% higher to electrolyze Si than Al, which results in 14.4 kWh_e. Air emissions of different pollutants are extrapolated from environmental reports. Casting: This dataset represents the casting of liquid silicon metallurgical grade from SiO_2 electrolysis. The refinement process of molten silicon involves introducing a gas mixture (oxygen/nitrogen) through a porous plug located at the base of the transport ladle. The addition of oxygen gas serves to reduce the content of slag-forming impurities, primarily calcium and aluminium. Following the oxygen refining stage, the molten silicon is cast into shallow open cast-iron moulds and left to cool to room temperature for about 24 hours. The resulting solid silicon lumps are hard, yet somewhat fragile, making it conducive to mechanical milling. In the concluding industrial phase, the metallurgical-grade silicon (MG-Si) undergoes crushing to achieve the desired size, employing large-scale crushers such as jaw crushers, cone crushers, and roll crushers [102].
Iron	Electrolysis: This dataset represents the production of sponge iron using the DRI-H_2 process. After iron ore mining, beneficiation and pelletisation, iron ore and iron pellets are fed as input to this process to produce direct reduced sponge iron (solid-state) with hydrogen. Due to the lack of data for hydrogen, the electricity consumption for Power-to-H2 production was estimated at 2.91 kWh_{el} per kg of sponge iron. Based on the literature, the specific hydrogen requirement is 637 Nm3H2/t of sponge iron. This amount is required both for the reduction of the iron ore and to compensate for the purging rate in the first preheating stage. Using a Power-to-H2 efficiency of 70%, this can be converted into an energy requirement of 3.01 MWh_e/tH_2. Preheating to the inlet temperature of 940 °C in the shaft furnace has a specific energy requirement of 0.23 MWh_e/tH_2. The energy requirement of the Arcelor Mittal Hamburg reaction plant of 0.07 MWh_e/tFe is used as a reference for the auxiliary equipment. This gives a total specific energy requirement of 3.31 MWh_e/tFe. The degree of metallisation, defined as the degree of conversion of iron oxide to metallic iron, is 92 to 96% in a typical DRI-H2 process.

Table 16: Description of the fabrication process to produce feedstock (granules or powder) for the oxidation reaction (conversion) of the various redox cycles.

	Feedstock Fabrication (Figure 35 – 3, section Power-to-Metal)
Aluminium	Aluminium in the form of granules is obtained directly in the casthouse by quenching molten aluminium in water or steam to produce a granular product that is dried and ground into specific geometries.
Silicon	After the electrolysis and casting, the silicon ingot is crushed to powder. The Ecoinvent reference dataset of this process is “rock crushing”.
Iron	After the electrolysis, sponge iron (solid pellets) is crushed into powder using a rock-crushing machine. The Ecoinvent reference dataset of this process is “rock crushing”.

Table 17: Description of the oxidation reaction (Metal-to-Energy conversion) to produce winter heat and electricity in buildings.

	Metal-to-Energy Conversion (Figure 35 – 4, section Metal-to-Energy)
Aluminium	In general, a dense protective oxide film is formed on the aluminium surface. This film is passive in a neutral aqueous solution but can be dissolved in an alkaline aqueous solution. A temperature of 65 °C was chosen for the Al-water reactions because the heat extraction of the Alu-to-Energy converter is expected to be of interest at this temperature for domestic hot water preparation and space heating. Based on the reaction: $2Al + 6\ H_2O(l) \rightarrow 2\ Al(OH)_3 + 3\ H_2$; $\Delta Hr, 298 = -839$ kJ/mol, a theoretical maximum of 0.111 kg of H2 can be produced from each kg of Al. The maximum amount of heat that can be expected from a reaction at 65 °C ($\Delta Hr, 333 = -879$ kJ/mol) is 4.53 kWh_{th} (16.3 MJ) per kg Al.
Silicon	In general, a dense protective oxide film is formed on the silicon surface. This film is dissolved via a potassium hydroxide solution. Based on the reaction: $Si + 4\ H2O(l) \rightarrow Si(OH)_4 + H_2$; $\Delta Hr, 298 = -333$ kJ/mol (3.3 kWh_{th} per kg of Si). In addition, a theoretical maximum of 0.14 kg of H_2 can be produced from each kg of Si.
Iron	Based on the reaction $3\ Fe + 4\ H_2O(l) \rightarrow Fe3O_4 + 4\ H_2$; $\Delta Hr, 298 = + 25$ kJ/mol (0.048 kg H_2), the reaction product obtained is iron oxide with a hydrogen yield of 0.05 kg per kg of Fe. This iron oxidation reaction with water is endothermic. The energy input required for continuous operation is 0.04 kWh_{th} per kg of Fe, which is provided by the fuel cell heat recovery after initial start-up.

Table 18: Description of the fuel cell system to convert hydrogen to electricity and heat.

Fuel cell system (Figure 35 – 5, section Metal-to-Energy	
All redox cycles	The hydrogen produced in the Metal-to-Energy conversion process is directly converted in a fuel cell system to produce electricity and heat. The assumed efficiency of the fuel cell is 50% for electricity and 47% for heat recovery.

Table 19: Description of the allocation of the total energy output of the redox cycles.

Energy output of the redox cycle (Figure 35 – 6, functional unit)	
All redox cycles	Depending on the Metal-to-Energy and fuel cell process, the produced heat and electricity are allocated to form 1 MJ of total energy (functional unit).

Table 20: Description of the reaction product treatment required for recycling and re-introduction of the source material to metal oxide reduction.

Reaction product treatment (Figure 35 – 7, section material processing)	
Aluminium	The Ecoinvent reference dataset for this treatment process is the production of aluminium hydroxide. Only data inputs such as energy and water requirements for washing and drying the obtained product are considered. However, the energy input is a rough estimate and cannot be validated at this research state.
Silicon	In general, no data are available for this process. As the reaction product is silicon hydroxide, it is assumed that the same treatment as for the aluminium redox cycle reaction product is required.
Iron	It is assumed that this process is not required because for the iron redox cycle, but this assumption remains to be proven.

In general, the LCI of each process is based on the Ecoinvent reference datasets as shown in D.2.

3.5.3 Life Cycle Inventory Assessment (LCIA) and interpretation

In this section, the LCIA results are presented for the production per 1 MJ of energy generated to be used in a multiple-dwelling building in Switzerland. The charging process (Power-to-Metal) is assumed to take place at an industrial site in Switzerland, while the discharging process (Metal-to-Energy) will be carried out decentral in buildings. Therefore, transportation of the materials is considered.

3.5.3.1 *Global Warming Potential (GWP)*

GWP is a climate change impact assessment method that expresses the integrated radiative forcing over time (100 years chosen) of a greenhouse gas relative to that of CO_2, expressed in units of, e.g., gCO_2eq.Since the idea of the ReMeF concept is to store renewables in an easy to store and transport energy carrier, it is assumed that 100% renewable energy is used for the charging process. It should be noted that the total GWP of ReMeF highly depends on the type of renewable energy used within the storage cycle. Figure 36 provides an overview of the GHG emissions related to various electricity sources from the United Nations report on Life Cycle Assessment of Electricity Generation Options (2021) [103]. Under European conditions, the GWP of hydropower is the most favourable choice, followed by wind and PV electricity. PV technologies show lifecycle GHG emissions of about 10 gCO_2eq/MJ_e. Frischknecht and Krebs (2020) estimate GHG emissions for a 3 kW_p PV rooftop installation in Switzerland at 11.7 gCO_2eq/MJ_e[2] based on an average global production [104].

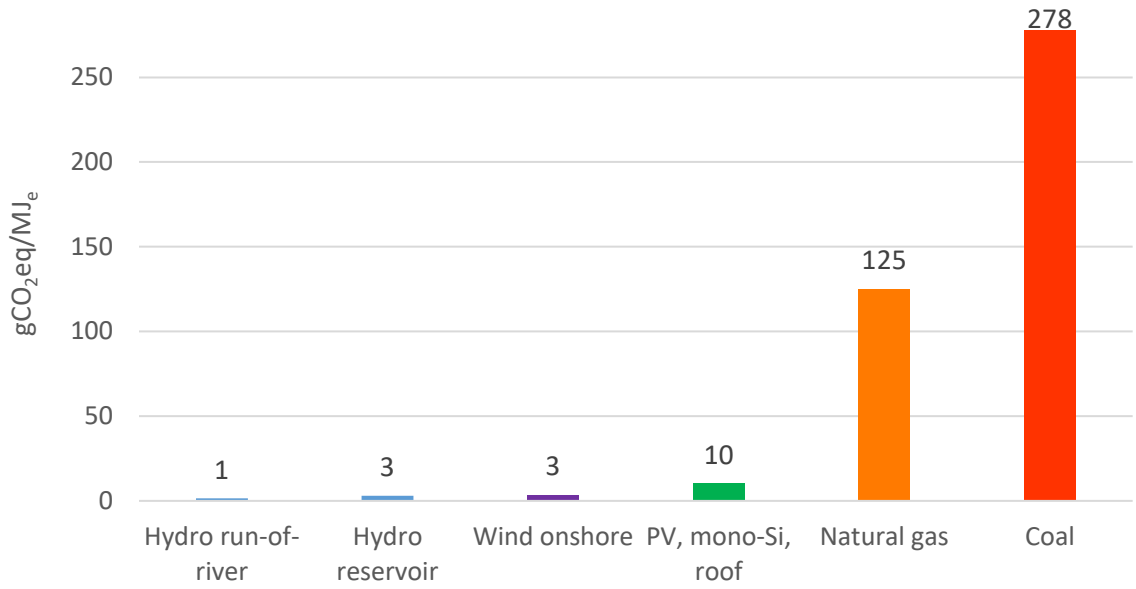

Figure 36: Comparison of the GHG emission for electricity production in Europe based on the United Nation report from 2021 [103].

To assess the life cycle GHG emissions of the ReMeF storage cycle, the following LCIA results are modelled assuming a GWP of 10 gCO_2eq/MJ_e for (PV) electricity input for charging. In addition, a sensitivity analysis of the electricity input was carried out, which allows for the assessment of GHG emissions independently on specific electricity impact parameters or assumptions (Chapter 4.2).

[2] annual electricity production 975 kWh/kW_p, lifetime 30 years for panel and 15 years for an inverter with module efficiency of 18 to 19.5%

Aluminium redox cycle

Figure 37 presents the GHG emissions for the different system processes in terms of raw materials, electricity, and other inputs. Overall, 58% of the GHG emissions can be attributed to the electricity input (assumption: PV), which is mainly used for the calcination, electrolysis, and reaction product treatment. GHG emissions from the considered fabrication process of aluminium granules are neglectable because the granules are produced at the electrolysis process by refining and quenching liquid aluminium which does not need any major additional energy input.

Within the Alu-to-Energy process, the material for the converter (steel), a loss rate of NaOH (10%) and a loss rate of the reaction product ($Al(OH)_3$) of 3% are considered. For the fuel cell system, material and maintenance requirements are included, contributing about 3% to the total GWP. Overall, the total GHG emissions for the aluminium storage cycle are estimated to be 26 gCO_2eq/MJ of energy output (26% electricity, 74% heat).

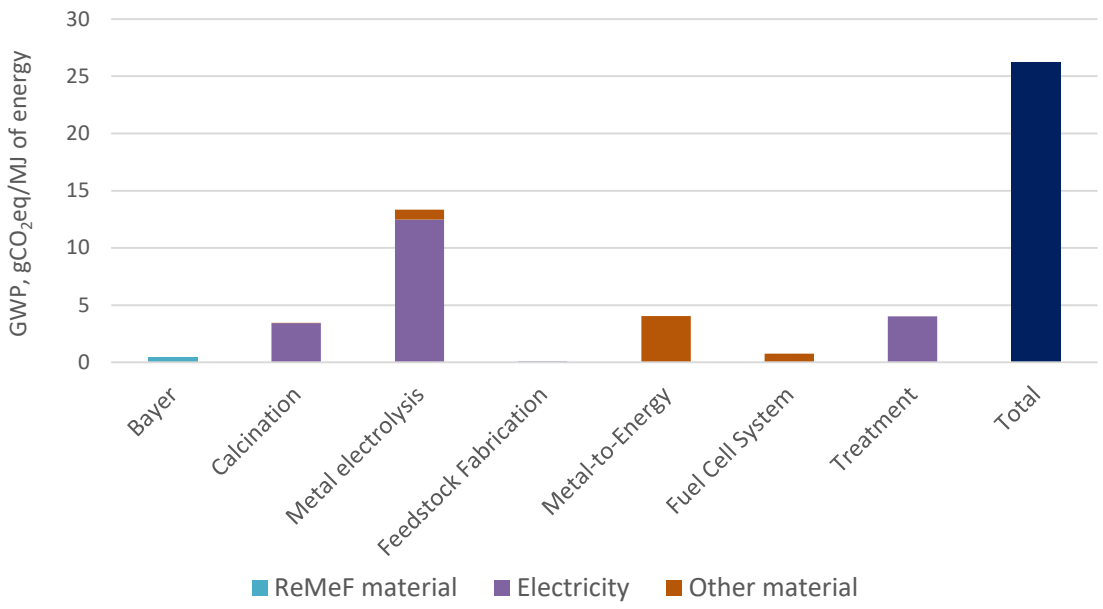

Figure 37: Share of GHG emissions related to the different processes and inputs (inclusive loss of NaOH: 10%, and loss of reaction product: 3% as $Al(OH)_3$. For electricity a GWP of 10 gCO_2eq/MJ_e was assumed. Total GWP: 26 gCO_2eq/MJ of energy (heat and electricity produced in winter).

Iron redox cycle

For iron production, the reaction product (iron oxide) is sent to the pelletizing process. Based on the Ecoinvent reference dataset “iron pellet production” this is a rather material-intensive process (e.g., other than iron oxide: lime, dolomite, bentonite, chromium). Furthermore, lost iron oxide of 3% is compensated leading to a total of 6 gCO_2eq/MJ of energy output (Figure 38). For the DRI-H_2 electrolysis to produce sponge iron, the electricity

input (assumption: PV) accounts for 70% of the GWP. However, the crushing of the sponge iron into powder is estimated to be negligible.

It is important to note that for the Fe-to-Energy process, the size of the converter is not adjusted when compared to the Alu-to-energy process, although it is known that twice the amount of feedstock needs to be converted to achieve an equivalent hydrogen output. However, the separation of the reaction product (iron oxide) may be less material-intensive compared to the Alu-to-Energy process. Therefore, this assumption can be justified.

The total GHG emissions of the iron redox cycle was estimated to be 24 gCO_2eq/MJ of energy output (50% electricity, 50% heat).

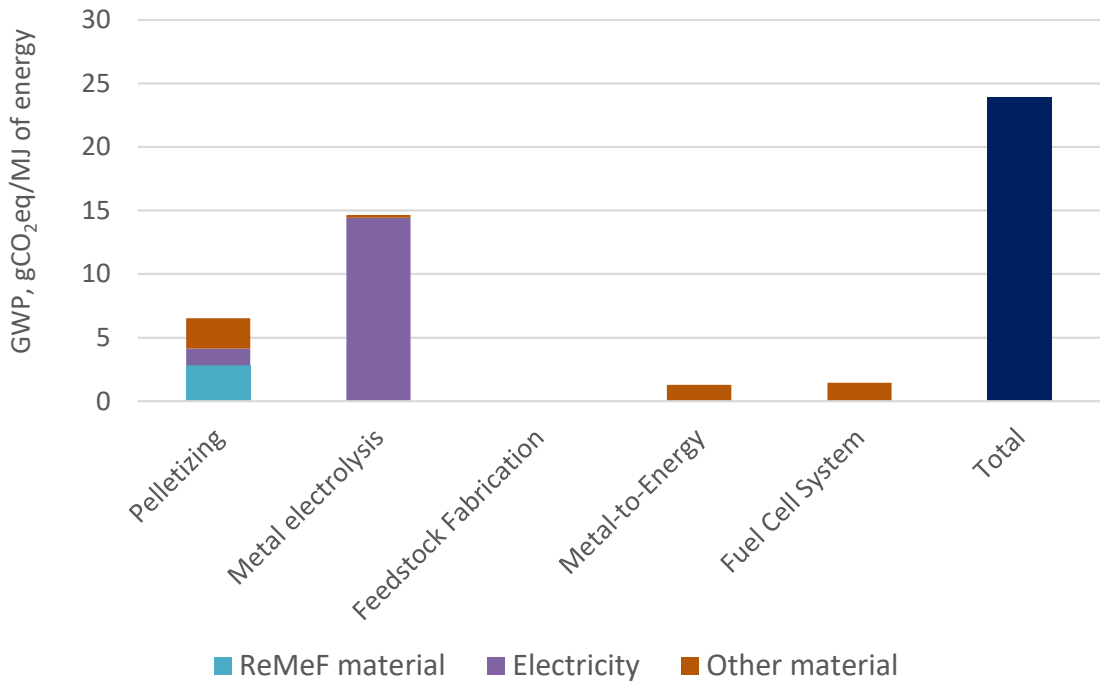

Figure 38: Share of GHG emissions related to the different processes and inputs (inclusive loss of reaction product: 3% as iron oxide. For electricity a GWP of 10 gCO_2eq/MJ_e was assumed. Total GWP: 24 gCO_2eq/MJ of energy (heat and electricity produced in winter).

Silicon redox cycle

The calcination process of silicon hydroxide includes a 3% loss rate that occurs in the Metal-to-Energy process. The electricity (assumption: PV) used for silicon production by electrolysis accounts for 54% of the total GWP of 20 gCO_2eq/MJ of energy stored in the silicon.

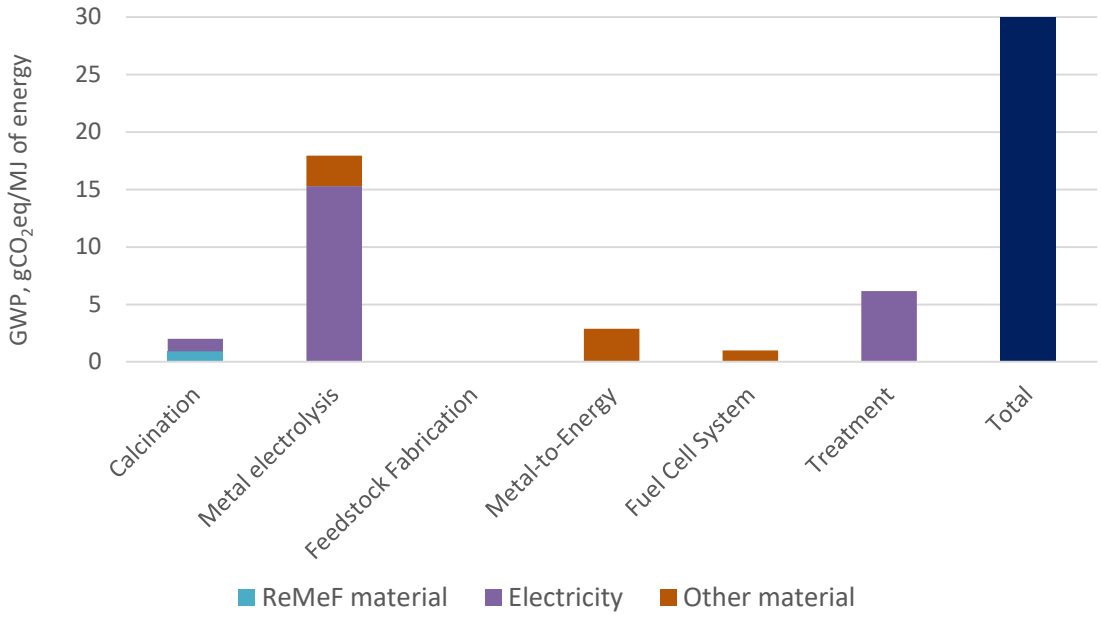

Figure 39: Share of GHG emissions related to the different processes and inputs (inclusive loss of KOH: 10%, and loss of reaction product: 3% as $Si(OH)_4$. For electricity a GWP of 10 gCO_2eq/MJ_e was assumed. Total GWP: 30 gCO_{2eq}/MJ of energy output (heat and electricity produced in winter).

In addition, it is estimated that 6 gCO_{2eq}/MJ of energy output can be attributed to the treatment of the reaction product before it can be reintroduced into the calcination process. Figure 39 shows the total GHG emission for the silicon storage cycle which is estimated at 30 gCO_{2eq}/MJ of energy output (32% electricity, 68% heat).

3.5.3.2 European Environmental Footprint

The Environmental Footprint (EF) method, endorsed by the European Commission, assesses the midpoint impact categories of products and organizations. Implemented in SimaPro, it includes the latest IPCC 2021 factors, making it a preferred method for LCA studies representing a political consensus and is seen as state-of-the-art in Europe.

The impact categories (Figure 40) evaluated by EF v3.1, which are described in detail in Annex D.6, shows the normalized results of the selected ReMeF redox cycles. The normalization refers to calculating the magnitude of category indicator results relative to reference information which is specified in each LCIA method [105].

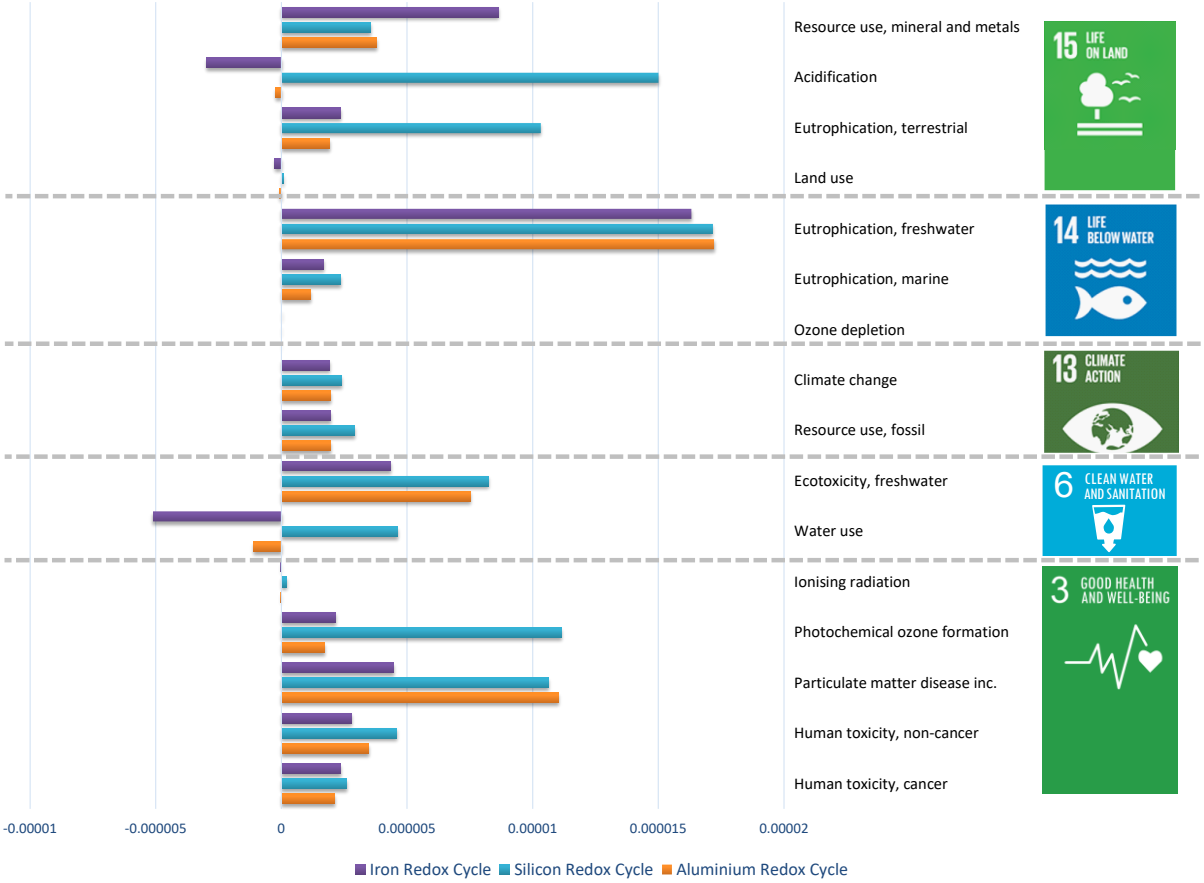

Figure 40: LCIA results (normalized) based on the EF v3.1 method of the selected ReMeF redox cycles (Annex D.7).

Other impact categories such as life on land, show that resource use on mineral and metals was highest for iron, followed by aluminium and iron, whereas acidification was highest for silicon. For the life below water, specifically freshwater eutrophication was estimated to be the highest for all ReMeF storage cycles compared to marine eutrophication marine and ozone depletion. In this case, the results for climate action categories were rather similar for all ReMeF storage cycles. Indicators for good health and well-being show overall the lowest values for iron, followed by aluminium, while particularly high results are estimated for silicon for photochemical ozone formation.

Land use, and water use result in negative numbers due to the chosen avoided burden approach which is an intrinsic consequence of this approach.

3.6 Impact on the Swiss energy system

3.6.1 Swiss energy system simulation

From the Energy Perspectives 2050+, the energy mix of the ZERO Basis scenario has been taken as a base to start with for the calculation with the Powercheck tool. Some deviations of inputs are described below. The calculation methodology of this tool differs somewhat from the calculation tools used for the Energy Perspectives 2050+, therefore, there are also minor differences in the results. A detailed list of input parameters can be found in the Annex E.

It is important to know that no fossil fuels or other fuel imports (no coal, gas, oil, uranium), and no Power-to-X or X-to-Energy are assumed yet before evaluation of the potential to use Power-to-Metal and Metal-to-Power.

3.6.2 Detailed results of heat and electricity demand

Heat demand

The heat demand is divided into multi-family houses and single-family houses. Office buildings and other large, heated buildings are also counted as multi-family houses to cover the entire Swiss heat demand of the building stock and not only that of residential buildings. In addition to space heating, the heat demand for domestic hot water and process heat is also calculated.

Figure 41 shows the result of the simulation for the year 2050. The heat demand is divided into space heating for MFH and SFH, domestic hot water and process heat, for each week of the year. As expected, the demand for space heating is close to zero in summer. Domestic hot water and process heat are required all year round.

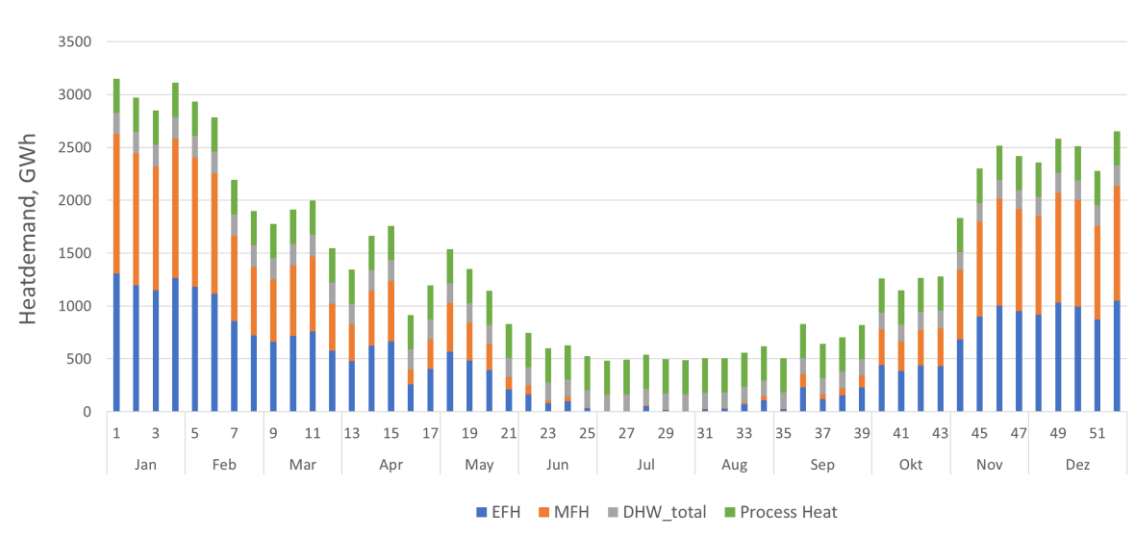

Figure 41: Swiss heat demand for each week of the year 2050.

Electricity balance

Four different simulations were carried out. Figure 42 shows the respective summer surpluses and winter deficits. The largest difference is between Pes and HighPV. The other two scenarios, in which more PV winter yield was targeted (and nothing else was changed from HighPV), each show a slight decrease in winter deficit compared with the previous scenario.

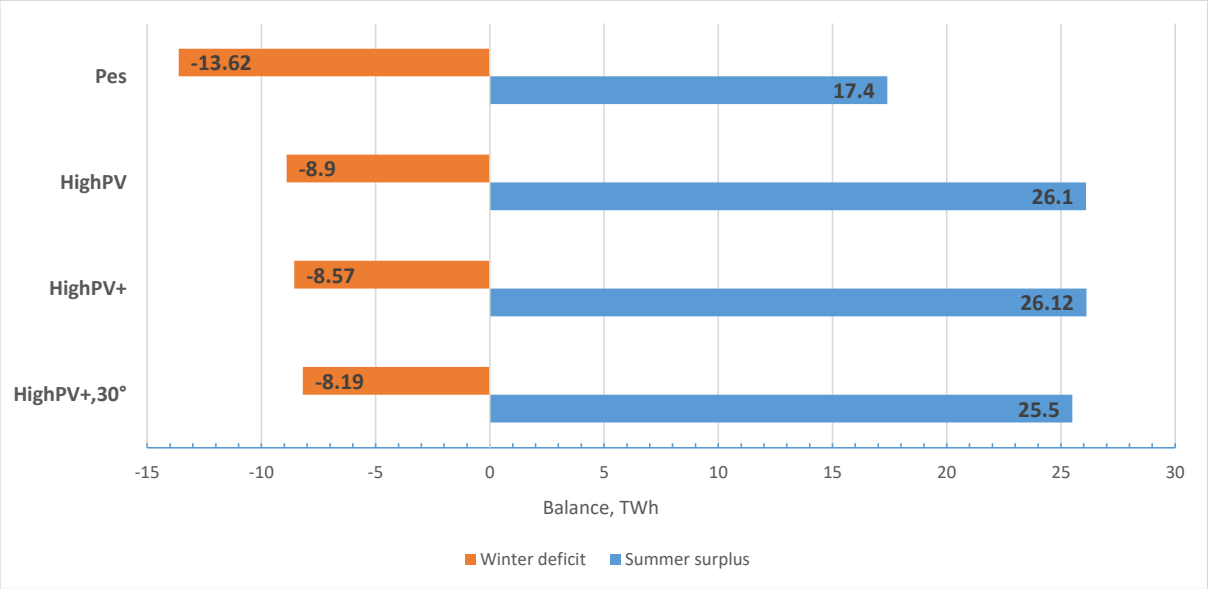

Figure 42: Electricity balance of the four simulated scenarios.

For the sake of simplicity, only the two scenarios Pes and HighPV+,30° are considered in more detail below and taken into account for the potential of ReMeF.

Figure 43 and Figure 44 show the electricity balances of 2050 with weekly values for the two scenarios PES and HighPV+,30°. As expected, the electricity balance is positive (surplus) in the summer half-year and negative (deficit) in the winter half-year. Table 21 shows the totals (summer and winter, where summer includes April to September and winter October to March).

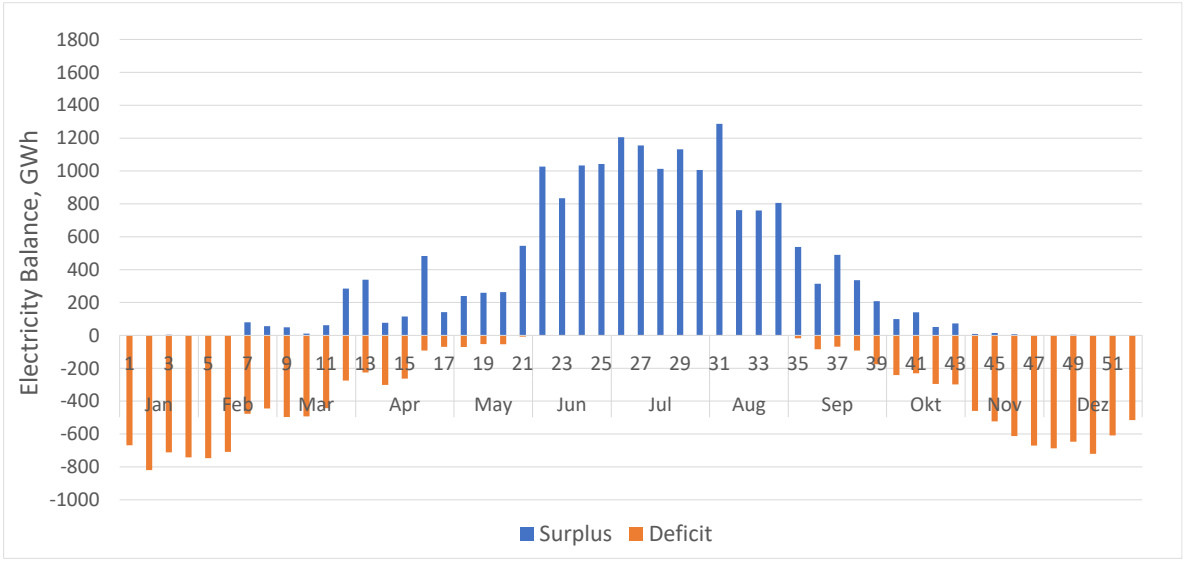

Figure 43: Weekly balance of the Swiss electricity system simulated for the year 2050 (PES).

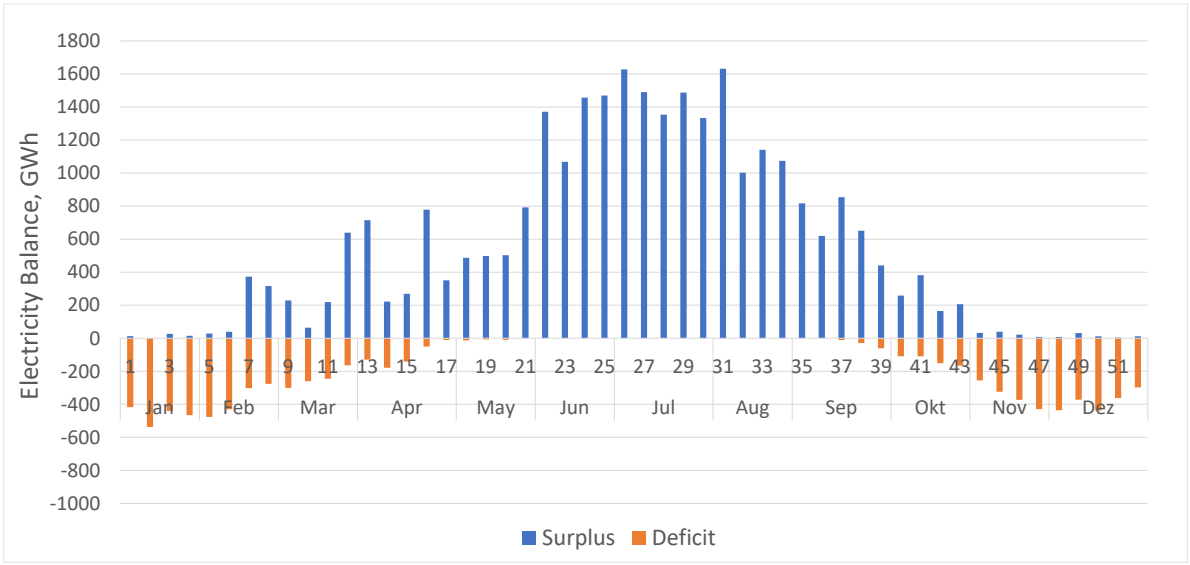

Figure 44: Weekly balance of the Swiss electricity system simulated for the year 2050 (HighPV+,30°).

Table 21: Electricity surplus/deficit in summer/winter half year.

		PES	HighPV+,30°	ZERO Basis
Summer surplus	**(Apr. – Sep.)**	17.4 TWh	25.5 TWh_{el}	9 TWh_{el}
Winter deficit	**(Oct. – Mar.)**	13.6 TWh	8.2 TWh_{el}	9 TWh_{el}

3.6.3 Potential of ReMeF

A total of four scenarios are used. Two different proportions (100% and 50%) of MFH equipped with Metal-to-Energy and two different total capacities of the installed units for each of the two proportions. The capacity of the units is chosen such that the units can be operated in full-load approximately four months of the year (higher capacity) or 6 months of the year (lower capacity) as shown in Table 22.

Table 22: The four assumptions with different heat demands covered.

Assumption Name	Amount of MFHs	Installed Power	Heat demand covered
100% / 2.4GW	100% MFHs	2.4 GW_{th}	400 GWh_{th} / Week
100% / 1.2GW	100% MFHs	1.2 GW_{th}	200 GWh_{th} / Week
50% / 1.2GW	50% MFHs	1.2 GW_{th}	200 GWh_{th} / Week
50% / 0.6GW	50% MFHs	0.6 GW_{th}	100 GWh_{th} / Week

Figure 45 and Figure 46 show the heat demand for 100% of the MFHs and 50% of the MFHs in the winter half-year (October to March) and the two different heat production capacities from ReMeF indicated by the horizontal lines.

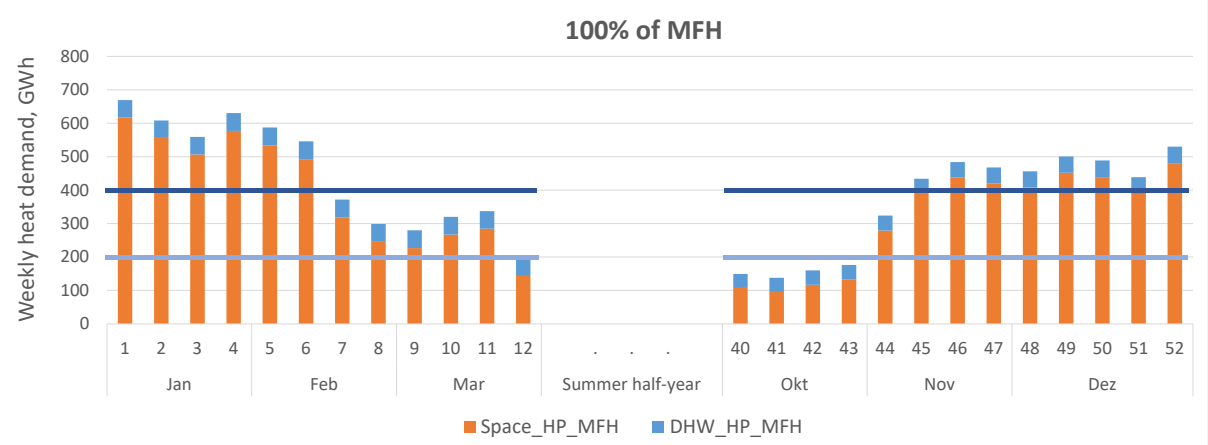

Figure 45: Weekly heat demand supplied by heat pumps for 100% multi-family houses (MFH). Orange bars represent space heating, and blue bars represent domestic hot water (DHW). The blue and dark blue lines show the installed heating power by ReMeF for the calculations of this report.

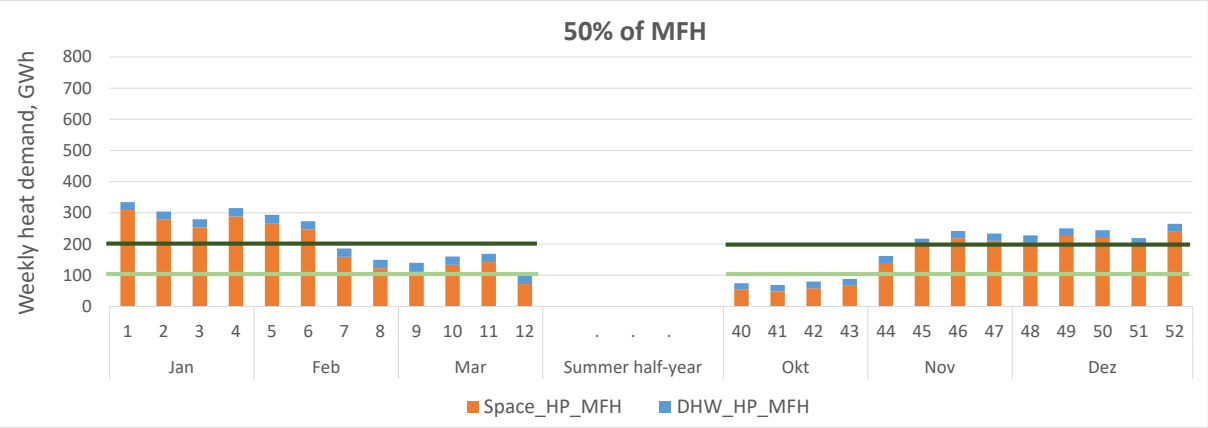

Figure 46: Weekly heat demand supplied by heat pumps for 50% of multi-family houses (MFH). Orange bars represent space heating, and blue bars represent domestic hot water (DHW). The green and dark green lines show the installed heating power covered by ReMeF for the calculations of this report.

Surplus electricity used for production of ReMeF

To see how much of the required ReMeF in Switzerland can be covered by the summer surplus, two assumptions were used for the installed capacity, corresponding to a full-load operation of 5 months (lower capacity) and of 3 months. The first leads to a dimensioning of 1.2 GW_{el} (consumption of 210 GWh_{el} per week), and the second to a dimensioning of 4.5 GW_{el} (consumption of 760 GWh_{el} per week) for the scenario PES (Figure 47).

For the scenario HighPV+,30°, the installed capacites are 2.6 GW_{el} (consumption of 440 GWh_{el} per week) and of 6 GW_{el} (consumption of 1000 GWh_{el} per week) (Figure 48).

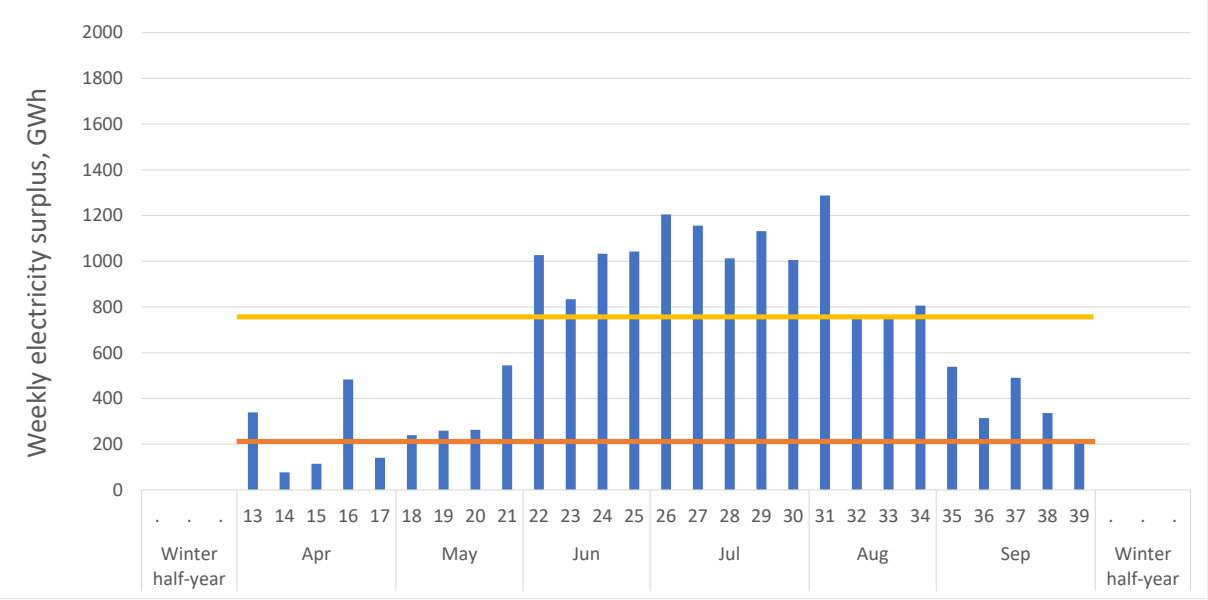

Figure 47: Electricity surplus in the summer half year (Apr. – Sep.) in Switzerland. The two lines show two different assumptions for the electricity used to produce ReMeF (PES).

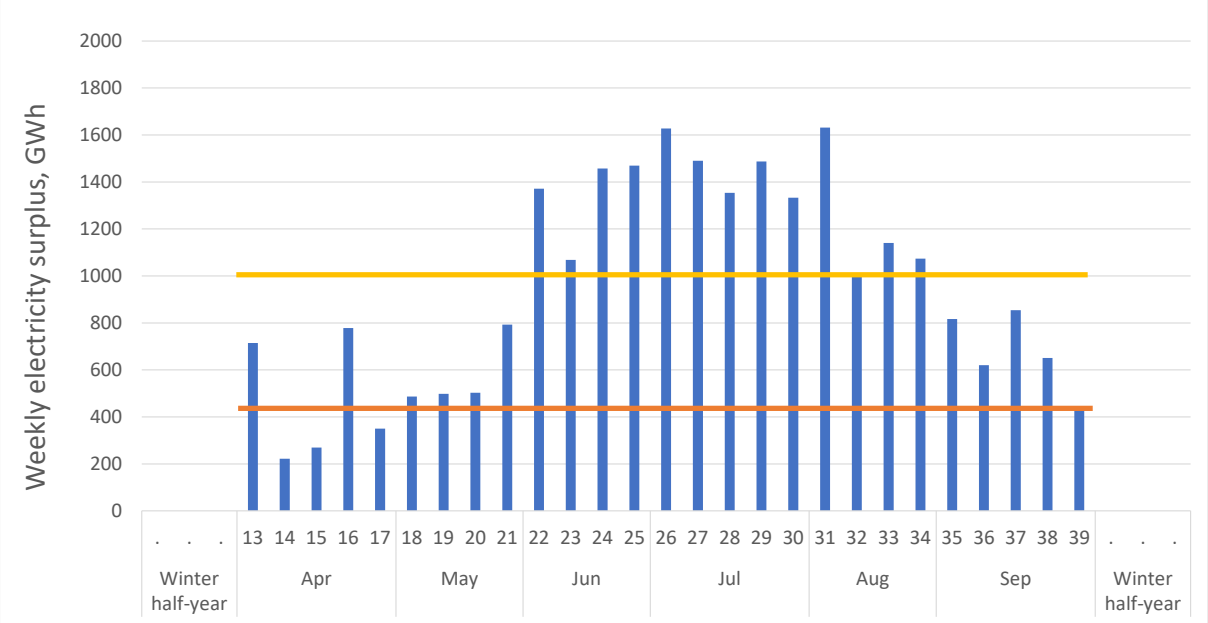

Figure 48: Electricity surplus in the summer half year (Apr. – Sep.) in Switzerland. The two lines show two different assumptions for the electricity used to produce ReMeF (HighPV+,30°).

Heat demand coverage

Table 23 shows the four assumptions of heat demand coverage. It shows how much total heat demand is covered in the winter half-year (October to March) and how much thermal power a ReMeF plant would need in each MFH to cover the demand. The heat demand is the same for both energy scenarios (PES and HighPV+,30°) and so is the covered heat demand.

Table 23: Overview of covered heat demand with ReMeF systems installed in the four different heat coverage assumptions.

	100% MFHs		**50% MFHs**	
	2.4 GW_{th}	**1.2 GW_{th}**	**1.2 GW_{th}**	**0.6 GW_{th}**
Covered heat demand (Oct.- Mar.)	9.0 TWh_{th}	5.1 TWh_{th}	4.5 TWh_{th}	2.5 TWh_{th}
Share of total MFH heat demand	82%	48%	41%	24%
Share of total building heat demand	30%	17%	15%	9%
Installed thermal power from ReMeF per MFH	10.3 kW_{th}	5.2 kW_{th}	10.3 kW_{th}	5.2 kW_{th}

Electricity savings

ReMeFs save electricity for two reasons. Firstly, they replace thermal power from heat pumps that would use electricity to provide heat. Secondly, electricity can be produced at the same time as heat in ReMeF Metal-to-Energy systems.

Figure 49 and Figure 50 (Pes and HighPV+,30°) show the comparison of electricity deficits in the winter half-year (October to March). The graphs show the deficits without the use of ReMeF and with the use of the three different metals as ReMeF in the four selected coverage assumptions.

A substantial decrease in the winter deficit can be seen when more MFH are equipped with Metal-to-Energy and when more total power is installed (from left to right for each metal).

For the energy scenario that uses pessimistic assumptions for the development of renewables (PES), the winter deficit decreases from almost 14 TWh to roughly 11 TWh for aluminium, 8 TWh for iron, and 10 TWh for silicon for a scenario with a high capacity (1.2 GW total) installed in 50% of the MFH.

For the scenario that uses more optimistic assumptions (HighPV+,30) the winter deficit can be reduced from 8 TWh to about 5 TWh for aluminium and silicon and to 2 TWh for iron, still considering the same case of 50% of the MFH equipped with a total of 1.2 GW. If all MFH were equipped with ReMeF based on iron with a total capacity of 2.4 GW, electricity could even be exported in winter (about 3 TWh).

The situation for iron is different from the other two metals due to the higher share of electricity generation. A more detailed balance sheet of the electricity savings can be found in E.3.

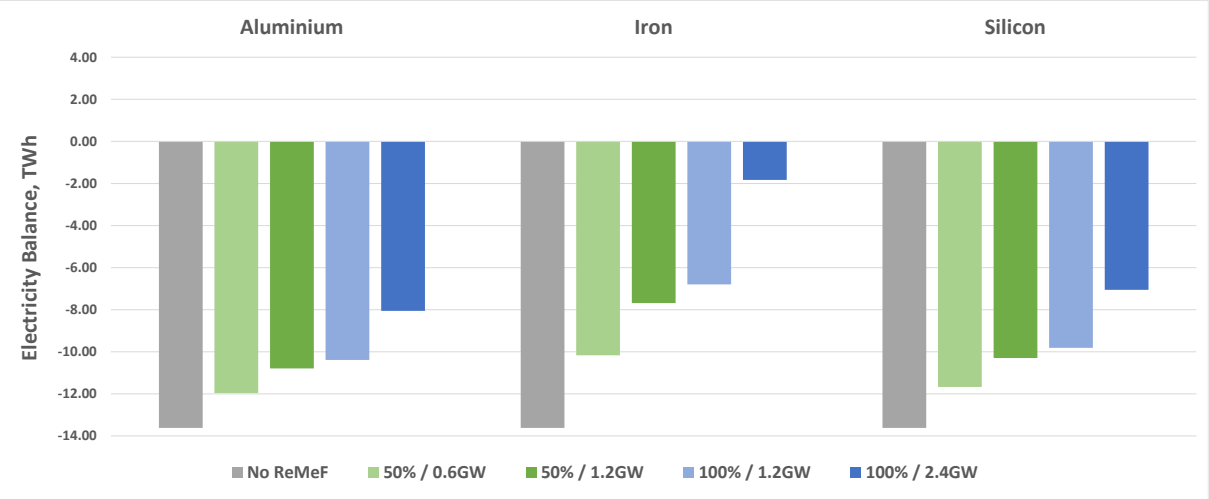

Figure 49: Comparison of the electricity balance in the winter half-year (Oct-Mar) before and after using ReMeF to produce heat and electricity. Negative values mean electricity imports or other electricity-producing technologies needed in addition for the scenario PES.

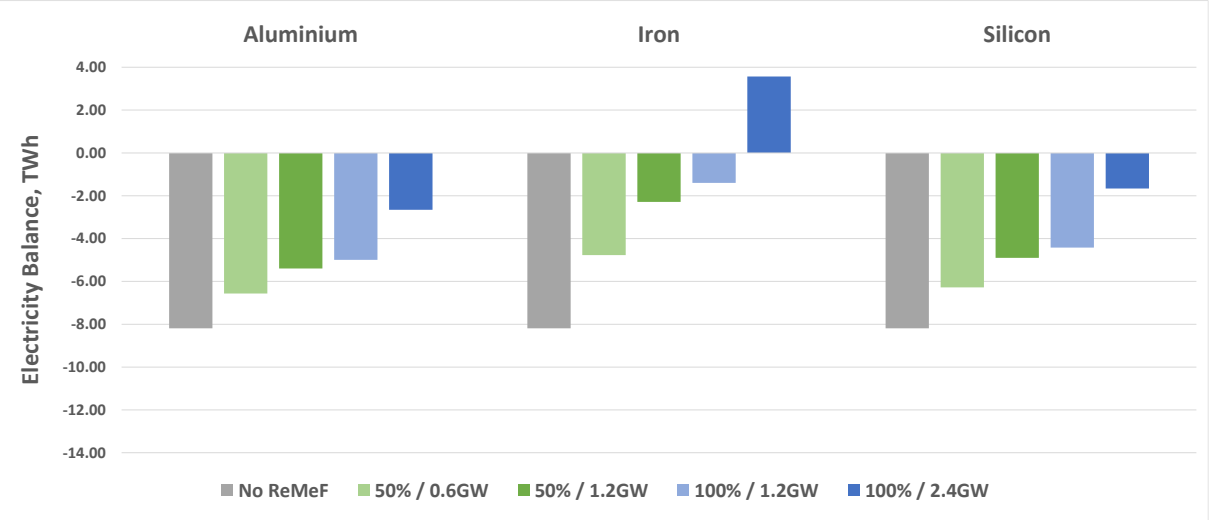

Figure 50: Comparison of the electricity balance in the winter half-year (Oct-Mar) before and after using ReMeF to produce heat and electricity. Negative values mean electricity imports or other electricity-producing technologies needed in addition for the scenario HighPV+,30°.

Figure 51 shows the amount of metal required in the four heat coverage assumptions. Here it is seen that although iron produces the most electricity, and therefore reduces the winter deficit the most, it also requires the most material. This is an effect of a higher share of electricity production on the one hand, i.e. more total energy turnover per kWh of heat produced, and a lower energy density per weight on the other hand.

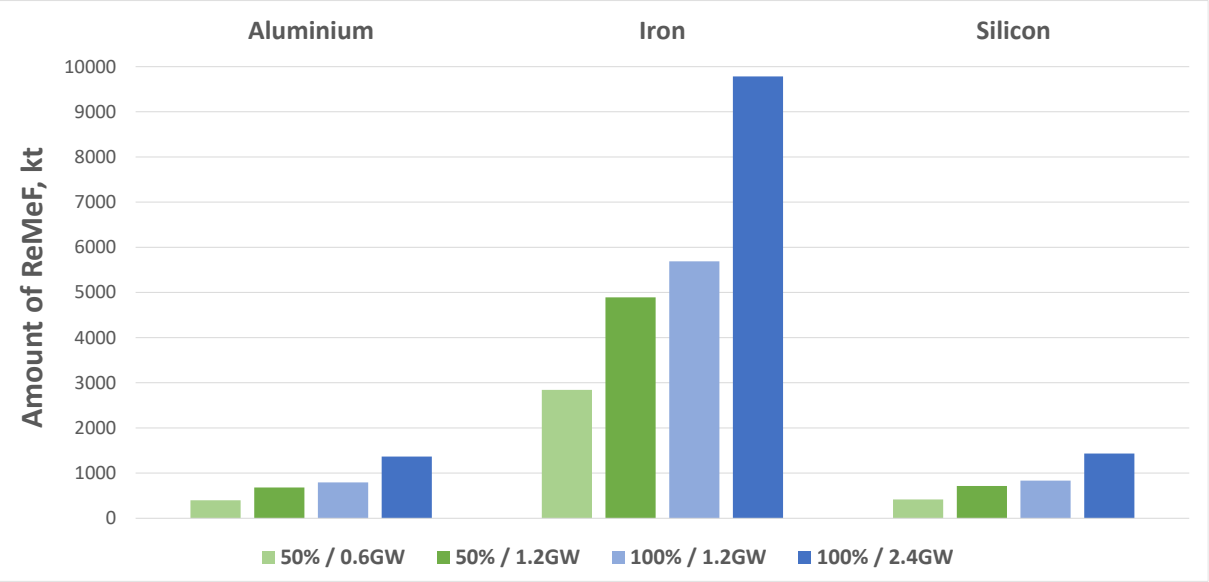

Figure 51: Theoretical amounts of ReMeF in kt needed to meet the heat demand of the four different heat coverage assumptions.

Production of ReMeF in the summer

In Scenario PES the two different production assumptions use 31% and 82% of the summer surplus, corresponding to a total amount of electricity of 5.3 TWh_e and 14.2 TWh_e respectively (Table 24).

In Scenario HighPV+,30° the two different production assumptions use 45% and 82% of the summer surplus, corresponding to a total amount of electricity of 11.4 TWh_e and 21 TWh_e respectively (Table 24).

Table 24: The two production capacity assumptions per energy scenario and how much electricity is used to produce ReMeFs in the summer half year, what share of the summer surplus is used and the needed electric power.

	PES		HighPV+,30°	
	1.2 GW_{el}	**4.5 GW_{el}**	**2.6 GW_{el}**	**6.0 GW_{el}**
Total electricity used	5.3 TWh_{el}	14.2 TWh_{el}	11.4 TWh_{el}	21 TWh_{el}
Share of summer surplus	31%	82%	45%	82%
weekly electricity demand	210 GWh_{el}	760 GWh_{el}	440 GWh_{el}	1000 GWh_{el}

Figure 52 and Figure 53 show the producible amounts of ReMeF in the two different production assumptions and the two energy scenarios PES and HighPV+,30°. The quantities that can be produced are very similar for aluminium and silicon, while they are slightly higher for aluminium. Much higher quantities can be produced with iron.

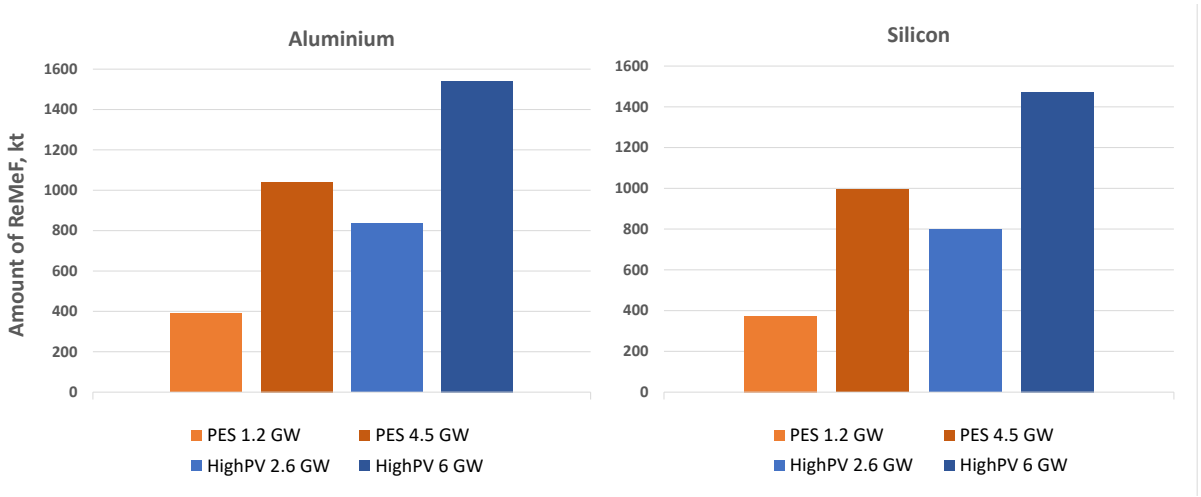

Figure 52: Amounts of ReMeF in kt producible in the two different production assumptions for both energy scenarios PES & HighPV+,30° with aluminium and silicon.

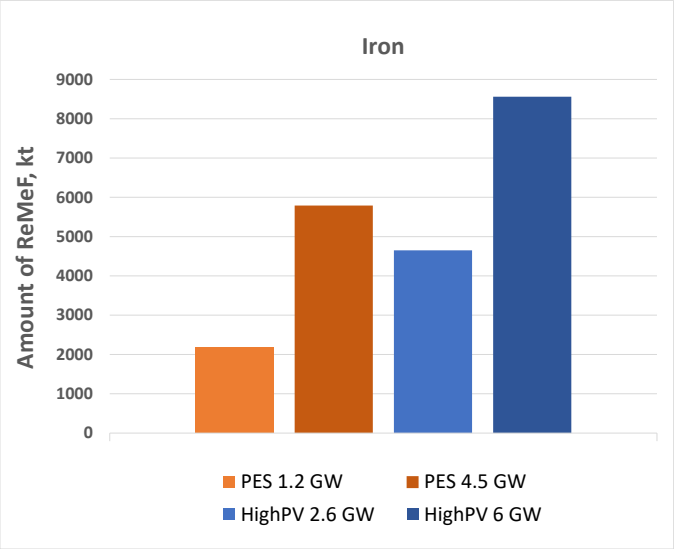

Figure 53: Amounts of ReMeF in kt producible in the two different production assumptions for both energy scenarios PES & HighPV+,30° with iron.

Winter coverage with ReMeF from summer surplus

Figure 54 and Figure 55 compare the amount of ReMeF required in the four winter coverage assumptions with the amount that can be produced in the two production assumptions described above.

In the PES scenario with the lower production assumption (1.2 GW), the amount of ReMeF produced is not sufficient to cover any of the winter coverage assumptions. On the other hand, with the higher production assumption (4.5 GW), all but the highest of the winter coverage assumptions (100% / 2.4 GW) can be covered by the produced ReMeF.

The HighPV+,30° energy scenario has a higher producible amount then PES and can therefore cover more of the needed amount of ReMeF: In the HighPV+,30° scenario with the lower production assumption (2.6 GW), the amount of ReMeF produced covers at least the lowest demand scenario. With the higher production assumption (4.5 GW), all but the highest of the winter coverage assumptions (100% / 2.4 GW) can be met with produced ReMeF based on iron or silicon, and with aluminium even the highest one.

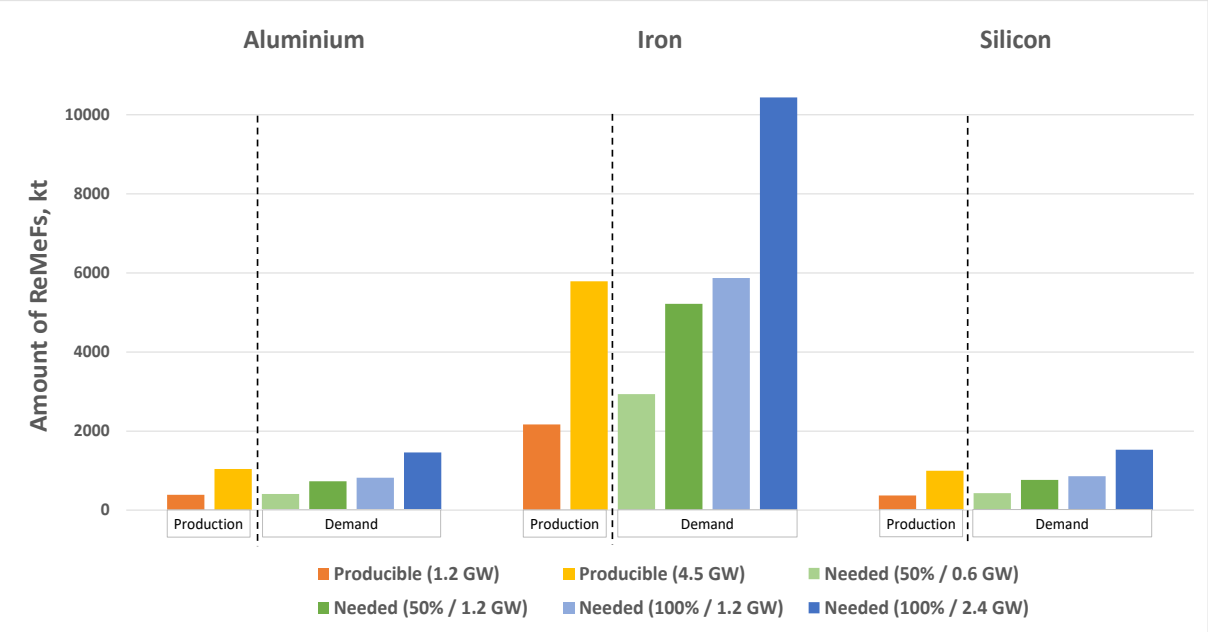

Figure 54: Comparison of needed amounts of ReMeF in the four heat coverage assumptions with the producible amounts of ReMeF with electricity surplus in the two production assumptions (PES).

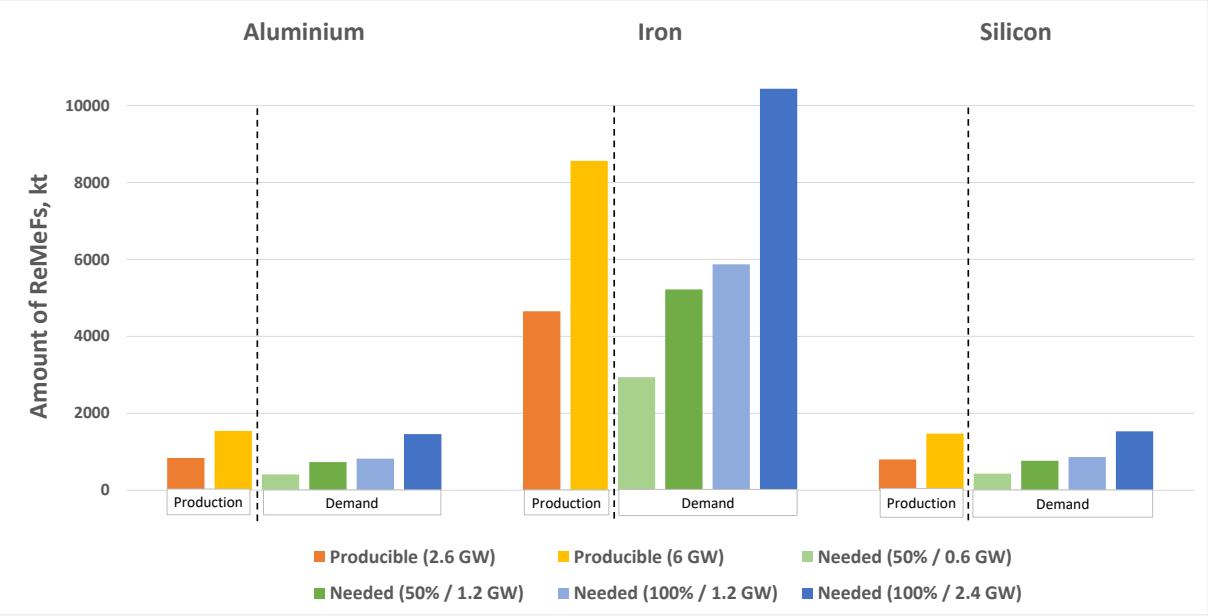

Figure 55: Comparison of needed amounts of ReMeF in the heat coverage assumptions with the producible amounts of ReMeF with electricity surplus in the two production assumptions (HighPV+,30°).

3.6.4 Potential CO_2-emission savings

The energy provided by Renewable Metal Fuels (ReMeF) effectively reduces the winter electricity deficit and thus potential CO_2 emissions associated with the coverage of this

deficit. This contribution is evaluated by comparing it with two alternative sources: natural gas-based electricity generation and electricity imports.

The analysis focuses on specific scenarios of winter electricity deficits as addressed by PES and HighPV+,30°, with ReMeF covering varying degrees of heat demand (100% / 2.4 GW, 100% / 1.2 GW, 50% / 1.2 GW, and 50% / 0.6 GW), as shown in Figure 49 and Figure 50. The potential CO_2-savings were calculated on the assumption that the winter energy supply by ReMeF is replacing (see also Chapter 2.2.2):

- winter electricity produced by gas turbine plants (GT scenario), or
- winter electricity imports from abroad (Import scenario)

The comparison is based on the production of ReMeF based on renewable (PV) electricity with GHG emissions of 10 gCO_2eq/MJ_e.

Replacing electricity from gas turbines

Estimated GHG emissions for winter electricity production based on conventional gas turbine plants is expected to be 204 gCO_2eq/MJ_e [106]. Figure 56 provides an overview of the total GWP for the PES and HighPV+, 30° scenarios without and with ReMeF implementation.

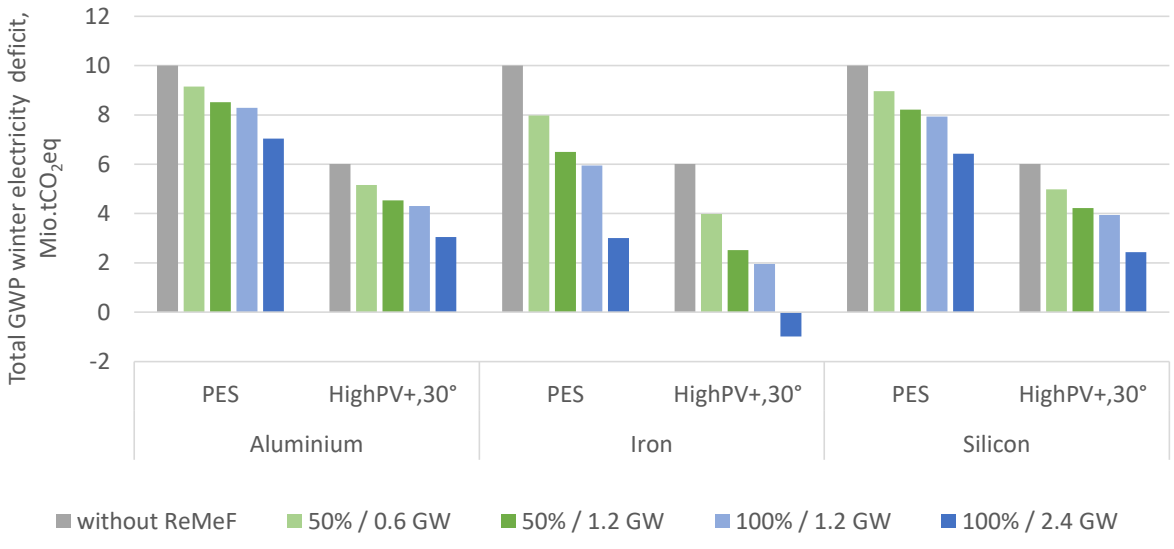

Figure 56: Scenario overview of the total GWP for the winter energy deficit without and with ReMeF storage cycles implemented, taking into account electricity produced from conventional gas turbines.

Without ReMeF storage cycles, the estimated total GWP of the winter electricity deficit is estimated at 10 Mio. tCO_2eq per year for the PES scenario, while in the case of the HighPV+, 30° scenario, total GHG emissions can be reduced by 3.99 Mio. tCO_2eq per year.

By implementing ReMeF storage cycles, the CO_2-savings for aluminium can be between 1.7 to 2.96 Mio. tCO_{2eq} per year. Iron achieved the maximum GHG savings of 4.06 to 7.00 Mio. tCO_{2eq} per year. Overall, silicon reached slightly higher CO_2-savings than aluminium (2.07 to 3.58 Mio. tCO_2eq). The much higher savings for iron are due to two effects. First, it was assumed that the amount of heat delivered by the ReMeF is the same for all of the three metals. Thus, if the share of electricity output is higher, which is the case for iron, more total energy is delivered and also more material (and more power input in summer) is needed in this case. The second effect is that delivering electricity replaces electricity from the gas turbine 1:1, whereas delivering heat only replaces electricity by 1:PF, where PF is the performance factor of heat delivered by a heat pump in the absence of heat from ReMeF.

Replacing winter electricity import

Rüdisüli et al. estimate GHG intensity of Swiss winter electricity imports to about 153 gCO_2eq/MJ_e in all of their 2018 scenarios [11]. This study was chosen as the basis to calculate the GHG emissions of ReMeF storage cycles in comparison to winter electricity imports from neighbouring countries. Figure 57 shows the total GWP for the PES and HighPV+, 30° scenarios.

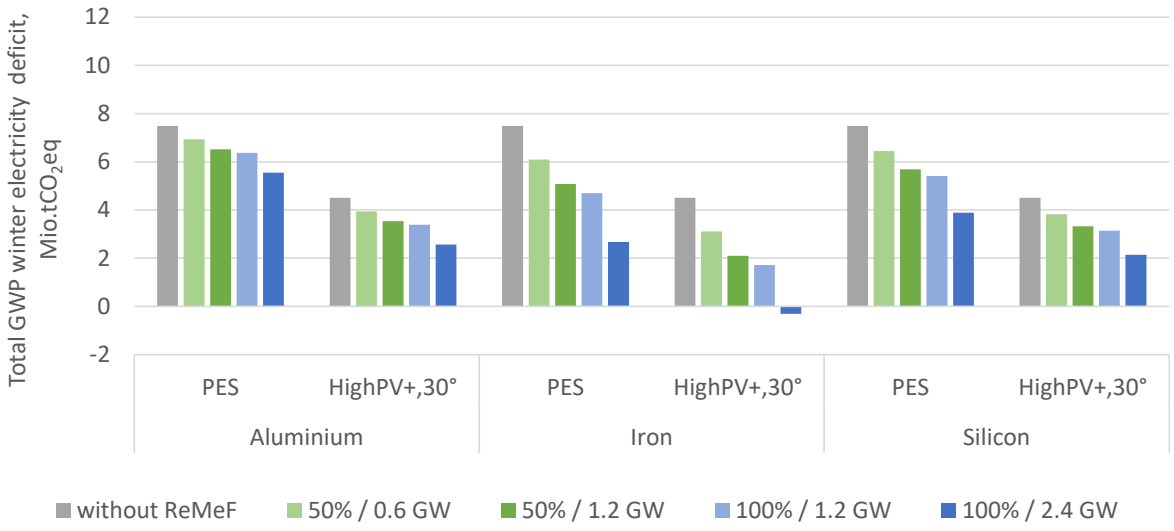

Figure 57: Scenario overview of the total GWP for the winter energy deficit without and with ReMeF storage cycles implemented, taking into account electricity imports from abroad.

Without ReMeF storage cycles, the expected total GHG emissions from winter electricity deficit is between 7.49 Mio. tCO_2eq per year in the PES scenario. For the HighPV+, 30° scenario, total GHG emissions can be cut by about 2.99 Mio. tCO_2eq per year.

For the aluminium ReMeF storage cycle, GHG emissions can be reduced by 1.12 to 1.94 Mio. tCO_2eq per year. The highest CO_2-savings are again achieved with iron, ranging from 2.79 to 4.82 Mio. tCO_2eq per year, followed by silicon, from 1.37 to 2.37 Mio. tCO_2eq.

Figure 58 presents an overview of the CO_2-savings achieved by both replacing scenarios.

It should be noted that ReMeF could also be produced in countries with an abundant renewable electricity potential based on hydropower and an already established metal industry, such as Iceland or Norway. In this case, total GHG emissions would increase by the emissions of transport by ship and then by truck or lorry on the one hand, and decrease because of the lower indirect emissions of hydropower compared to PV on the other hand.

Due to the very high energy density of ReMeF, the emissions from shipping from Iceland or Norway to Switzerland are minor and much lower than the advantage (i.e. reduction of emissions) of producing electricity from hydropower instead of PV. In this case, Switzerland would import ReMeF produced with lower CO_2 emissions and further reduce its total GHG emissions (exact figures not calculated or shown in this report).

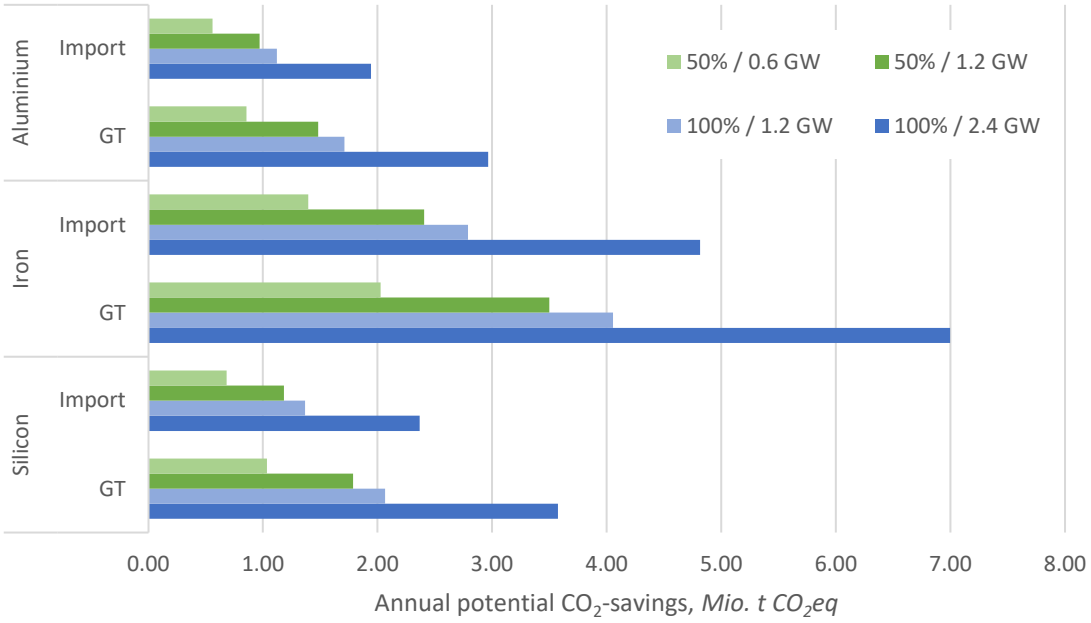

Figure 58: Annual CO_2-savings of ReMeF produced with PV electricity for the winter energy deficit replacing winter electricity production by gas turbine plants with 204 gCO_2eq/MJ_e and/or imported electricity from neighbouring countries with 153 gCO_2eq/MJ_e.

4 Conclusions

In general, it can be concluded that aluminium, iron, and silicon are potentially promising candidates as renewable energy carriers and seasonal storage media which are safe, easy to handle and very efficient to store. A metal oxidation reaction with water at low temperatures (< 100 °C) can produce heat and hydrogen, which is further converted in a fuel cell to electricity and additional heat that can be used to cover winter energy demands in buildings with very low storage volume requirements. Other conversion possibilities exist at higher temperatures, that may potentially also deliver a higher electrical efficiency of the Metal-to-Energy conversion or process heat at higher temperatures.

4.1 Technology Assessment

Power-to-Metal

Conventional metal reduction processes for aluminium and iron use carbon as a reducing agent. Electrolytic reduction with “inert” anodes that replace conventional carbon anodes or chemical reduction by hydrogen are the two state-of-the art processes to reduce metals while avoiding CO_2 emissions. For CO_2-free aluminium production, inert electrode electrolysis is considered to be at TRL 4-6, while technological development of direct reduction of iron using hydrogen to produce sponge iron with a purity of 94% to 98% is further advanced, large demonstration plants being built and TRL may be considered 6-7.

Power-to-Metal	Aluminium	Iron		Silicon
Technology	Inert electrolysis	Direct reduction with H_2	Inert electrolysis	Inert electrolysis
Material input	Al_2O_3	Fe_2O_3 & Fe_3O_4		SiO_2
Emission	O_2	H_2O	O_2	O_2
Reduction output	Al (liquid)	Sponge iron (solid)	Fe (liquid)	MG-Si (liquid)*
Metal reduction efficiency, max. %	65	60	65	65
TRL	4-7	6/7	6/7	4
Power-to-Storage Efficiency, max. %	**63**	**57**	**57**	**63**
Gravimetric Energy Density, kWh/kg	8.6	2.0	1.85	9
Volumetric Energy Density, kWh/m³	~ 23'300	~ 11'300		~ 21'000

* metallurgical grade

Figure 59: Key parameters of the analysed Power-to-Metal processes. The gravimetric energy density is the maximum amount of energy that can be released in the oxidation reaction (Metal-to-Energy).

For silicon, only a TRL of 4 has been achieved so far because research and industry are focusing more on directly producing poly- and even monocrystalline silicon grades to overcome the need for the highly energy intensive Siemens process (purification process of MG-Si).

The most relevant carbon-free Power-to-Metal technologies are summarized in Figure 59. In comparison, other Power-to-X options such as the clean production of hydrogen, methane, methanol, and ammonia reach efficiencies between 38 and 54% for producing a chemical energy carrier that can be seasonally stored (i.e. including compression or liquification and storage for gases).

Metal-to-Energy

The Alu-to-Energy and Silicon-to-Energy processes achieve similar shares of hydrogen and heat yields. However, silicon seems to be less reactive at room temperature, potentially requiring a higher surface-area ratio, and therefore, the need to use silicon in the form of powder as a source material. Nevertheless, even in powder form, silicon is safe to handle and non-explosive but should be stored in an inert environment to prevent natural oxidation, i.e., the formation of a passivation layer.

Most advanced in development is the Alu-to-Energy process below 100 °C, approaching a TRL of 5 to 6. For the silicon water oxidation processes, current development seems to reach a TRL of 4 to 5. Whereas for the Iron-to-Energy process at low temperatures, no advanced technology development could be identified, reaching only a TRL of 2 at the moment of writing.

Figure 60 provides key parameters of the metal oxidation reaction with water and indicates today's TRL levels.

Metal-to-Energy	Aluminium	Iron	Silicon
Feedstock form	Granules	N/A	Powder
Hydrogen yield per kg material input, kg	**0.11**	**0.048**	**0.14**
Metal-to-Energy heat output, kWh	**4.3**	**0**	**3.3**
Metal-to-Electric efficiency, %	**25**	**51**	**31**
Metal-to-Thermal efficiency, %	**70**	**44**	**64**
TRL	5/6	2	4/5
Low temperature pathway			

Figure 60: Key parameters of the analysed Metal-to-Energy processes for the low-temperature pathway.

Total ReMeF storage cycle efficiency was estimated to reach (Figure 33):

- 60% for aluminium
- 55% for iron
- 59% for silicon (considering the molten salt electrolysis) and
- 38% for silicon (carbothermal reduction including CCS).

4.2 Environmental assessment and GWP

Figure 61 provides an overview of the total GWP results of the selected ReMeF storage cycles with GHG emissions of 10 gCO_2eq/MJ_e for the electricity input, which represents the described 2050 PES and HighPV+,30° electricity mix scenarios in Chapter 2.3.2.

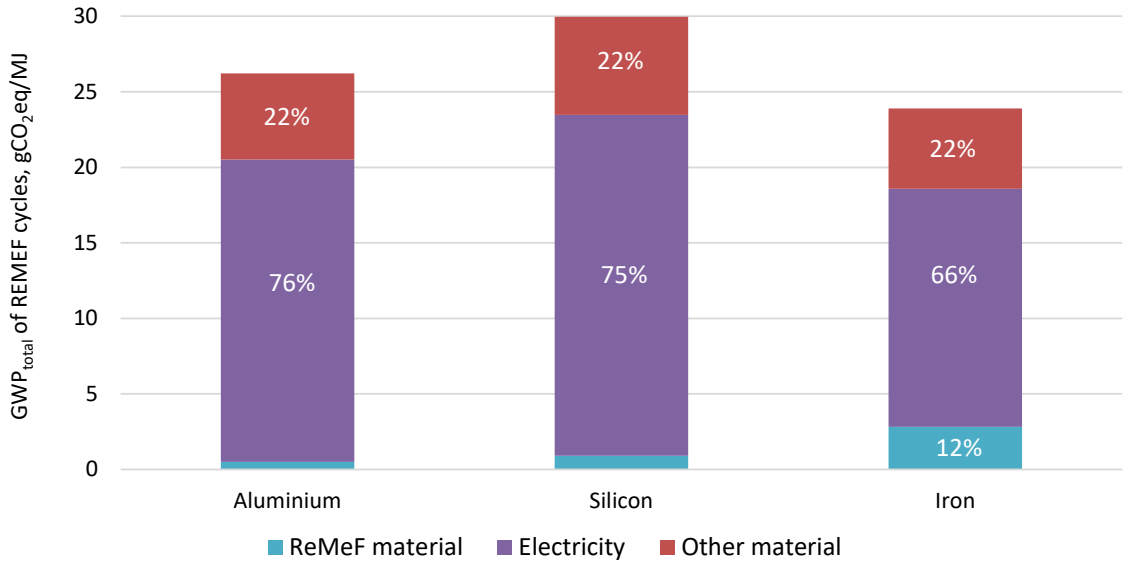

Figure 61: GHG emissions of the three ReMeF energy cycles related to material and energy inputs including a loss rate of 3 % as reaction product based on electric energy input with a burden of 10 gCO_2eq/MJ_e (PV electricity).

In general, most of the GHG emissions (76% for aluminium, 75% for silicon, and 66% for iron redox cycle) can be attributed to the electricity required for the reduction of the metal-oxide. Other material efforts as described in Chapter 3.5.2 contribute 22% to the total GWP of the ReMeF cycles.

The initial raw material input is estimated to be low for aluminium and silicon. However, the iron redox cycle contributes 12% because the environmental impact of iron oxide production appears in this category, whereas for aluminium and silicon the production of metal oxide is part of the process chain.

However, if ReMeF are not produced from low-carbon electricity, total GHG emissions will increase. Therefore, Figure 62 shows the total GWP of the ReMeF redox cycles in relation to the GWP of the electricity input. Compared to a mini-CHP plant (2 kW_e) burning natural gas with an estimated GHG emission of about 77 gCO_2eq/MJ of energy output, the ReMeF storage cycle is expected to reach an equivalent GWP using electricity with the following GHG emissions:

- 39 gCO_2eq/MJ_e for the aluminium cycle
- 48 gCO_2eq/MJ_e for the iron cycle
- 34 gCO_2eq/MJ_e for the silicon cycle

Considering the electricity input from PV of around 10 gCO_2eq/MJ_e, the total CO_2 savings of around 60 to 70% can be achieved if the ReMeF storage cycles are used instead of the natural gas mini-CHP plant. Note that the GHG emissions for the PES and HighPV+,30° scenarios are also estimated at 10 gCO_2eq/MJ_e.

It can be concluded that if the ReMeF using electricity with a GWP below 5 gCO_2eq/MJ_e, the total GHG emissions of all ReMeF storage cycles are estimated to be similar at around 15 gCO_2eq/MJ of energy output (Figure 62). However, when using electricity with higher GHG emissions per MJ_e, such as 10 gCO_2eq/MJ_e, the iron storage cycle achieves the most favourable total GWP and the silicon storage cycle achieves the least favourable total GWP.

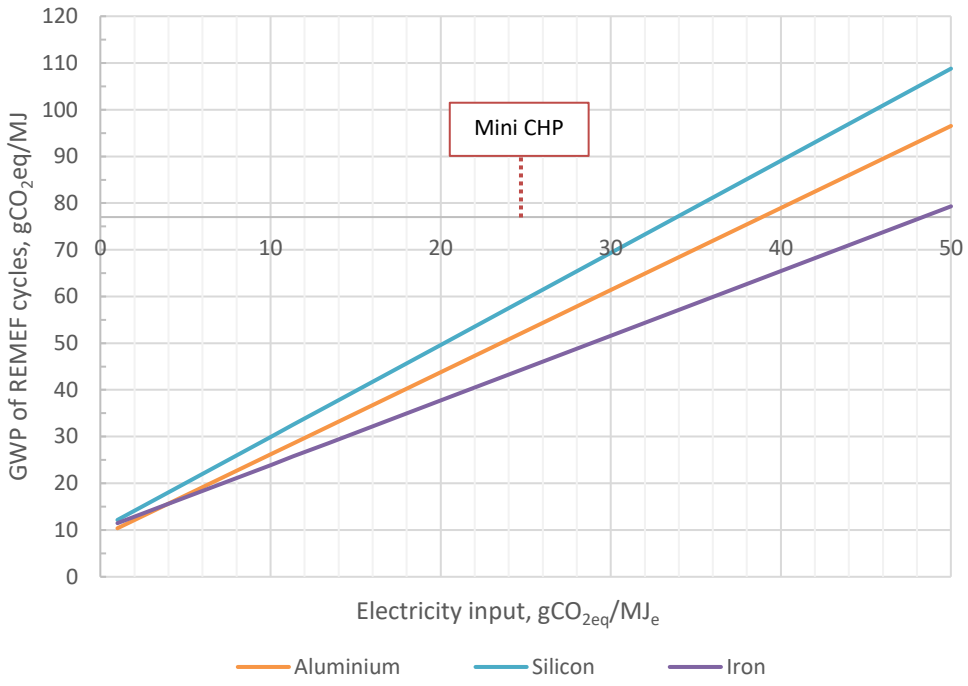

Figure 62: Sensitivity analysis of ReMeF redox cycles regarding the GWP results in relation to the GWP of the electricity input used. The results are compared to the GWP of a natural gas mini-CHF plant, 2 kW_e.

The positive result for iron is due to the fact that the share of hydrogen compared to heat, and thus the share of electricity after the fuel cell compared to heat, is much higher for the iron conversion than for the other metals. If the proportion of electricity from the energy content of aluminium or silicon could be increased, the results might change.

The environmental impact of resource use, minerals and metals is highest for the iron redox cycle. In comparison, the silicon redox cycle was the least favourable for most impact categories, in particular for the “acidification”, “eutrophication, terrestrial” and “photochemical ozone formation”. Overall, the impact indicator “eutrophication, freshwater” generally results in the highest normalized value for all ReMeF storage cycles.

4.3 Potential impact of ReMeF on the Swiss energy system

Depending on the assumptions for energy scenarios, a Swiss energy system with a 100% renewable supply of energy based on domestic resources in 2050 starts with a deficit between 13.6 TWh (pessimistic) and 8.2 TWh (high penetration of PV).

Renewable metal fuels applied exclusively in multifamily buildings with production capacities from 5-10 kW_{th} per unit may reduce the winter deficit by 2 to 12 TWh. In some extreme assumptions this would even lead to winter exports of electricity, which underlines the enormous potential of this technology. Additional potential for applications in district heating or for industrial processes were not even included in these scenarios.

While aluminium and silicon have a similar effect on electricity savings, the situation is very different for iron. This is because iron conversion can produce heat and electricity in roughly equal proportions, whereas the heat production of aluminium and silicon is 2 to 3 times higher than electricity production. On the other hand, iron conversion has a lower overall efficiency and a lower energy storage density. The amount of metal required is therefore many times higher for iron than for aluminium and silicon, when producing the same amount of heat.

Regardless of which assumption and scenario was considered, any use of ReMeFs can reduce the electricity deficit in the winter half-year substantially and thus also reduce the need for gas-fired power plants or other Power-to-X energy carriers.

Overall, the implementation of ReMeF storage cycles in the Swiss energy system has the potential to reduce GHG emissions when compared to scenarios such as winter electricity production from gas turbine plants or winter electricity imports from neighbouring countries.

In general, more GHG emissions can be reduced by applying the HighPV+,30° scenario. This is due to the higher reduction in the winter electricity deficit achieved (see Figure 56, Figure 57).

Table 25 provides an overview of the potential CO_2-savings that could be achieved by implementing ReMeF storage cycles to replace winter electricity from conventional gas turbines or imports from neighbouring countries.

Table 25: Annual CO_2-savings in Mio. t CO_{2eq} achieved by ReMeF heat and electricity production in 100% of MFH, compared to electricity from gas turbines (GT) with 204 gCO_2eq/MJ_e and imported electricity (Import) with 152 gCO_2eq/MJ_e, based on equal amounts of heat delivered by the different metal energy carriers.

Mio.tCO_2eq savings per year	vs. Gas Turbines		vs. Import	
Total power of ReMeF installed	**1.2 GW**	**2.4 GW**	**1.2 GW**	**2.4 GW**
Aluminium	1.71	2.96	1.12	1.94
Iron	4.06	7.00	2.79	4.82
Silicon	2.07	3.58	1.37	2.37

Under the assumption of equal amounts of heat delivered by the different energy carriers, it can be concluded that iron can achieve the most CO_2-savings (up to 7 Mio. tCO_2eq per year), followed by silicon (up to 3.58 Mio. tCO_2eq per year), and aluminium (up to 2.96 Mio. tCO_2eq per year).

By importing ReMeFs which are produced in countries with excess low-carbon renewable energy, potential CO_2-savings could even be increased.

5 References

[1] Bergthorson JM. Recyclable metal fuels for clean and compact zero-carbon power. Progress in Energy and Combustion Science 2018;68:169–96. https://doi.org/10.1016/j.pecs.2018.05.001.

[2] Mineral Commodity Summaries 2023. U.S. Department of the Interior and U.S. Geological Survey; 2023.

[3] Miller KA, Thompson KF, Johnston P, Santillo D. An Overview of Seabed Mining Including the Current State of Development, Environmental Impacts, and Knowledge Gaps. Front Mar Sci 2018;4:418. https://doi.org/10.3389/fmars.2017.00418.

[4] The promise and risks of deep-sea mining. Reuters 2023.

[5] International Organization for Standardization. ISO 14044 Environmental management—life cycle assessment—requirements and guidelines. Geneva, Switzerland: ISO; 2006.

[6] Dubreuil A, Young SB, Atherton J, Gloria TP. Metals recycling maps and allocation procedures in life cycle assessment. Int J Life Cycle Assess 2010;15:621–34. https://doi.org/10.1007/s11367-010-0174-5.

[7] Jungbluth N. Description of life cycle impact assessment methods n.d.

[8] How Gas Turbine Power Plants Work. EnergyGov n.d. https://www.energy.gov/fecm/how-gas-turbine-power-plants-work (accessed March 22, 2024).

[9] Swiss Federal Office of Energy BFE. Faktenblatt temporäres Reservekraftwerk Birr. 2023.

[10] ENTSO-E Transparency Platform n.d. https://transparency.entsoe.eu/ (accessed March 22, 2024).

[11] Rüdisüli M, Romano E, Eggimann S, Patel MK. Decarbonization strategies for Switzerland considering embedded greenhouse gas emissions in electricity imports. Energy Policy 2022;162:112794. https://doi.org/10.1016/j.enpol.2022.112794.

[12] BFE. Energieperspektiven 2050+. 2021.

[13] PowerCheck n.d. https://powercheck.ch/ (accessed November 21, 2023).

[14] Kemmler A, Trachsel T. Analyse des schweizerischen Energieverbrauchs 2000–2022 nach Verwendungszwecken. Prognos AG / Bundesamt für Energie; 2023.

[15] Haller MY, Dott R, Ruschenburg J, Ochs F, Bony J. The Reference Framework for System Simulations of the IEA SHC Task 44 / HPP Annex 38 2013.

[16] Axpo Power Switcher. Axpo Power Switcher n.d. https://powerswitcher.axpo.com (accessed February 28, 2024).

[17] Bergthorson JM, Goroshin S, Soo MJ, Julien P, Palecka J, Frost DL, et al. Direct combustion of recyclable metal fuels for zero-carbon heat and power. Applied Energy 2015;160:368–82. https://doi.org/10.1016/j.apenergy.2015.09.037.

[18] Lithium and Boron. Ioneer n.d. https://www.ioneer.com/projects/about-rhyolite-ridge/lithium-and-boron/ (accessed March 9, 2023).

[19] Trowell KA, Goroshin S, Frost DL, Bergthorson JM. Aluminum and its role as a recyclable, sustainable carrier of renewable energy. Applied Energy 2020;275:115112. https://doi.org/10.1016/j.apenergy.2020.115112.

[20] Andersson J, Grönkvist S. Large-scale storage of hydrogen. International Journal of Hydrogen Energy 2019;44:11901–19. https://doi.org/10.1016/j.ijhydene.2019.03.063.

[21] Brinkman L, Bulfin B, Steinfeld A. Thermochemical Hydrogen Storage via the Reversible Reduction and Oxidation of Metal Oxides. Energy Fuels 2021;35:18756–67. https://doi.org/10.1021/acs.energyfuels.1c02615.

[22] Dudita M, Farchado M, Englert A, Carbonell Sanchez D, Haller M. Heat and power storage using aluminium for low and zero energy buildings. E3S Web Conf 2019;111:04008. https://doi.org/10.1051/e3sconf/201911104008.
[23] Depken J, Dyck A, Roß L, Ehlers S. Safety Considerations of Hydrogen Application in Shipping in Comparison to LNG 2022:20.
[24] Multiview. Pricing Trends for Minor Metals: Magnesium, Silicon, and Manganese. Belmont Metals 2021. https://www.belmontmetals.com/pricing-trends-for-minor-metals-magnesium-silicon-and-manganese-raw-materials/ (accessed March 9, 2023).
[25] About Magnesium - International Magnesium Association n.d. https://www.intlmag.org/page/basics_about_mg_ima (accessed March 10, 2023).
[26] Multiview. Aluminum and Nickel Industries Experience Market Surges Due To Russia Supply Risks. Belmont Metals 2022. https://www.belmontmetals.com/aluminum-and-nickel-industries-experience-market-surges-due-to-russia-supply-risks/ (accessed March 10, 2023).
[27] Zinc - 2023 Data - 1960-2022 Historical - 2024 Forecast - Price - Quote - Chart n.d. https://tradingeconomics.com/commodity/zinc (accessed March 10, 2023).
[28] Magnesium 99.9%Min China Spot Price. InvestingCom n.d. https://www.investing.com/commodities/magnesium-99.9-min-china-futures (accessed March 10, 2023).
[29] Aluminium Historical Prices. InvestingCom n.d. https://www.investing.com/commodities/aluminum-historical-data (accessed March 10, 2023).
[30] Mike. Metal silicon price index. Businessanalytiq 2021. https://businessanalytiq.com/procurementanalytics/index/metal-silicon-price-index/ (accessed February 17, 2023).
[31] Manganese Flake 99.7% min Price $US / MT in CIF India, Ex-VAT FOB China, EXW China, FOB China, Warehouse Rotterdam. ScrapMonster n.d. https://www.scrapmonster.com//metal-prices/manganese-flake-997-min-price/738 (accessed March 10, 2023).
[32] Steel - 2023 Data - 2009-2022 Historical - 2024 Forecast - Price - Quote - Chart n.d. https://tradingeconomics.com/commodity/steel (accessed March 10, 2023).
[33] Erdkruste häufigste Elemente. Statista n.d. https://de.statista.com/statistik/daten/studie/1124582/umfrage/haeufigste-elemente-der-erdkruste/ (accessed February 3, 2023).
[34] Manganese. Giyani Metals Corp n.d. https://giyanimetals.com/manganese (accessed March 10, 2023).
[35] Reserves of zinc globally 2022. Statista n.d. https://www.statista.com/statistics/1185295/reserves-ofzinc-worldwide/ (accessed March 10, 2023).
[36] Zinc - Historical Statistics (Data Series 140) | U.S. Geological Survey n.d. https://www.usgs.gov/media/files/zinc-historical-statistics-data-series-140 (accessed March 10, 2023).
[37] Historical Statistics for Mineral and Material Commodities in the United States | U.S. Geological Survey n.d. https://www.usgs.gov/centers/national-minerals-information-center/historical-statistics-mineral-and-material-commodities (accessed February 17, 2023).
[38] Suopajärvi H, Umeki K, Mousa E, Hedayati A, Romar H, Kemppainen A, et al. Use of biomass in integrated steelmaking – Status quo, future needs and comparison to other

low-CO2 steel production technologies. Applied Energy 2018;213:384–407. https://doi.org/10.1016/j.apenergy.2018.01.060.
[39] Haller MY, Dudita M, Baeuerle Y. AlEnCycles – Aluminium-Redox-Cycles for the Production of Heat and Electricity for Buildings based on Renewable Energie. Rapperswil, CH: SPF Institute for Solar Technology; 2022.
[40] Obaidat M, Al-Ghandoor A, Phelan P, Villalobos R, Alkhalidi A. Energy and Exergy Analyses of Different Aluminum Reduction Technologies. Sustainability 2018;10:1216. https://doi.org/10.3390/su10041216.
[41] Haller MY, Carbonell D, Dudita M, Zenhäusern D, Häberle A. Seasonal energy storage in aluminium for 100 percent solar heat and electricity supply. Energy Conversion and Management: X 2020;5:100017. https://doi.org/10.1016/j.ecmx.2019.100017.
[42] REVEAL. Horizon Europe Research Project n.d. https://www.reveal-storage.eu (accessed August 25, 2022).
[43] Vasile BS, Dobra G, Iliev S, Cotet L, Neacsu IA, Nicoara AI, et al. Thermally Activated Al(OH)3: Part I—Morphology and Porosity Evaluation. Ceramics 2021;4:265–77. https://doi.org/10.3390/ceramics4020021.
[44] Gupta A, Basu B. Sustainable Primary Aluminium Production: Technology Status and Future Opportunities. Trans Indian Inst Met 2019;72:2135–50. https://doi.org/10.1007/s12666-019-01699-9.
[45] Allanore A. Features and Challenges of Molten Oxide Electrolytes for Metal Extraction. J Electrochem Soc 2015;162:E13–22. https://doi.org/10.1149/2.0451501jes.
[46] Debiagi P, Rocha RC, Scholtissek A, Janicka J, Hasse C. Iron as a sustainable chemical carrier of renewable energy: Analysis of opportunities and challenges for retrofitting coal-fired power plants. Renewable and Sustainable Energy Reviews 2022;165:112579. https://doi.org/10.1016/j.rser.2022.112579.
[47] Pineau A, Kanari N, Gaballah I. Kinetics of reduction of iron oxides by H2 Part II. Low temperature reduction of magnetite. Thermochimica Acta 2007.
[48] Sherwood SC, Dixit V, Salomez C. The global warming potential of near-surface emitted water vapour. Environ Res Lett 2018;13:104006. https://doi.org/10.1088/1748-9326/aae018.
[49] Dias V, Pochet M, Contino F, Jeanmart H. Energy and Economic Costs of Chemical Storage. Front Mech Eng 2020;6:21. https://doi.org/10.3389/fmech.2020.00021.
[50] Vogl V, Åhman M, Nilsson LJ. Assessment of hydrogen direct reduction for fossil-free steelmaking. Journal of Cleaner Production 2018;203:736–45. https://doi.org/10.1016/j.jclepro.2018.08.279.
[51] Pei M, Petäjäniemi M, Regnell A, Wijk O. Toward a Fossil Free Future with HYBRIT: Development of Iron and Steelmaking Technology in Sweden and Finland. Metals 2020;10:972. https://doi.org/10.3390/met10070972.
[52] Green Steel Solution. Boston Metal n.d. https://www.bostonmetal.com/green-steel-solution/ (accessed May 30, 2023).
[53] A. September L, Kheswa N, S. Seroka N, Khotseng L. Green synthesis of silica and silicon from agricultural residue sugarcane bagasse ash – a mini review. RSC Advances 2023;13:1370–80. https://doi.org/10.1039/D2RA07490G.
[54] Andrews RN, Clarson SJ. Pathways to Solar Grade Silicon. Silicon 2015;7:303–5. https://doi.org/10.1007/s12633-014-9235-x.
[55] Tseng M-F, Ricci L, Tao M. Multi-potential electropurification of a reusable CaCl2-CaF2 eutectic salt for solar-grade Si electrorefining. Separation and Purification Technology 2021;274:119030. https://doi.org/10.1016/j.seppur.2021.119030.

[56] Padamata SK, Saevarsdottir G. Silicon electrowinning by molten salts electrolysis. Frontiers in Chemistry 2023;11.
[57] Sakanaka Yoshihide, Goto Takuya. Electrodeposition of Si film on Ag substrate in molten LiF–NaF–KF directly dissolving SiO2. Electrochimica Acta 2015;164:139–42. https://doi.org/10.1016/j.electacta.2014.12.159.
[58] Mattei RCD, Elwell D, Feigelson RS. Electrodeposition of Silicon at Temperatures above Its Melting Point. J Electrochem Soc 1981;128:1712. https://doi.org/10.1149/1.2127716.
[59] Lee S-C, Hur J-M, Seo C-S. Silicon powder production by electrochemical reduction of SiO2 in molten LiCl–Li2O. Journal of Industrial and Engineering Chemistry 2008;14:651–4. https://doi.org/10.1016/j.jiec.2008.04.010.
[60] Jiang T, Xu X, Chen GZ. Silicon prepared by electro-reduction in molten salts as new energy materials. Journal of Energy Chemistry 2020;47:46–61. https://doi.org/10.1016/j.jechem.2019.11.005.
[61] Yu Z, Wang N, Fang S, Qi X, Gao Z, Yang J, et al. Pilot-Plant Production of High-Performance Silicon Nanowires by Molten Salt Electrolysis of Silica. Industrial & Engineering Chemistry Research 2019. https://doi.org/10.1021/acs.iecr.9b04430.
[62] Tian F, Pang Z, Hu S, Zhang X, Wang F, Nie W, et al. Recent Advances in Electrochemical-Based Silicon Production Technologies with Reduced Carbon Emission. Research 2023;6:0142. https://doi.org/10.34133/research.0142.
[63] Coxon P, Coto M, Juzeliunas E, Fray DJ. The use of electro-deoxidation in molten salts to reduce the energy consumption of solar grade silicon and increase the output of PV solar cells. Progress in Natural Science: Materials International 2015;25. https://doi.org/10.1016/j.pnsc.2015.11.006.
[64] Saevarsdottir G, Kvande H, Magnusson T. Greenhouse Gas Emissions from Silicon Production -Development of Carbon Footprint with Changing Energy Systems. SSRN Electronic Journal 2021. https://doi.org/10.2139/ssrn.3926088.
[65] Kim KH, Lee DJ, Cho KM, Kim SJ, Park J-K, Jung H-T. Complete magnesiothermic reduction reaction of vertically aligned mesoporous silica channels to form pure silicon nanoparticles. Sci Rep 2015;5:9014. https://doi.org/10.1038/srep09014.
[66] He X-C, Xie G, Li H-R, Li R-X, Yang D-J, Xu Q-X. Technology of dehydration and transformation of silicic acid. Rare Met 2013;32:532–6. https://doi.org/10.1007/s12598-013-0087-0.
[67] Environmental, social and corporate governance (ESG) report. Elkem; 2022.
[68] TOPBIO: Turn Wood Waste into Biocarbon for Metallurgical Industries - WAI Environmental Solutions 2023. https://waies.no/wai-is-granted-3-mnok-by-rff-vestfold-og-telemark-to-turn-wood-waste-into-biocarbon-for-metallurgical-industries/ (accessed June 2, 2023).
[69] Scientist ISR, Vegar Andersen PhD candidate D of MS and E, Ragnhild Jensen Elkem Technology SPM. Recirculating off-gas contributes to carbon capture. SINTEF 2021. https://www.sintef.no/en/latest-news/2021/recirculating-off-gas-contributes-to-carbon-capture/ (accessed May 23, 2023).
[70] Nagwa. Lesson Explainer: Corrosion | Nagwa n.d. https://www.nagwa.com/en/explainers/385157238120/ (accessed November 26, 2023).
[71] Dudita M, Farchado M, Englert A, Carbonell Sanchez D, Haller M. Heat and power storage using aluminium for low and zero energy buildings. E3S Web Conf 2019;111:04008. https://doi.org/10.1051/e3sconf/201911104008.
[72] Elitzur S, Rosenband V, Gany A. Study of hydrogen production and storage based on aluminum–water reaction. International Journal of Hydrogen Energy 2014;39:6328–34.

[73] Elsarrag E, Elhoweris A, Alhorr Y. The production of hydrogen as an alternative energy carrier from aluminium waste. Energy, Sustainability and Society 2017;7:9. https://doi.org/10.1186/s13705-017-0110-7.
[74] Gao X, Wang C, Bai W, Hou Y, Che D. Experimental investigation of the catalyst-free reaction characteristics of micron aluminum powder with water at low and medium temperatures. Journal of Energy Storage 2023;59:106543. https://doi.org/10.1016/j.est.2022.106543.
[75] Barelli L, Baumann M, Bidini G, Ottaviano PA, Schneider RV, Passerini S, et al. Reactive Metals as Energy Storage and Carrier Media: Use of Aluminum for Power Generation in Fuel Cell-Based Power Plants. Energy Technol 2020;8:2000233. https://doi.org/10.1002/ente.202000233.
[76] Barelli L, Trombetti L, Di Michele A, Gammaitoni L, Asenbauer J, Passerini S. Aluminum Steam Oxidation in the Framework of Long-Term Energy Storage: Experimental Analysis of the Reaction Parameters Effect on Metal Conversion Rate. Energy Technology 2022;10:2200441. https://doi.org/10.1002/ente.202200441.
[77] Wochele J, Ludwig Chr. Aluminium als Brennstoff und Speicher. Paul Scherrer Institute; 2004.
[78] Using aluminum and water to make clean hydrogen fuel—when and where it's needed. Main n.d. https://energy.mit.edu/news/using-aluminum-and-water-to-make-clean-hydrogen-fuel-when-and-where-its-needed/ (accessed June 20, 2023).
[79] Stages and Types of Steel Corrosion n.d. https://www.huyett.com/blog/steel-corrosion (accessed June 3, 2023).
[80] Dudziak T. Steam Oxidation of Fe-Based Materials. High Temperature Corrosion, IntechOpen; 2016. https://doi.org/10.5772/62935.
[81] Fry A, Osgerby S, Wright M. Oxidation of Alloys in Steam Environment - A Review. NPL Report MATC(A)90, National Physical Laboratory; 2002.
[82] Thompson M de K. The Reaction Between Iron and Water in the Absence of Oxygen. Trans Electrochem Soc 1940;78:251. https://doi.org/10.1149/1.3071303.
[83] SOLID - A compact and clean fuel. SOLID n.d. https://teamsolid.org/ (accessed June 5, 2023).
[84] Metal fuels. ENGIE Innovation n.d. http://innovation.engie.com/en/sustainable_technologies/detail/metal-fuels/27092 (accessed June 5, 2023).
[85] TU/e demonstrates iron fuel at brewery Bavaria: a new circular and CO2-free fuel for the industry n.d. https://www.tue.nl/en/news-and-events/news-overview/29-10-2020-tue-demonstrates-iron-fuel-at-brewery-bavaria-a-new-circular-and-co2-free-fuel-for-the-industry?_lrsc=%22%3E%3Cscript%3Ealert%281%29%3C%2Fscript%3E&cHash=8e8897f2fbe34cacbf55ca91e4daa7fa (accessed June 5, 2023).
[86] Steam Iron. SOLID n.d. https://teamsolid.org/steam-iron/ (accessed June 5, 2023).
[87] Ultra-thin Layers of Rust Generate Electricity from Flowing Water. California Institute of Technology 2019. https://www.caltech.edu/about/news/ultra-thin-layers-rust-generate-electricity-flowing-water (accessed June 5, 2023).
[88] Goller B, Kovalev D, Sreseli O. Nanosilicon in water as a source of hydrogen: size and pH matter. Nanotechnology 2011;22:305402. https://doi.org/10.1088/0957-4484/22/30/305402.
[89] Ning R, Jiang Y, Zeng Y, Gong H, Zhao J, Weisse J, et al. On-demand production of hydrogen by reacting porous silicon nanowires with water. Nano Res 2020;13:1459–64. https://doi.org/10.1007/s12274-020-2734-8.

[90] Taft EA. Steam Oxidation of Silicon. J Electrochem Soc 1989;136:3476. https://doi.org/10.1149/1.2096488.
[91] Mussabek G, Alekseev SA, Manilov AI, Tutashkonko S, Nychyporuk T, Shabdan Y, et al. Kinetics of Hydrogen Generation from Oxidation of Hydrogenated Silicon Nanocrystals in Aqueous Solutions. Nanomaterials 2020;10:1413. https://doi.org/10.3390/nano10071413.
[92] Tan N, Li H, Ding Z, Wei K, Ma W, Wu D, et al. Hydrogen generation during the purification of metallurgical-grade silicon. International Journal of Hydrogen Energy 2020. https://doi.org/10.1016/j.ijhydene.2020.10.117.
[93] Nakayama S, Kuwata S, Imai S. Simple hydrogen gas production method using waste silicon. Results in Materials 2022;13:100254. https://doi.org/10.1016/j.rinma.2022.100254.
[94] Just Add Water: How Scientists Are Using Silicon to Produce Hydrogen on Demand n.d. https://www.buffalo.edu/news/releases/2013/01/017.html (accessed June 5, 2023).
[95] https://newatlas.com/author/loz-blain. Another hydrogen transport powder emerges, promising double the density. New Atlas 2022. https://newatlas.com/energy/eat-si-hydrogen-generating-powder/ (accessed June 5, 2023).
[96] Products | EPRO Advance Technology. EPRO-ATech n.d. https://www.epro-atech.com/products (accessed June 5, 2023).
[97] Green hydrogen cost reduction: Scaling up electrolysers to meet the 1.5C climate goal n.d.
[98] Pastushenko A, Litvinenko S, Lysenko V, Skryshevsky V. Self-regulated hydrogen generation with the use of nano-powders: application for portable fuel cells. Physical Sciences and Technology 2018;5:50–9. https://doi.org/10.26577/phst-2018-1-144.
[99] Kanehira S, Kanamori S, Nagashima K, Saeki T, Visbal H, Fukui T, et al. Controllable hydrogen release via aluminum powder corrosion in calcium hydroxide solutions. Journal of Asian Ceramic Societies 2013;1:296–303. https://doi.org/10.1016/j.jascer.2013.08.001.
[100] Yavor Y, Goroshin S, Bergthorson JM, Frost DL. Comparative reactivity of industrial metal powders with water for hydrogen production. International Journal of Hydrogen Energy 2015;40:1026–36. https://doi.org/10.1016/j.ijhydene.2014.11.075.
[101] PEM Fuel Cell Stack Technology | Nedstack n.d. https://nedstack.com/en/pem-fuel-cell-stack-technology (accessed March 5, 2024).
[102] Leblanc D, Hovington P, Kim C, Guerfi A, Bélanger D, Zaghib K. Silicon as anode for high-energy lithium ion batteries: From molten ingot to nanoparticles. Journal of Power Sources 2015;299:529–36. https://doi.org/10.1016/j.jpowsour.2015.09.040.
[103] Life Cycle Assessment of Electricity Generation Options. Geneva, Switzerland: United Nations Economic Comission for Europe; 2021.
[104] Frischknecht R, Krebs L. Ökobilanz Strom aus Photovoltaikanlagen. Factsheet, treeze fair life cycle thinking; 2020.
[105] European Commission. Joint Research Centre. Updated characterisation and normalisation factors for the environmental footprint 3.1 method. LU: Publications Office; 2023.
[106] Wernet G, Bauer C, Steubing B, Reinhard J, Moreno-Ruiz E, Weidema B. The ecoinvent database version 3 (part I): overview and methodology. Int J Life Cycle Assess 2016;21:1218–30. https://doi.org/10.1007/s11367-016-1087-8.
[107] National Institute of Standards and Technology. NIST 2024. https://www.nist.gov/ (accessed April 28, 2024).

Annex A: Criteria evaluation

Scale definition: **10 – favourable** **0 – unfavourable**

A.1 Energy density

Linear scoring function:

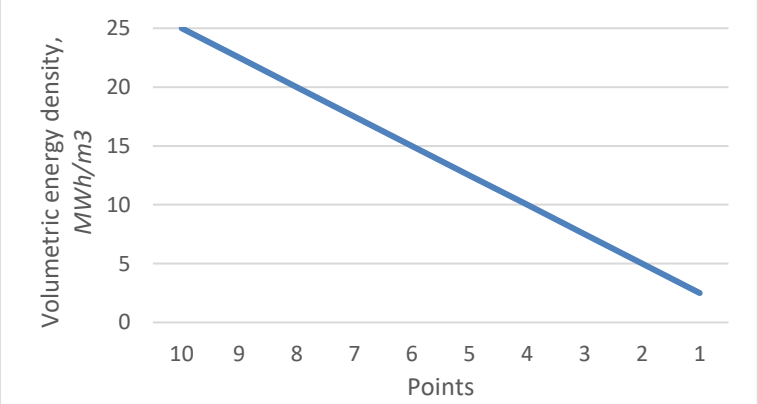

Scoring: Energy density						
	Aluminium	Iron	Magnesium	Manganese	Silicon	Zinc
Specific energy density, *MWh/m3*	23	11	12	19	21	11
Points	**10**	**4**	**5**	**8**	**9**	**4**

A.2 Market price development

Linear scoring function:

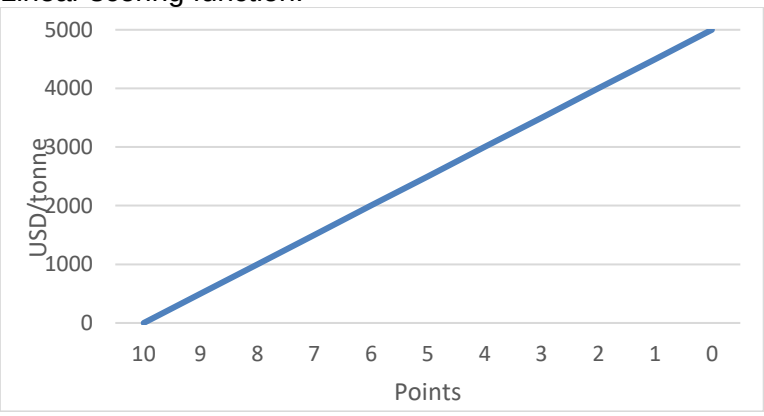

Scoring: Market price						
	Aluminium	Iron	Magnesium	Manganese	Silicon	Zinc
Avg. price 2018 to 2023, *USD/tonne*	2,180	1,315	2,248	2,228	2,490	2,836
Points	**6**	**7**	**6**	**6**	**5**	**4**

A.3 Abundancy

Exponential scoring function:

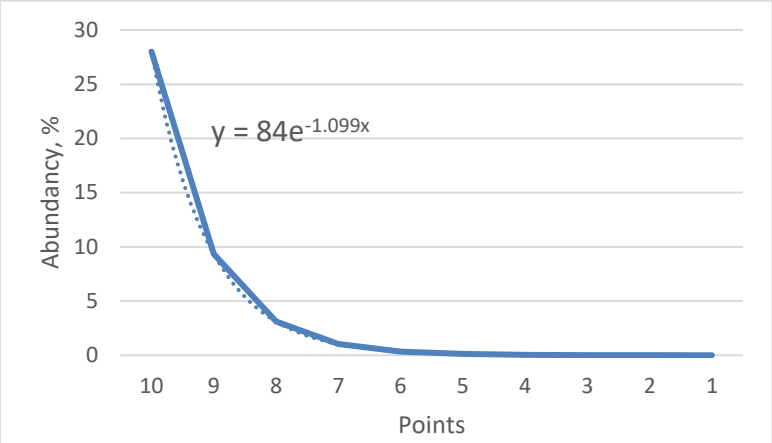

Scoring: Abundancy						
	Aluminium	Iron	Magnesium	Manganese	Silicon	Zinc
Abundancy, *%*	8.2	5.6	2.3	0.095	28.2	0.007
Points	**9**	**8**	**7**	**3**	**10**	**2**

A.4 World reserves

Exponential scoring function:

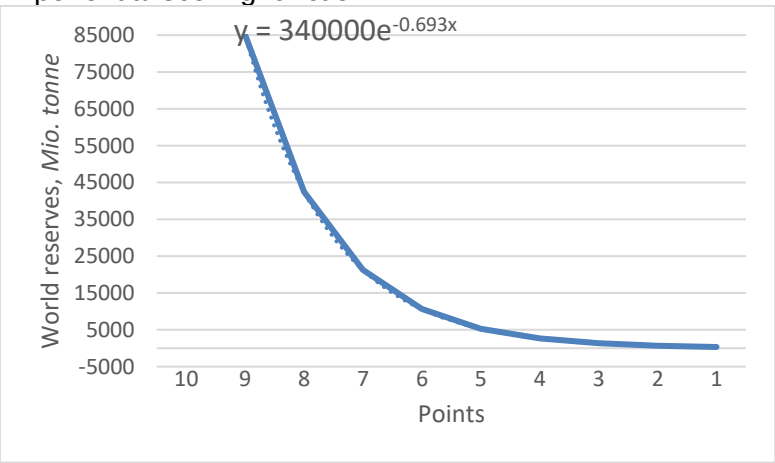

Scoring: World reserves						
	Aluminium	Iron	Magnesium	Manganese	Silicon	Zinc
World reserves,	7425	85000	2400	340	*quasi*	251

Mio. tonne					*unlimited*	
Points	**7**	**9**	**4**	**1**	**10**	**1**

A.5 Production increase for ReMeF

Exponential scoring function:

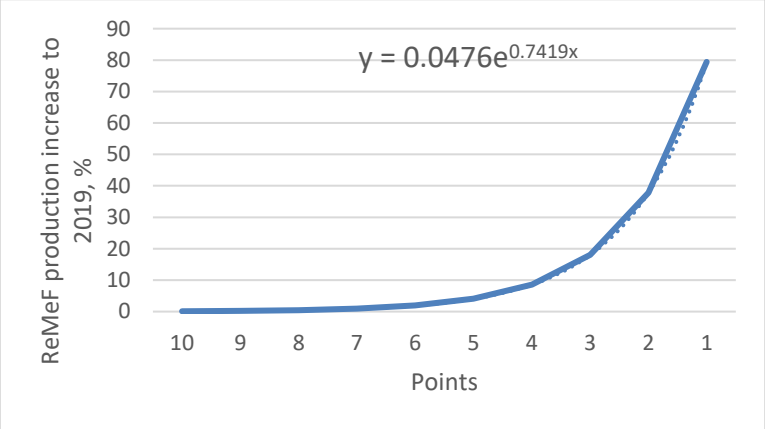

Scoring: ReMeF production increase compared to global production in 2019						
	Aluminium	Iron	Magnesium	Manganese	Silicon	Zinc
Production increase, *%*	1	0.3	48	26	9	37
Points	**7**	**9**	**1**	**3**	**4**	**2**

Annex B: Thermodynamic properties

Symbols

- $\Delta H°_{f,298}$ Standard molar enthalpy (heat) of formation at 298.15 K in kJ/mol
- $S°_{298}$ Standard molar entropy at 298.15 K in J/mol K
- $\Delta G°_{f,298}$ Standard molar Gibbs energy of formation at 298.15 K in kJ/mol
- $C°_{p,298}$ Molar heat capacity at constant pressure at 298.15 K in J/mol K
- $C°_p$ Heat capacity [J/(mol·K)] at temperature T, in the temperature range indicated in the table and expressed by the equation: $C°_p = a + bT + c'/T^2$

Thermodynamic data

From the standard enthalpy of formation ($\Delta H°_{f,298}$) presented in Table 26, the enthalpy of the reaction is calculated using (47).

$$\Delta H°_{reaction,298} = (\Sigma\ n_p\ \Delta H°_{f,298})_{products} - (\Sigma\ n_r\ \Delta H°_{f,298})_{reactants} \quad (47)$$

Table 26: Standard thermodynamic data at 298 K for the species involved in the presented reactions [107].

Symbol	$\Delta H°_{f,298}$ (kJ/mol)	$S°_{298}$ J/(mol·K)	$\Delta G°_{f,298}$ (kJ/mol)	$C°_{p,298}$ J/(mol·K)	Coefficients of the equation $C°_{p,298} = f(T)$			ΔT K
					a	$b·10^3$	$c'·10^{-5}$	
Al (cr)	0	28	0		20.67	12.38	0	298-933
H_2 (g)	0	131	0	28.8	27.28	3.26	0.50	298-3000
$C_{graphite}$	0	6	0	8.53	17.15	4.27	-8.79	298-2300
CO (g)	-110.53	197.6			25.5	6.09	4.05	298-1300
CO_2 (g)	-394	214	-394					298-1200
O_2 (g)	0							
$Al2O_3$ (cr)	-1675	51	1582	79	114.6	12.89	-34.31	298-1800
H_2O (l)	-286	70	-237	75.3	-	-	-	298
H_2O (g)	-242	189	-229	33.6	30	10.71	0.33	298-2500
$Al(OH)_3$ (s)	−1277	85	-1150					
Fe (cr)	0	27.3			18.42	24.64	-8.91	298-700
FeO (s)	-272	60.75			45.75	18.78	-5.95	298-1650
Fe_3O_4 (s)	-1118.4	146.4						
Fe_2O_3 (s)	-824	87.4	-717.8					
$Fe(OH)_3$ (s)	-823	106.7						
$Fe(OH)_2$ (s)	-574	87.9			56.7	132.1	-83.6	298-1500
Si (cr)	0	18.8			14.59	5.22	-1.078	3504-6000
SiO_2 (s)	-910.7	41.8			-6.07	251.6	-324.79	298 - 847

Annex C: Technology Readiness Level (TRL)

Scale of development for a technology

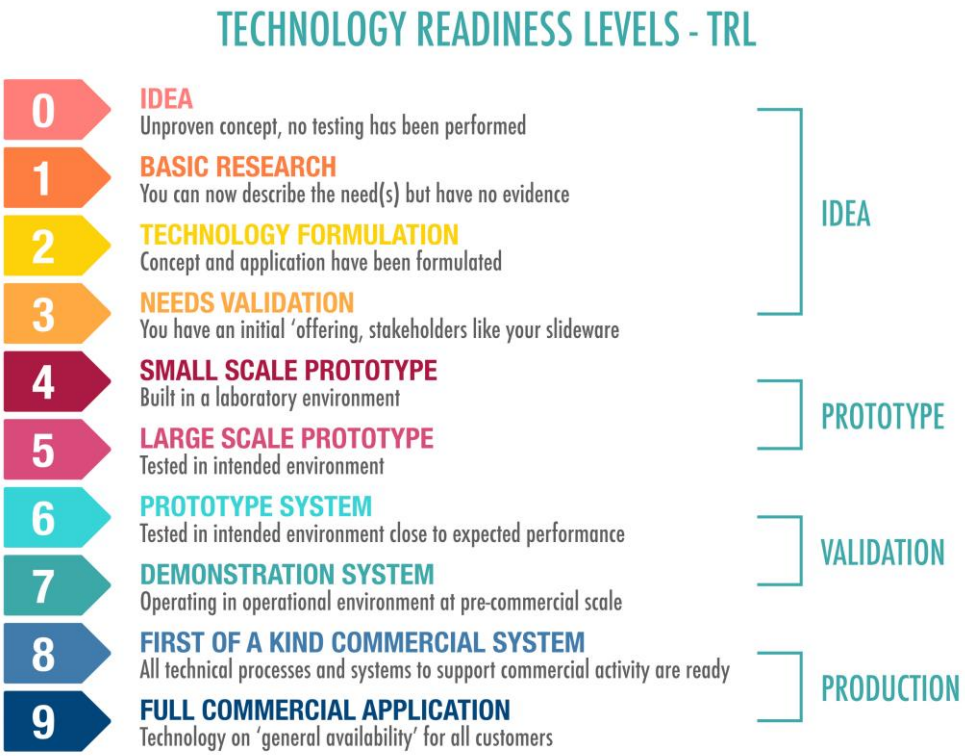

Annex D: LCA details

D.1 General cut-off rules

Included	Excluded
Raw material extraction	Anode production for aluminium inert smelter process
Energy and fuel inputs	Voltage transmission losses of the Power-to-Metal process
Extraction, processing and delivery of energy and the fuel inputs	Reaction product separation of Metal-to-Energy process
Extraction and processing of auxiliary materials (e.g. chemicals, solvents, lubricants, packaging, etc.)	Maintenance and operation of the Metal-to-Energy process
Production of the source material and processing it	Heat exchanger losses and heat distribution for the Metal-to-Energy process
Transportation of raw and processed materials and products	Human labour
Source material recycling	
Waste treatment and disposal	
Main production facilities construction	
Construction material for Metal-to-Energy converter	

D.2 Inventory – Ecoinvent reference dataset

	Aluminium	Iron	Silicon
Material Processing			
	aluminium hydroxide		sand
	aluminium oxide production	iron pellet production	silica sand production
Power-to-Metal			
Metal Electrolysis	aluminium production primary, liquid	sponge iron production	silicon production, metallurgical grade
	aluminium production primary, ingot		silicon production, multi-Si, casted
Feedstock Fabrication	granulate blast furnace slag	rock crushing	rock crushing
Metal-to-Energy			
Energy Conversion	Results from Chapter 3.4, 3.4.4		
Fuel Cell System	biomethane, low pressure burned in polymer electrolyte membrane fuel cell 2kWe, future		
Reaction Product Separation	Results from Chapter 3.4, 3.4.4		

D.3 LCI Aluminium Redox Cycle

LCI Dataset: **Aluminium Redox Cycle**

Exchange Summary: Calcination

Reference product	Amount	
aluminium hydroxide production, renewable, al-to-energy	1	kg

Input from technosphere	Amount	
aluminium hydroxide factory	1.64E-11	unit
bauxite	1.41	kg
electricity, medium voltage, renewable energy products	0.046	kWh
electricity, medium voltage, renewable energy products [a]	7.28	MJ
quicklime, milled, loose	0.0198	kg
sodium hydroxide, without water, in 50% solution state	0.031	kg

Input from technosphere, waste	Amount	
inert waste, for final disposal	-0.00047	kg
redmud from bauxite digestion	-0.536	kg

Input from environment	Amount	
occupation, unspecified	4.30E-10	m2*year
water, unspecified natural origin	0.00233	m3

Emissions to air	Amount	
mercury II	1.30E-07	kg
nitrogen oxides	1.87E-04	kg
particulate matter, < 2.5 um	2.88E-06	kg
particulate matter, > 10 um	1.60E-06	kg
particulate matter, > 2.5 um and < 10 um	3.52E-06	kg
sulfur dioxide	1.62E-04	kg
water	9.00E-04	m3

Emissions to water	Amount	
BOD5, biological oxygen demand	4.59E-05	kg
COD, chemical oxygen demand	4.59E-05	kg
DOC, dissolved organic carbon	1.80E-05	kg
mercury II	3.00E-10	kg
sodium I	1.28E-03	kg
suspended solids, unspecified	1.10E-04	kg
TOC, total organic carbon	1.80E-05	kg
water	1.77E-03	m3

[a] heat

LCI Dataset: **Aluminium Redox Cycle**

Exchange Summary: Calcination

Reference product	Amount	
aluminium oxide, al-to-energy	1	kg

Input from technosphere	Amount	
aluminium oxide factory	2.50E-11	unit
electricity, medium voltage, renewable energy products	0.008	kWh
electricity, medium voltage, renewable energy products [a]	6.8	MJ
aluminium hydroxide, renewable, al-to-energy	1.53	kg
transport, freight train	8.24E-06	tkm
transport, freight, lorry	1.77E-05	tkm

Input from technosphere, waste	Amount

Input from environment	Amount

Emissions to air	Amount	
water	1.20E-03	m3

Emissions to water	Amount

[a] heat

LCI Dataset: **Aluminium Redox Cycle**

Exchange Summary: Electrolysis

Reference product	Amount	
aluminium production primary, liquid, al-to-energy	1	kg

Input from technosphere	Amount	
aluminium electrolysis factory	7.70E-11	unit
aluminium oxide, al-to-energy	1.91E+00	kg
electricity, medium voltage, renewable energy products	1.32E+01	kWh
cryolite	8.00E-04	kg
aluminium fluoride	7.80E-03	kg
cathode, for aluminium electrolysis	2.78E-03	kg
refractory, fireclay, packed	3.35E-03	kg
blasting	2.01E-04	kg
cast iron	4.02E-04	kg
reinforcing steel	2.63E-03	kg

Input from technosphere, waste	Amount	
inert waste	-1.40E-03	kg
inert waste, for final disposal	-2.59E-01	kg
scrap steel	-3.50E-03	kg
filter dust from Al electrolysis	-5.30E-04	kg

Input from environment	Amount	
water, unspecified natural origin	3.65E-02	m3
fluoride	2.10E-04	kg

Emissions to air	Amount	
water	2.30E-03	kg
particulate matter, < 2.5 um	7.06E-04	kg
particulate matter, > 10 um	1.52E-04	kg
particulate matter, > 2.5 um and < 10 um	1.45E-04	kg
hydrogen fluoride	5.00E-04	kg

Emissions to water	Amount	
fluoride	2.10E-04	kg
water	3.65E-02	m3

LCI Dataset: **Aluminium Redox Cycle**

Exchange Summary: Casting

Reference product	Amount	
aluminium production primary, casted, al-to-energy	1	kg

Input from technosphere	Amount	
aluminium casting factory	1.54E-10	unit
aluminium, primary, liquid, al-to-energy	1.00E+00	kg
electricity, medium voltage, renewable energy products	9.50E-02	kWh
refractory, fireclay, packed	7.00E-04	kg
stone wool	1.10E-04	kg
nitrogen, liquid	6.00E-04	kg

Input from technosphere, waste	Amount	
dross from Al electrolysis	-1.72E-01	kg
inert waste, for final disposal	-3.67E-03	kg
filter dust from Al electrolysis	-4.25E-04	kg

Input from environment	Amount	
water, unspecified natural origin	5.01E-03	m3

Emissions to air	Amount	
water	7.00E-04	kg
particulate matter, < 2.5 um	1.37E-05	kg
particulate matter, > 10 um	7.60E-05	kg
particulate matter, > 2.5 um and < 10 um	1.67E-05	kg
hydrogen chloride	1.50E-05	kg
nitrogen oxides	1.10E-04	kg

Emissions to water	Amount	
treatment of wastewater	4.31E-03	m3

LCI Dataset: **Aluminium Redox Cycle**

Exchange Summary: Fabrication

Reference product	Amount	
aluminium production primary, granules, al-to-energy	1	kg

Input from technosphere	Amount	
aluminium, primary, casted, al-to-energy	1.00E+00	kg
electricity, medium voltage, renewable energy products	1.80E-03	kWh
tap water	4.78E-01	kg

Input from technosphere, waste	Amount

Input from environment	Amount

Emissions to air	Amount	
water	4.78E-04	kg
particulate matter, > 2.5 um and < 10 um	8.39E-06	kg

Emissions to water	Amount

LCI Dataset: **Aluminium Redox Cycle**

Exchange Summary: Conversion

Reference product	Amount	
heat production, multiple-dwelling, al-to-energy	1	MJ
hydrogen production, multiple-dwelling, al-to-energy	7.10E-03	kg
aluminium hydroxide, al-to-energy	1.81E-01	kg

Input from technosphere	Amount	
aluminium, primary, granules, al-to-energy	6.46E-02	kg
sodium hydroxide	1.03E-03	kg
carbon steel	5.98E-04	kg
stainless steel	7.69E-04	kg
water	1.32E-04	m3
transport, freight, train	6.56E-07	tonkm
transport, freight, lorry, unspecified	6.37E-07	tonkm

Input from technosphere, waste	Amount	
inert waste, for final disposal	-5.60E-03	kg

Input from environment	Amount

Emissions to air	Amount

Emissions to water	Amount	
sodium hydroxide	1.03E-03	kg

LCI Dataset: **Aluminium Redox Cycle**

Exchange Summary: Fuel cell system

Reference product	Amount	
electricity, low voltage, multiple-dwelling, al-to-energy	1	kWh
heat production, multiple-dwelling, fuel cell, al-to-energy	3.42E+00	MJ

Input from technosphere	Amount	
hydrogen production, multiple-dwelling, al-to-energy	5.00E-02	kg
fuel cell, polymer electrolyte membrane, 2 kW, electrical future	1.51E-05	unit
maintenance, polymer electrolyte membrane fuel cell, 2kW electrical	2.10E-04	unit

Input from technosphere, waste	Amount

Input from environment	Amount

Emissions to air	Amount

Emissions to water	Amount

LCI Dataset: **Aluminium Redox Cycle**

Exchange Summary: Aluminium Redox Cycle total

Reference product	Amount

heat production, fuel cell, al-to-energy	7.47E-01	MJ
electricity, low voltage, al-to-energy	2.53E-01	MJ

Input from technosphere	Amount	
heat production, multiple-dwelling, al-to-energy	5.07E-01	MJ
heat production, multiple-dwelling, fuel cell, al-to-energy	2.40E-01	MJ
electricity, low voltage, multiple-dwelling, al-to-energy	2.53E-01	MJ

Input from technosphere, waste	Amount

Input from environment	Amount

Emissions to air	Amount

Emissions to water	Amount

D.4 : LCI Silicon Redox Cycle

LCI Dataset: **Silicon Redox Cycle**

Exchange Summary: Calcination

Reference product	Amount	
silicon oxide production, si-to-energy	1	kg

Input from technosphere	Amount	
aluminium oxide factory	2.50E-11	unit
electricity, medium voltage, renewable energy products	0.008	kWh
electricity, medium voltage, renewable energy products [a]	1.36	MJ
silicon hydroxide production, renewable, si-to-energy	1.552	kg
sand	0.048	kg
transport, freight train	8.24E-06	tkm
transport, freight, lorry	1.77E-05	tkm

Input from technosphere, waste	Amount

Input from environment	Amount

Emissions to air	Amount	
water	6.00E-04	m3

Emissions to water	Amount

[a] heat

LCI Dataset: **Silicon Redox Cycle**

Exchange Summary: Electrolysis

Reference product	Amount	
silicon production metlalurgical grade, liquid, si-to-energy	1	kg

Input from technosphere	Amount	
silicon electrolysis factory	1.00E-11	unit
silicon oxide, al-to-energy	2.70E+00	kg
electricity, medium voltage, renewable energy products	1.44E+01	kWh
calcium chloride	4.91E-03	kg
sodium chloride	2.46E-03	kg
magnesium chloride	1.23E-03	kg
refractory, fireclay, packed	5.26E-03	kg
cast iron	6.43E-04	kg
reinforcing steel	4.20E-03	kg

Input from technosphere, waste	Amount	
inert waste	-1.40E-03	kg
inert waste, for final disposal	-2.59E-01	kg
scrap steel	-6.70E-03	kg
filter dust from Al electrolysis	-5.30E-04	kg

Input from environment	Amount

Emissions to air	Amount	
particulate matter, > 10 um	7.75E-03	kg
hydrogen fluoride	5.00E-04	kg
sulfur dioxide	1.22E-02	kg
silicon	7.75E-03	kg
nitrogen oxides	9.74E-03	kg

Emissions to water	Amount

LCI Dataset: **Silicon Redox Cycle**

Exchange Summary: Casting

Reference product	Amount	
silicon metallurgical grade, casted, si-to-energy	1	kg

Input from technosphere	Amount	
silicon factory	1.54E-10	unit
silicon production metallurgical grade, liquid, si-to-energy	1.14E+00	kg
oxygen, liquid	2.00E-02	kg

Input from technosphere, waste	Amount	
dross from Al electrolysis	-1.72E-01	kg
inert waste, for final disposal	-3.67E-03	kg
filter dust from Al electrolysis	-4.25E-04	kg

Input from environment	Amount

Emissions to air	Amount

Emissions to water	Amount

LCI Dataset: **Silicon Redox Cycle**

Exchange Summary: Fabrication

Reference product	Amount

silicon metallurgical grade, powder, si-to-energy	1	kg

Input from technosphere	Amount	
industrial machine, heavy duty, unspecific	4.41E-07	unit
silicon metallurgical grade, casted, si-to-energy	1.00E+00	kg
electricity, medium voltage, renewable energy products	7.16E-04	kWh
lubricating oil	4.50E-07	kg
cast iron	7.00E-06	kg

Input from technosphere, waste	Amount

Input from environment	Amount

Emissions to air	Amount

Emissions to water	Amount

LCI Dataset: **Silicon Redox Cycle**

Exchange Summary: Conversion

Reference product	Amount	
heat production, multiple-dwelling, al-to-energy	1	MJ
hydrogen production, multiple-dwelling, al-to-energy	1.18E-02	kg
siliocon hydroxide, al-to-energy	2.78E-01	kg

Input from technosphere	Amount	
silicon metalurgical grade, powder, si-to-energy	8.42E-02	kg
potassium hydroxide	1.69E-03	kg
carbon steel	4.82E-04	kg
stainless steel	6.20E-04	kg
water	2.21E-04	m3
transport, freight, train	1.05E-06	tonkm
transport, freight, lorry, unspecified	1.02E-06	tonkm

Input from technosphere, waste	Amount	
inert waste, for final disposal	-8.59E-03	kg

Input from environment	Amount

Emissions to air	Amount

Emissions to water	Amount

potassium hydroxide	1.69E-03	kg

LCI Dataset: **Silicon Redox Cycle**

Exchange Summary: Fuel cell system

Reference product	Amount	
electricity, low voltage, multiple-dwelling, al-to-energy	1	kWh
heat production, multiple-dwelling, fuel cell, al-to-energy	3.42E+00	MJ

Input from technosphere	Amount	
hydrogen production, multiple-dwelling, al-to-energy	5.00E-02	kg
fuel cell, polymer electrolyte membrane, 2 kW, electrical future	1.51E-05	unit
maintenance, polymer electrolyte membrane fuel cell, 2kW electrical	2.10E-04	unit

Input from technosphere, waste	Amount

Input from environment	Amount

Emissions to air	Amount

Emissions to water	Amount

LCI Dataset: **Silicon Redox Cycle**

Exchange Summary: Silicon Redox Cycle total

Reference product	Amount	
electricity, low voltage, si-to-energy	3.11E-01	MJ
heat production, fuel cell, si-to-energy	6.43E-01	MJ

Input from technosphere	Amount	
heat production, multiple-dwelling, si-to-energy	3.48E-01	MJ
heat production, multiple-dwelling, fuel cell, si-to-energy	2.95E-01	MJ
electricity, low voltage, multiple-dwelling, si-to-energy	3.11E-01	MJ

Input from technosphere, waste	Amount

Input from environment	Amount

Emissions to air	Amount

Emissions to water	Amount	

LCI Dataset: **Silicon Redox Cycle**

Exchange Summary: Reaction Product Treatment

Reference product	Amount	
silicon hydroxide production, renewable, si-to-energy	1.00E+00	kg

Input from technosphere	Amount	
silicon hydroxide, si-to-energy	1.00E+00	kg
electricity, medium voltage, renewable energy products [a]	2.17E+00	MJ

Input from technosphere, waste	Amount	
inert waste, for final disposal	-4.70E-04	kg

Input from environment	Amount	
water, unspecified natural origin	2.33E-03	m3

Emissions to air	Amount	

Emissions to water	Amount	
suspended solids, unspecified	1.10E-04	kg
water	2.33E-03	m3

[a] heat

D.5 : LCI Iron Redox Cycle

LCI Dataset: **Iron Redox Cycle**

Exchange Summary: Pelletizing

Reference product	Amount	
iron pellet production, fe-to-energy	1	kg

Input from technosphere	Amount	
aluminium oxide factory	2.50E-11	unit
electricity, high voltage, renewable energy products	0.008	kWh
electricity, high voltage, renewable energy products [a]	0.714	MJ
iron oxide, renewable production, fe-to-energy	9.90E-01	kg
iron ore	4.42E-02	kg
bentonite	4.44E-03	kg
chromium	1.83E-04	kg
lime	1.75E-02	kg
dolomite	3.77E-02	kg
lubricating oil	1.68E-05	kg
sodium hydroxide	1.01E-04	kg
solvent, organic	3.76E-06	kg
steel, unalloyed	1.04E-03	kg
tap water	6.11E-01	kg
transport, freight train	8.24E-06	tkm
transport, freight, lorry	1.77E-05	tkm

Input from technosphere, waste	Amount	
scrap steel	-1.00E-04	kg
spent solvent mixture	-3.76E-06	kg
waster mineral oil	-2.66E-06	kg

Input from environment	Amount	

Emissions to air	Amount	
water	6.00E-04	m3
particulate matter, < 2.5 um	1.05E-05	kg
particulate matter, > 10 um	1.80E-05	kg
particulate matter, > 2.5 / < 10 um	1.23E-05	kg

Emissions to water	Amount	
water	5.62E-04	m3

[a] heat

LCI Dataset: **Iron Redox Cycle**

Exchange Summary: Electrolysis

Reference product	Amount	
sponge iron production DRI-H, fe-to-energy	1	kg

Input from technosphere	Amount	
blast furnace	1.33E-11	unit
iron pellet production, fe-to-energy	1.42E+00	kg
electricity, high voltage, renewable energy products	3.00E-01	kWh
electricity, high voltage, renewable energy products	2.91E+00	kWh
dolomite	1.31E-02	kg
nitrogen, liquid	4.88E-02	kg

Input from technosphere, waste	Amount	
inert waste, for final disposal	-3.00E-01	kg
wastewater from pig iron production	-1.44E-03	m3
blast furnace sludge	-1.00E-01	kg

Input from environment	Amount	
water	2.76E-03	m3

Emissions to air	Amount	
water	3.60E-04	m3
particulate matter, < 2.5 um	2.87E-05	kg
particulate matter, > 10 um	1.60E-06	kg
particulate matter, > 2.5 / < 10 um	1.60E-06	kg

Emissions to water	Amount

LCI Dataset: **Iron Redox Cycle**

Exchange Summary: Fabrication

Reference product	Amount	
iron production, powder, fe-to-energy	1	kg

Input from technosphere	Amount	
industrial machine, heavy duty, unspecific	4.41E-07	unit
sponge iron production DRI-H, fe-to-energy	1.00E+00	kg
electricity, medium voltage, renewable energy products	7.16E-04	kWh
lubricating oil	4.50E-07	kg
cast iron	7.00E-06	kg

Input from technosphere, waste	Amount

Input from environment	Amount

Emissions to air	Amount

Emissions to water	Amount

LCI Dataset: **Iron Redox Cycle**

Exchange Summary: Conversion

Reference product	Amount	
hydrogen production, multiple-dwelling, al-to-energy	1.00E+00	kg
iron oxide, renewable production, fe-to-energy	2.78E+01	kg

Input from technosphere	Amount	
iron production, powder, fe-to-energy	2.08E+01	kg
carbon steel	1.55E-02	kg
stainless steel	1.99E-02	kg
water	2.75E-02	m3
transport, freight, train	7.65E-05	tonkm
transport, freight, lorry, unspecified	7.42E-05	tonkm

Input from technosphere, waste	Amount	
inert waste, for final disposal	-9.20E-01	kg

Input from environment	Amount

Emissions to air	Amount

Emissions to water	Amount

LCI Dataset: **Iron Redox Cycle**

Exchange Summary: Fuel cell system

Reference product	Amount	
electricity, low voltage, multiple-dwelling, al-to-energy	1	kWh
heat production, multiple-dwelling, fuel cell, al-to-energy	3.42E+00	MJ

Input from technosphere	Amount	
hydrogen production, multiple-dwelling, al-to-energy	5.00E-02	kg
fuel cell, polymer electrolyte membrane, 2 kW, electrical future	1.51E-05	unit
maintenance, polymer electrolyte membrane fuel cell, 2kW electrical	2.10E-04	unit

Input from technosphere, waste	Amount

Input from environment	Amount

Emissions to air	Amount

Emissions to water	Amount

LCI Dataset: **Iron Redox Cycle**

Exchange Summary: Iron Redox Cycle total

Reference product	Amount	
electricity, low voltage, fe-to-energy	5.00E-01	MJ
heat production, fuel cell, fe-to-energy	5.00E-01	MJ

Input from technosphere	Amount	
heat production, multiple-dwelling, fuel cell, fe-to-energy	5.25E-01	MJ
electricity, low voltage, multiple-dwelling, fe-to-energy	5.00E-01	MJ

Input from technosphere, waste	Amount

Input from environment	Amount

Emissions to air	Amount

Emissions to water	Amount

LCI Dataset: **Iron Redox Cycle**

Exchange Summary: Reaction Product Treatment

Reference product	Amount	
iron oxide, renewable production, fe-to-energy	1.00E+00	kg

Input from technosphere	Amount	
iron oxide, si-to-energy	1.00E+00	kg
electricity, medium voltage, renewable energy products [a]	2.17E+00	MJ

Input from technosphere, waste	Amount	
inert waste, for final disposal	-4.70E-04	kg

Input from environment	Amount	
water, unspecified natural origin	2.33E-03	m3

Emissions to air	Amount	

Emissions to water	Amount	
suspended solids, unspecified	1.10E-04	kg
water	2.33E-03	m3

[a] heat

D.6 Midpoint impact categories for the European EF 3.1 LCIA method [105].

Impact category	Impact assessment model	Indicator unit	Source
Climate change	The Global Warming Potential (GWP) calculates the radiative forcing over a 100 year time horizon. It assesses the potential impact of different gaseous emissions on climate change.	kg CO_2 eq	IPCC 2021 + JRC adaptions
Ozone depletion	The Ozone Depletion Potential (ODP) calculates the destructive effects on the stratospheric ozone layer over a time horizon of 100 years. The stratospheric ozone layer reduces the amount of UV-radiation that reaches the ground, and which can cause damages for humans, animals, plants and materials.	kg CFC-11 eq	EDIP model based on the ODPs of WMO 2014 + integrations from other sources
Ionizing radiation	This category estimates the effect of radioactive emissions on human health. Most radiation stems from normal operation of nuclear power plants including the nuclear fuel production and treatment of radioactive wastes (accidents are not included). Quantification of the impact of ionizing radiation on the population is made with reference to Uranium 235.	kg U^{235} eq	Frischknecht et al. 2000
Photochemical ozone formation	This category calculates the effect of summer smog on human health. Ozone and other reactive oxygen compounds are formed as secondary contaminants in the troposphere (close to the ground). Ozone is formed by the oxidation of the primary contaminants VOC (Volatile Organic Compounds) or CO (carbon monoxide) in the presence of NOx (nitrogen oxides) under the influence of light. Expression of the potential contribution to photochemical ozone formation close to the ground. The method used includes spatial differentiation and is only valid for Europe. Considering a marginal increase in ozone formation, the LOTOS-EUROS spatially differentiated model averages over 14000 grid cells to define European factors.	kg NMVOC eq	Van Zelm et al. 2008 as applied in ReCiPe
Human toxicity, non-cancer	The unit "CTUh" (Comparative Toxic Unit for Humans) expresses the estimated increase in morbidity in the total human population due to different types of emissions entering into the environment. The calculation is based on USEtox® 2.1, which is a model that describes chemical fate, exposure, effect and optionally severity of emissions. No spatial differentiation beyond continent and world compartments. Specific groups of chemicals require further works (cf. details in other sections). Impact indicator: Comparative Toxic Unit for human (CTUh) expressing the estimated increase in morbidity in the total human population per unit mass of a chemical emitted (cases per kilogram).	CTUh	Fantke et al. 2017 Rosenbaum et al. 2008 as in Saouter et al. 2018
Human toxicity, cancer	Based on USEtox 2.1 model, see above	CTUh	Fantke et al. 2017 Rosenbaum et al. 2008 as in Saouter et al. 2018
Acidification	This impact category describes potential impacts on soil and freshwater that becomes more acid due to the deposition of certain pollutants from air: The "Accumulated Exceedance" model characterizes the change in critical load exceedance of the sensitive area in terrestrial and main freshwater ecosystems, to which acidifying substances deposit.	molc H+ eq	Posch et al. 2008 Seppälä et al. 2006
Particulate matter	This category estimates the potential effect of fine dust emissions on human health: The indicator is calculated applying the average slope between the Emission Response Function (ERF) working point and the theoretical minimum-risk level. Exposure model based on archetypes that include urban environments, rural environments, and indoor environments within urban and rural areas.	Disease incidence	Fantke et al. 2016
Eutrophication, freshwater	Expression of the degree to which the nutrients emitted in Europe reach the freshwater and lead to the problem of eutrophication. Only phosphorus emissions are evaluated since it is considered as the limiting factor in freshwater. EUTREND model used to model atmospheric emissions. Impact indicator: Phosphorus equivalents: European validity. Averaged characterization factors from country dependent characterization factors.	kg P eq	Struijs et al. 2009 as implemented in ReCiPe
Eutrophication, marine	Expression of the degree to which nutrients emitted in Europe reach the oceans and lead to eutrophication. Only nitrogen emissions evaluated since it is considered as the limiting factor in marine water. EUTREND model used to model atmospheric emissions. Impact indicator: Nitrogen equivalents.	kg N eq	Struijs et al. 2009 as implemented in ReCiPe
Eutrophication, terrestrial	Eutrophication means that too many nutrients reach ecosystems and harm the plants and animals living in sensitive systems: The "Accumulated Exceedance" model characterizes the change in critical load exceedance of the sensitive terrestrial area, to which eutrophying substances ("excess nutrients") deposit. It is European-country dependent which is not considered with the LCI data used in this study.	molc N eq	Posch et al. 2008 Seppälä et al. 2006
Ecotoxicity, freshwater	Measurement of environmental toxicity in freshwater due to emissions: The unit "CTUe" (Comparative Toxic Unit for ecosystems) is an expression of an estimate of the potentially affected fraction of species (PAF) integrated over time and volume per unit mass of a chemical emitted (PAF m3 year/kg). Specific groups of chemicals require further works. USEtox consensus model (multimedia model). No spatial differentiation beyond continent and world compartments. Specific groups of chemicals requires further works.	CTUe	Fantke et al. 2017 Rosenbaum et al. 2008 as in Saouter et al. 2018
Land use	Land use refers here to the amount and quality deficit of land occupied or transformed. This model is based on soil quality index as in LANCA model. CFs set was re-Calculated by JRC starting from LANCA® v 2.5 as baseline model. Out of 5 original indicators (Erosion resistance, Mechanical filtration, Physicochemical filtration, Groundwater regeneration, Biotic production) only 4 have been included in the aggregation (Physicochemical filtration was excluded due to the high correlation with the mechanical filtration). Biodiversity impacts are not covered in this method.[7]	Pt	De Laurentiis et al. 2019; Horn et al. 2018
Water use	Assessment of the water use related to local scarcity of water in different countries. Relative Available WAter REmaining (AWARE) per area in a watershed, after the demand of humans and aquatic ecosystems has been met.	m^3 deprived	Boulay et al. 2018
Resource use, fossils	Abiotic resource depletion fossil fuels (ADP-fossil); based on lower heating value	MJ eq	van Oers et al. 2002
Resource use, minerals and metals	Ultimate reserves model. The model takes both the annual production as well as the availability of the resource into account. (CML 2002 model). ADP for energy carriers, based on van Oers et al. 2002 as implemented in CML, v. 4.8 (2016). Depletion model based on use-to-availability ratio. Full substitution among fossil energy carriers is assumed.	kg Sb eq	van Oers et al. 2002

D.7 LCIA results, EF v3.1

	Aluminium Redox Cycle	Silicon Redox Cycle	Iron Redox Cycle
Human toxicity, cancer	2.12967E-06	2.60938E-06	2.36199E-06
Human toxicity, non-cancer	3.47793E-06	4.58648E-06	2.79412E-06
Particulate matter disease inc.	1.10256E-05	1.06224E-05	4.47245E-06
Photochemical ozone formation	1.70693E-06	1.11358E-05	2.13071E-06
Ionising radiation	-2.13872E-08	2.05201E-07	-2.26615E-08
Water use	-1.10824E-06	4.62065E-06	-5.11278E-06
Ecotoxicity, freshwater	7.51021E-06	8.23021E-06	4.34871E-06
Climate change	1.96237E-06	2.39768E-06	1.90564E-06
Resource use, fossil	1.9466E-06	2.89747E-06	1.94156E-06
Ozone depletion	5.10708E-09	-1.1301E-08	2.10733E-08
Eutrophication, marine	1.17773E-06	2.36082E-06	1.68658E-06
Eutrophication, freshwater	1.72186E-05	1.71764E-05	1.63153E-05
Land use	-8.68462E-08	7.12452E-08	-2.58962E-07
Eutrophication, terrestrial	1.90941E-06	1.03268E-05	2.35965E-06
Acidification	-2.41584E-07	1.50086E-05	-2.97467E-06
Resource use, mineral and metals	3.80092E-06	3.55049E-06	8.64366E-06

Annex E: Energy scenarios

E.1 Swiss energy scenario assumptions

Electricity System:

Scenario: PES

PowerCheck Parameter	Unit	Value
Flatlands PV	Power [GW]	37.5
Wind	Power [GW]	0
Thermal Power Plant	Power [GW]	0.9

Scenario: HighPV+,30°

PowerCheck Parameter	Unit	Value
Flatlands PV	Power [GW]	43.6
Alpine PV	Power [GW]	1.4
Wind	Power [GW]	2.2
Thermal Power Plant	Power [GW]	1.3

Both Scenarios:

PowerCheck Parameter	Unit	Value
Battery (Elektrochemical)	Power [GW]	10
	Capacity [GWh]	10
Pump Storage Power Plant	Power [GW]	3
	Capacity [GWh]	240
	Initial Level [GWh]	20
Hydro Storage Power Plant	Power [GW]	10
	Capacity [GWh]	10885
	Initial Level [GWh]	6500
Elecrolysis	Power [GW]	0
H2 (or others)	Capacity [GWh]	0
H2 (or others) Power Plant	Power [GW]	0
Run-of-river Power Plant	Power [GW]	3.5

PowerCheck Parameter	Distribution over year	Yearly Value (Same as 2050+)
E-Mobility	Evenly	17 TWh
Base Consumption	Like 2019 (20% higher in winter)	31.5 TWh
Big HP for District Heating	Proportional to Heat demand	2.7 TWh

Heating System General:

Share of Heating Systems for Space Heating:

PowerCheck Parameter	Unit	Value
New buildings	% of current (2019) ERA [%]	+18
Future Renovation Rate	% of yearly ERA [%]	1.1
Passiv Houses	% of new/renovated ERA [%]	10
Share of HPs with Air Source	% in target year [%]	80
DHW Change	% change compared to 2019 [%]	-13
DHW Heatrecovery	% revovered heat of total demand [%]	10

Share of Heating Systems for Domestic Hot Water:

Domestic Hot Water Type of heating system	Share of all ERA [%]
	Same for SFH and MFH
District heating	31
Electric	0
Oil	0
Biogas	7
Wood	2
Heat pumps	59
Other	1

E.2 Scenario comparison from AXPO Web-Tool

Scenarios Unit: TWh	PV	Wind	Run-of-River	Hydro Storage	Other Renewables	Hydrogen	Fossil	Nuclear Power
2050+	36	4.3	19	19	5	0	0.5	0
Axpo Ern.	36	10	18	18	6	7	0.5	0
Axpo Land.	32	0.4	18	17.5	6	0	0.5	30
WWB	16.5	1	16	17	4	0	0.5	0
Grossen	48	2.2	20	20	4	4.5	1.9	0
Nordmann	77	7	18	19	2.2	6	1.9	0
Wasserfallen	16.5	0.5	19.5	20	3	10	0.5	9
Schwarz	38	43	19	24.5	0	0	0	0
Helion	55	3.5	18	18	6	2.3	0.5	0
Swisssolar	45	4.3	18	17.5	7	2.3	0.5	0
ESC Nexus-e	40	0.2	20.5	19	4	0	0.6	0
Economiesuisse	40	0.15	20.5	19	4	0	0.6	17.3
Rechsteiner	48	3	30.5	30.5	2	0.5	0	0

Scenarios Unit: TWh	Total Demand	Total Demand (w/o Electrolysis)	E-Mobility	Heat Pumps	Electrolysis
2050+	77	74	13	12	3
Axpo Ern.	88	79	15	10	9
Axpo Land.	88	79	15	10	9
WWB	80	77	13	9	3
Grossen	90	73	23	5	17
Nordmann	115	91	17	6	24
Wasserfallen	-	-	-	-	-
Schwarz	112	112	16	22	0
Helion	88	78	22	6	10
Swisssolar	90	78	17	12	12
ESC Nexus-e	-	-	-	-	-
Economiesuisse	-	-	-	-	-
Rechsteiner	78	75	14.5	12	3

Scenarios Unit: TWh	Summer (half-year) Surplus	Winter (half-year) Deficit
2050+	9	-9
Axpo Ern	8	-1.2
Axpo Land	18	-3.5
WWB	-4.5	-23
Grossen	10	-2.3
Nordmann	11.3	-3.5

Wasserfallen	7	-4.2
Schwarz	17	-3.2
Helion	22	-6.7
Swisssolar	13	-4.7
ESC Nexus-e	18	-11
Economiesuisse	26	-1
Rechsteiner	36	-3

E.3 Electricity deficit in winter for different scenarios

Scenario: PES

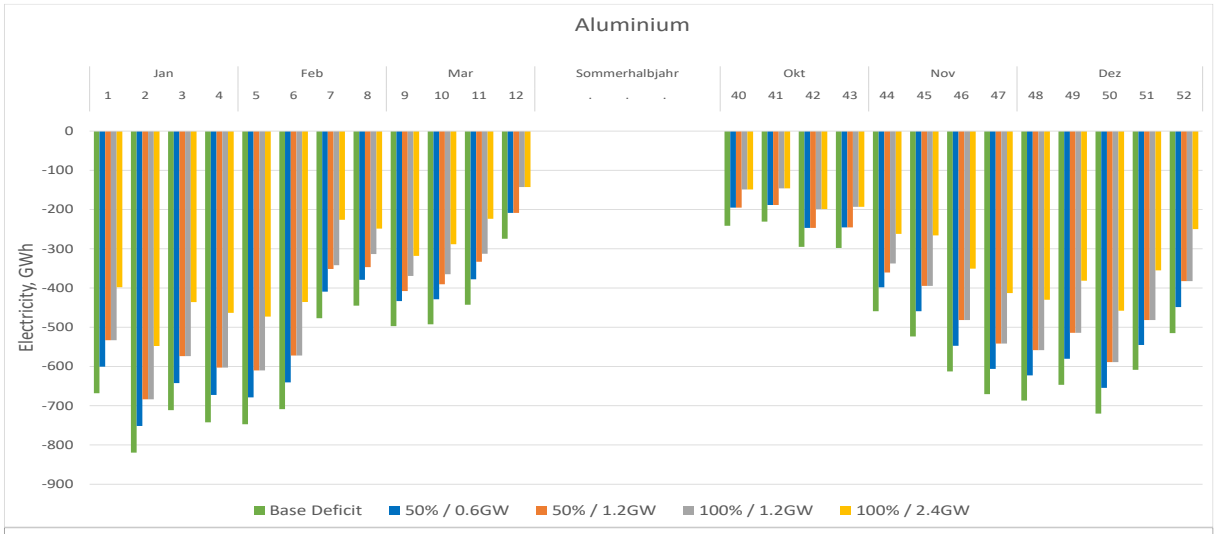

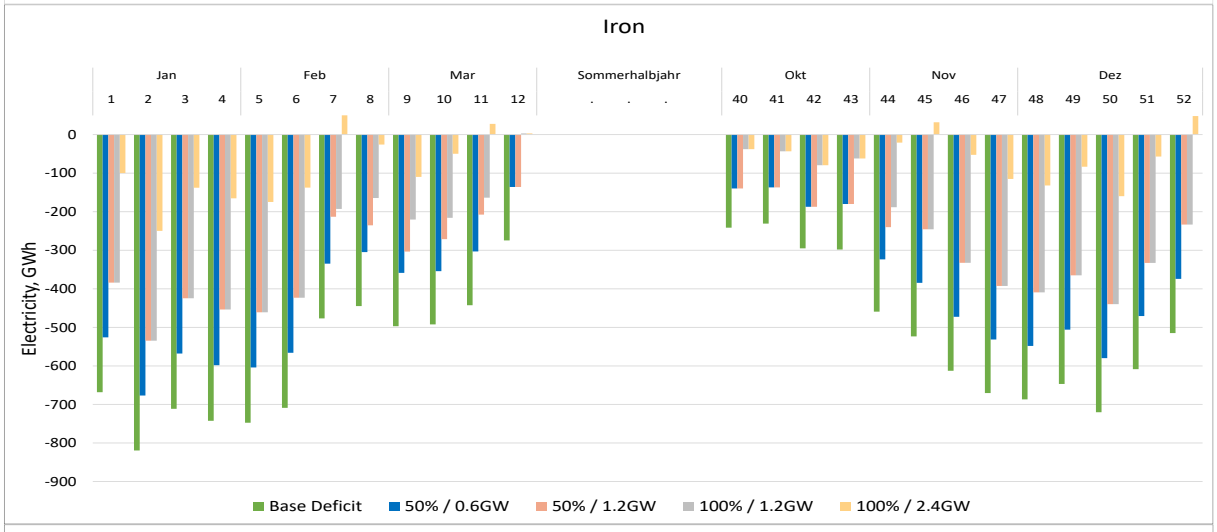

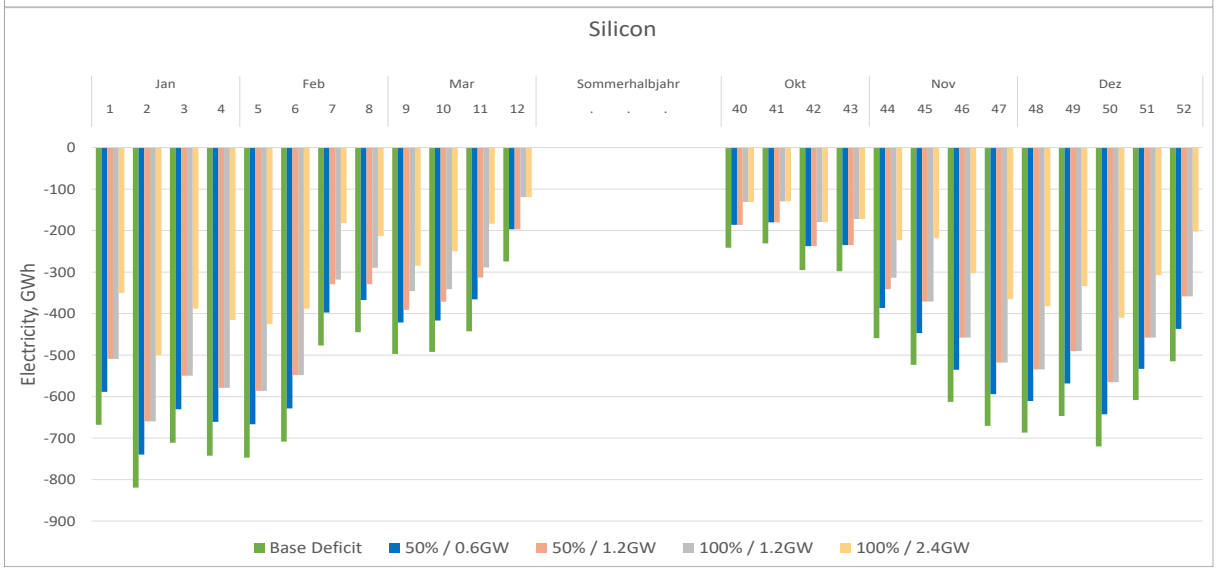

Scenario: HighPV+,30°

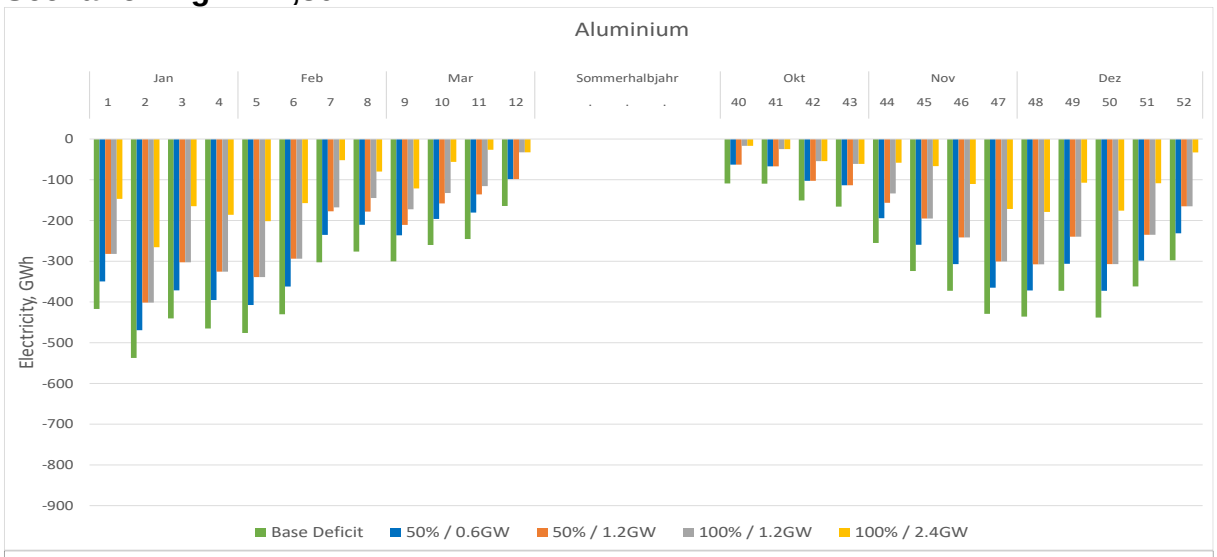

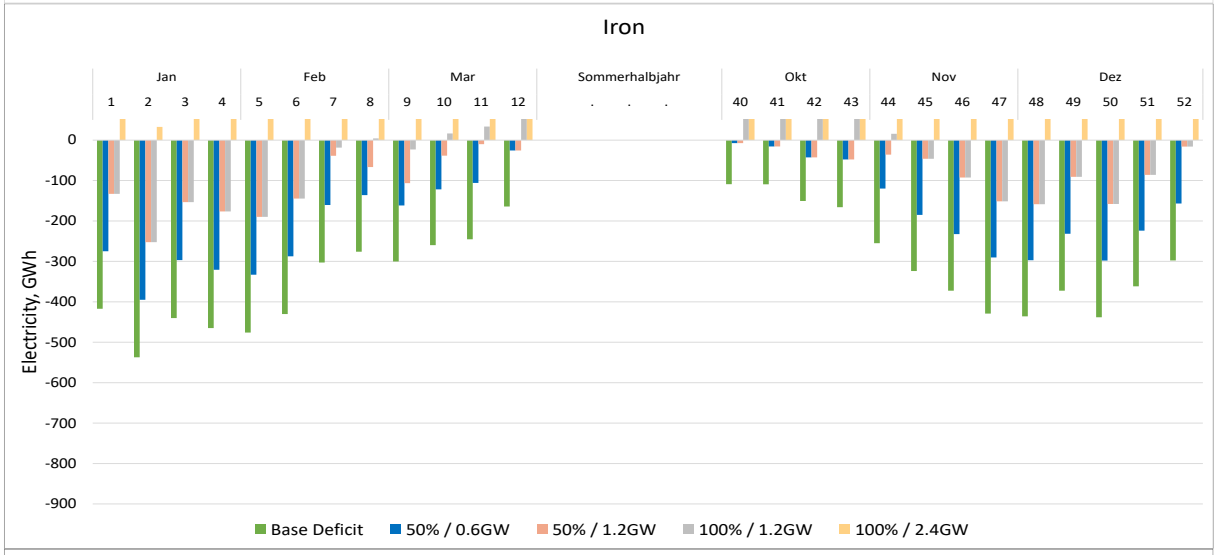

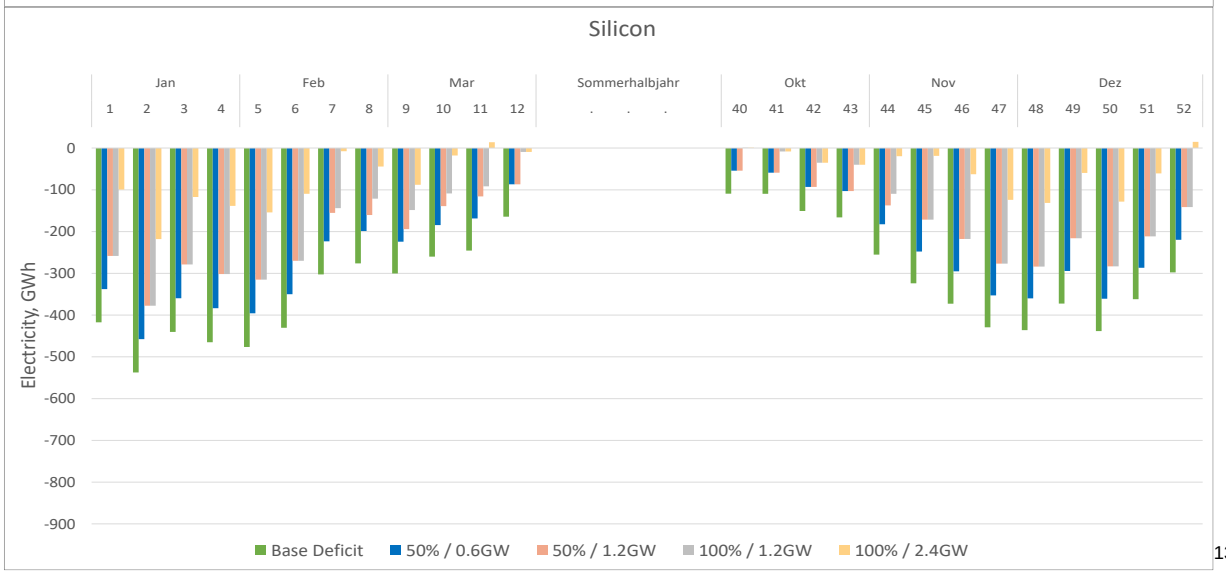

E.4 Comparison of Results

Electricity production and consumption 2050

Production Unit: TWh	PES	HighPV+,30°	ZERO Basis
PV	35.8	46.0	33.6
Wind	0.0	4.3	4.3
Thermal (Other Ren.)	1.8	4.2	4.2
Run-of-River	18.6	18.6	18.6
Hydro Storage	19.5	19.5	19
Pump Storage	4.2	4.2	6.2
Total	**79.9**	**95.8**	**82.7**
Consumption Unit: TWh	**PES**	**HighPV+,30°**	**ZERO Basis**
Base Consumpion	31.6	31.6	31.4
E-Mobility	16.9	16.9	17
Space Heat	8.2	8.2	7.2
DHW	3.8	3.8	2
Process Heat	3.5	3.5	5.2
District Heat	2.7	2.7	2.7
Pump Storage	5.2	5.2	8.5
Losses	5.7	5.7	5.3
Total	**77.6**	**77.6**	**79.3**